UNIVERSITY OF LIÈGE

FACULTY OF APPLIED SCIENCES

Numerical Modeling of a High-Temperature Heat Pump in the Context of CO_2 Capture

Master's thesis completed to obtain the Master's degree in Electromechanical Engineering, by VAN LIEROP Théo

Promotors:
LEMORT Vincent
LÉONARD Grégoire
Supervisor:
BEGUIN Brieuc

Jury:
CASETTA Damien
LEMORT Vincent
LÉONARD Grégoire
QUOILIN Sylvain

ACADEMIC YEAR 2023-2024

Abstract

In the current context of energy transition, CO_2 capture technologies are part of the solutions to help reduce greenhouse gas emissions and global warming. The main challenge accompanying these technologies is their energy consumption. Therefore, this thesis investigates the technical feasibility of integrating a high-temperature heat pump into a CO_2 capture pilot project to reduce its energy consumption.

First, a comprehensive review of heat pump technologies and their previous integrations into CO_2 capture processes is presented. Then, the heat sources available from the cooling requirements of the CO_2 capture process are explored, considering two cases: a single-evaporator heat pump connected to the process's cooling circuit and a two-evaporator heat pump utilizing the high-temperature CO_2-water mixture exiting the stripper.

A complete theoretical model is developed, particularly for the compressor, to simulate the performance and energy consumption of different heat pump configurations based on operating conditions. The results show a potential reduction in energy demand, demonstrating the feasibility and benefits of this integration. For the first case study, the optimal configuration allows a 54% reduction in energy consumption. For the second case study, two configurations achieved similar results, allowing a reduction of 59% and 60% in initial energy consumption. The simulation results of the system's behavior under variable load demonstrate that, depending on the pilot's needs, it would be appropriate to size the compressors for lower power than the nominal power. An additional analysis is then conducted where the capture process itself is modified. The analysis of reducing the pressure in the stripper shows that the best performance is obtained at a pressure of 1.25 bar, allowing a 65% reduction compared to the initial process.

Acknowledgment

First of all, I want to thank my academic supervisors, Prof. Vincent Lemort and Prof. Grégoire Léonard, for their advice, support, and guidance throughout this work.

I am also grateful to Brieuc Beguin for his presence and willingness to answer all my questions, as well as his advice and proofreading of this report.

Additionally, I extend my thanks to the research team of the CO_2 capture pilot plant project for their welcome and daily assistance.

Lastly, I would like to express my heartfelt gratitude to my family, especially my parents, who have always believed in me and supported me in all my projects.

I would like to end by thanking my friends, my roommates, and my girlfriend for their moral support during my studies and for this project.

Contents

List of Figures

Chapter 1

Introduction

1.1 Context

In the current global climate crisis, the urgency surrounding energy and its consumption has never been more pronounced. With the adoption of the Paris Agreement during COP21 in 2015, the international community set forth a landmark framework with the ambitious aim of limiting the rise in global temperatures below 2°C above pre-industrial levels, with an even more ambitious aspiration of limiting it to 1.5°C. This agreement underscores the imperative for an immediate and comprehensive energy transition. The energy transition, as illustrated Figure 1.1 necessitates a drastic decrease in global greenhouse gas emissions.

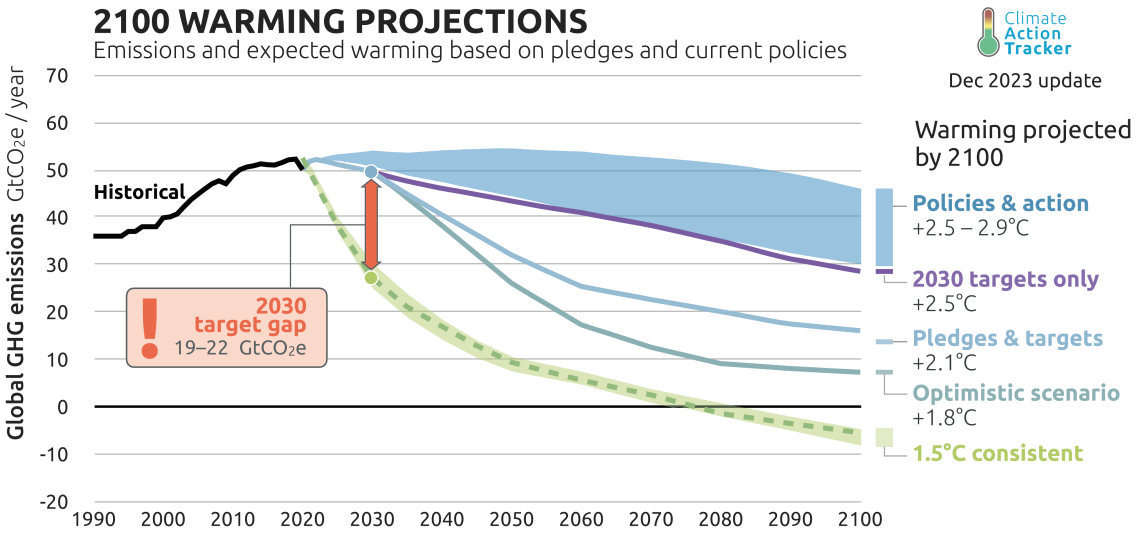

Figure 1.1: Greenhouse gas emissions projection [1].

CO_2 stands out as the primary contributor to the greenhouse effect on a global scale [2]. Consequently, it becomes imperative to address CO_2 emissions directly. Two key solutions involve transitioning to renewable energies, which entails gradually replacing fossil fuel sources with clean and sustainable alternatives such as solar, wind, and hydroelectric power. Simultaneously, enhancing energy efficiency aims to reduce the amount of energy consumed, thereby lowering CO_2 emissions associated with energy production and use.

The transition towards renewable energies represents a complex and gradual process rather than an immediate shift. Figure 1.2 indicate that a significant portion, around 84%, of global CO_2 emis-

sions stems from energy consumption, underscoring the pivotal role of transitioning to cleaner energy sources. However, it is essential to acknowledge that approximately 16% of CO_2 emissions originate from industrial processes themselves. For instance, industrial activities like cement production release CO_2 as an inherent byproduct, irrespective of the energy source employed, whether it be fossil fuels or renewables.

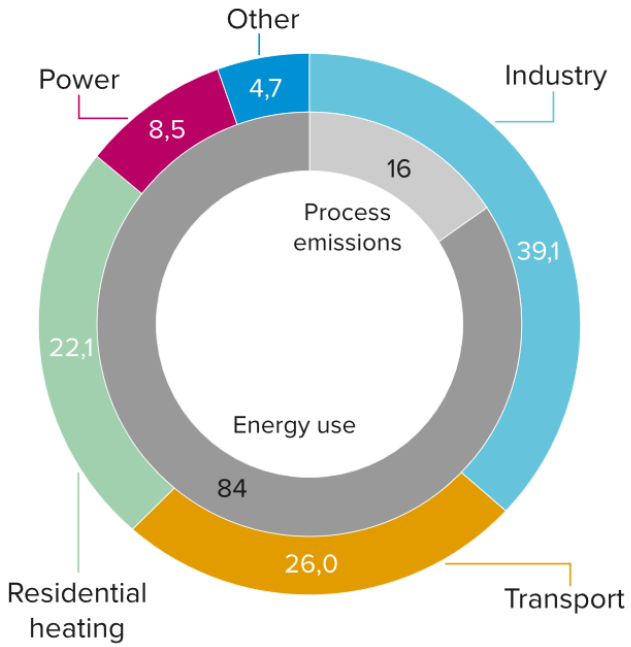

Figure 1.2: CO_2 emissions by sector [3].

This nuanced understanding highlights the multifaceted nature of emissions reduction efforts. In the short term, carbon capture technology can plays a pivotal role in capturing emissions associated with energy consumption, providing a crucial bridge towards a cleaner energy future. Moreover, it is imperative to emphasize that carbon capture technology also holds long-term significance. By deploying carbon capture solutions, industries can effectively mitigate emissions from inherently carbon-intensive processes, ensuring a more sustainable pathway forward. Therefore, alongside the adoption of renewable energies, the deployment of carbon capture technology becomes imperative.

1.2 Carbon capture, utilization and storage (CCUS)

Carbon Capture, Utilization, and Storage (CCUS) encompasses a range of technologies designed to prevent the release of CO_2 into the atmosphere. These technologies capture CO_2 either from concentrated emission sources, such as industrial facilities and power plants, or directly from the ambient air. Once captured, it can be either used in various industrial processes or permanently stored underground.

1.2.1 Capture technologies

When capture is conducted from concentrated sources, there are three primary capture modes [4] :

- **Pre-combustion capture:**

In this mode, CO_2 is captured before the combustion of fossil fuels. Typically, this occurs during the gasification process, where the fossil fuel is converted into a syngas, containing CO_2, hydrogen, and carbon monoxide. The CO_2 is then separated from the syngas before combustion.

- **Post-combustion capture :**

  Post-combustion capture involves the removal of CO_2 from flue gases emitted after the combustion of fossil fuels. The flue gases, containing CO2, pass through a capture unit where the CO2 is extracted, resulting in a high-purity CO_2 stream. Post-combustion carbon capture (PCC) offers several advantages that make it an attractive technology for reducing CO_2 emissions from existing power plants [5]. One of the primary benefits of PCC is its retrofitting capability, allowing it to be implemented in existing power plants and industrial facilities without requiring significant structural modifications. Additionally, PCC exhibits flexibility in handling flue gas streams with varying CO_2 concentrations, making it applicable to a wide range of combustion sources.

- **Oxyfuel combustion :**

  Oxyfuel combustion entails burning fossil fuels with pure oxygen and recycled flue gas, resulting in a flue gas stream enriched with CO_2. This facilitates the subsequent capture of CO_2, as the flue gas is predominantly composed of CO_2 and water vapor, with minimal nitrogen dilution. The disadvantages of oxy-combustion include the significant material requirements due to the high operating temperatures, a decrease in efficiency as the oxygen production process consumes a lot of energy, and the high initial capital investment needed.

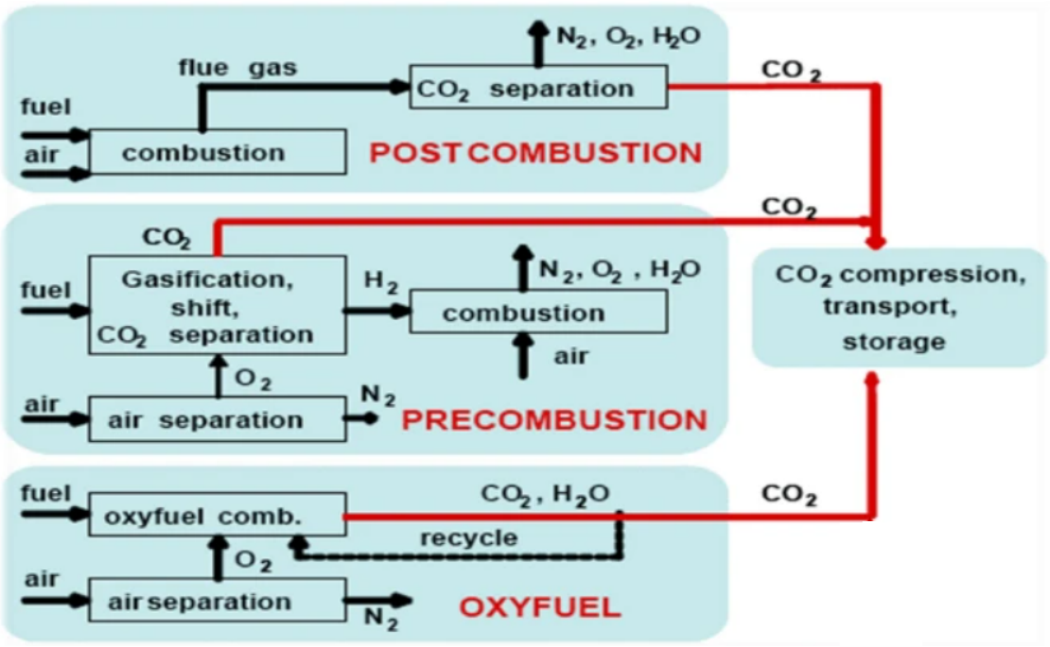

Figure 1.3: Primary carbon capture modes [6].

1.2.2 Post-combustion separation technologies

When employing post-combustion capture, there are several methods for separating CO_2 from flue gases. These methods include chemical absorption, physical adsorption, membrane separation, and cryogenic separation [7]. Here is a summary of how each method operates.

- **Chemical absorption:**

Among these various techniques, the most commonly used is the amine-based chemical absorption method for CO_2 separation. This is primarily due to its long-standing history of development and widespread application across diverse industries like the desulfurization of petrochemical products. It offers high capture efficiency and adaptability to different operational conditions, with simple integration into existing industrial infrastructure [8]. This method represented in Figure 1.4 involves using chemical solvents to capture CO_2 from flue gases. The solvent selectively absorbs CO_2 molecules, separating them from other gases. The captured CO_2 is then released through a regeneration process, typically involving heating or depressurization, allowing for the reuse of the solvent.

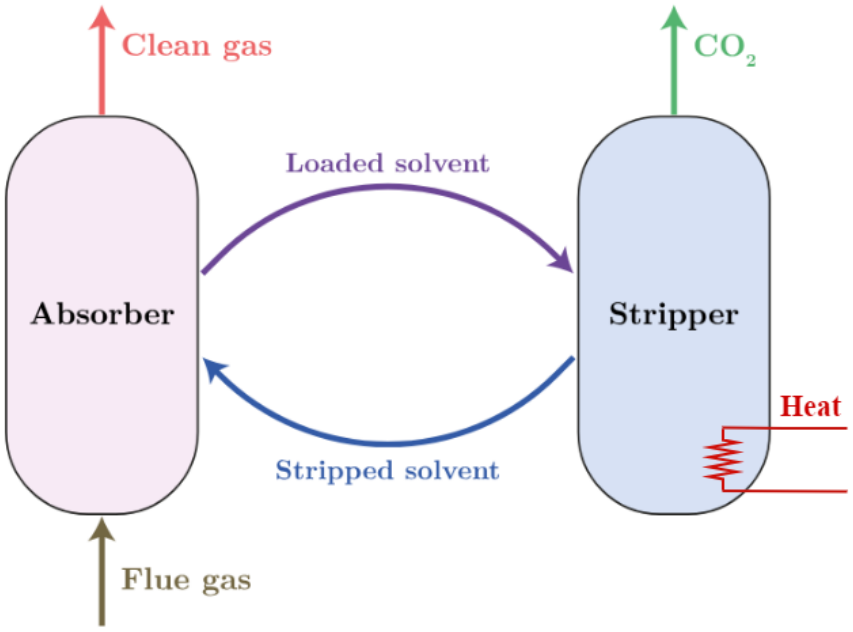

Figure 1.4: Chemical absorption process [9].

- **Physical adsorption:** Physical adsorption relies on porous solid materials, such as activated carbons, zeolites, or metal-organic frameworks (MOFs), to capture CO_2 molecules from gas streams. These materials have high surface areas and specific pore structures that enable them to selectively adsorb CO_2 while allowing other gases to pass through. After adsorption, the CO_2 can be desorbed from the adsorbent material using changes in temperature or pressure, making it available for storage or utilization.

- **Membrane separation:** Membrane separation technologies utilize selective permeable membranes to separate CO_2 from gas mixtures based on differences in molecular size, shape, or solubility. Membrane separation offers advantages such as scalability, simplicity, and potentially lower operating costs compared to traditional absorption or adsorption processes. However, membrane separation may face challenges related to membrane stability, selectivity, and fouling [10].

- **Cryogenic separation:** Cryogenic separation involves cooling the gas mixture to very low temperatures to condense and separate CO_2 from other gases. Cryogenic separation is particularly effective for high-purity CO_2 streams and can achieve high levels of CO_2 recovery. However, cryogenic separation requires significant energy inputs for refrigeration and may not be economically viable for low CO_2 concentration streams or small-scale applications [10].

1.2.3 Utilization and Storage

Once captured, carbon dioxide (CO_2) presents a lot of opportunities for utilization across various industrial sectors [11]. For instance, CO_2, combined with hydrogen, can undergo conversion into synthetic fuels, through processes like Fischer-Tropsch synthesis. These synthetic fuels are carbon neutral and can serve as sustainable alternatives to fossil fuels, particularly in transportation. Moreover, captured CO_2 can be utilized as a feedstock in the production of chemicals and materials. Through processes like carbonation or mineralization, CO_2 can be chemically transformed into valuable compounds such as methanol, urea, or polymers. These chemicals find applications in numerous industries, including agriculture, pharmaceuticals, and construction, contributing to the circular economy by closing the carbon loop and reducing reliance on conventional feedstocks derived from fossil fuels.

On the storage front, geological sequestration of CO_2 involves injecting captured CO_2 into underground geological formations, such as saline aquifers or depleted oil and gas reservoirs. Once injected, the CO_2 is securely trapped within the pore spaces of the rock formation, preventing its release into the atmosphere. Geological storage provides a long-term solution for carbon mitigation by permanently isolating CO2 from the atmosphere [11].

After reviewing various CO_2 capture technologies and more specifically the post combustion amine-based chemical absorption process, the following section introduces the CO_2 capture pilot plant project currently undertaken by the research team led by Mr. Leonard Grégoire from the Department of Chemical Engineering in the University of Liège.

1.3 Pilot plant Project

The goal of the project is to implement a smale-scale pilot for de-risking the existing but not yet commercially available post-combustion carbon capture with amine-based chemical absorption. The pilot project will have a capacity to capture approximately 1 tonne of CO_2 per day, allowing for substantial data collection and analysis. Its operations will encompass a wide range of scientific activities, including studying solvent degradation, dynamic behavior while varying operating conditions such as flue gas flow rate and CO_2 concentration, evaluating the overall performance of the carbon capture process and cost estimations.

1.3.1 Amine-based CO_2 capture process description

As previously introduced and developped in the preceding section, the most mature and promising technology for CO_2 capture is post-combustion capture, achieved through CO_2 separation utilizing chemical absorption with amines. The complete process is illustrated in Figure 1.5.

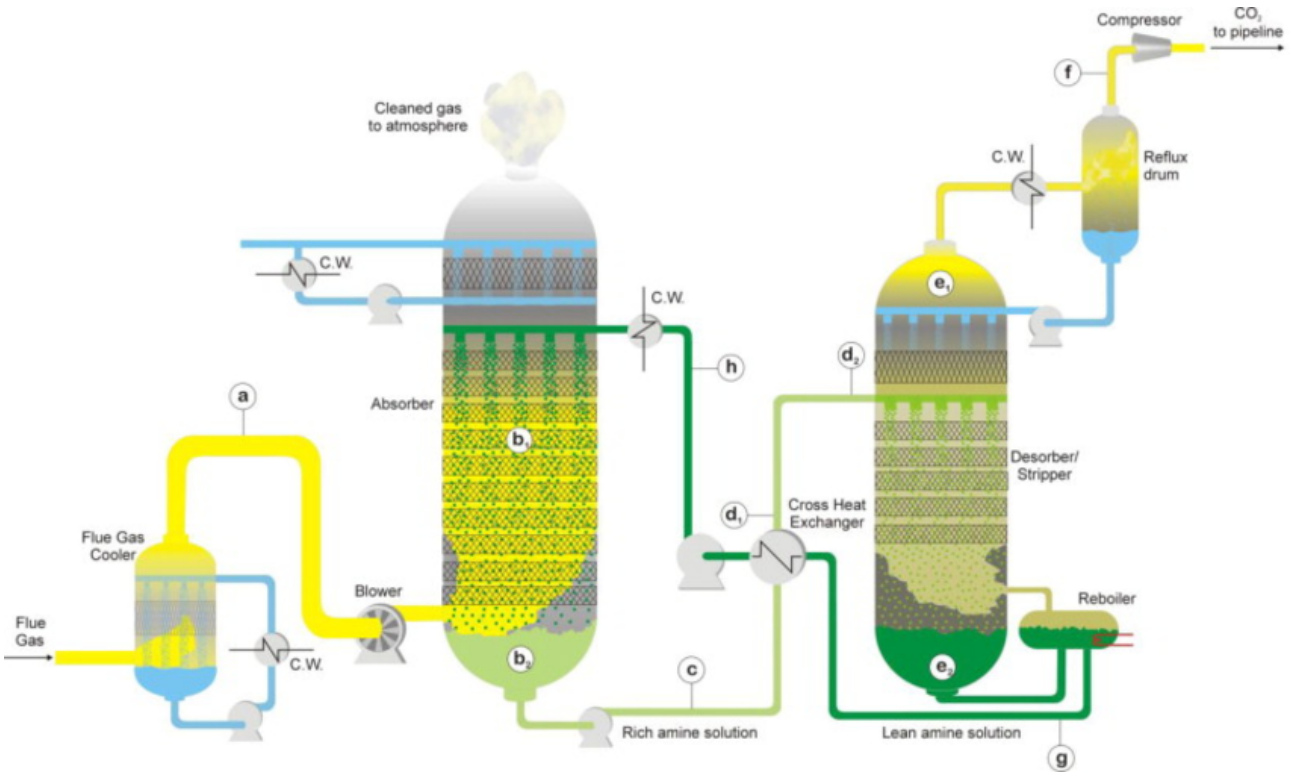

Figure 1.5: Amine-based CO_2 capture process diagram [12].

For a better understanding, here are the key steps :

a) The flue gases are cooled and washed in a direct contact exchanger before entering the absorber.

b) 1. The cooled and washed flue gases come into contact with the liquid amine in the absorber, where CO_2 is absorbed and the CO_2-depleted gas is released to the atmosphere

2. The amine solution becomes rich in CO_2 after absorbing it in the absorber.

c) The rich amine solution is pumped first to the cross heat exchanger and then finally to the stripper

d) The rich amine solution is preheated using the hot lean amine solution exiting the desorber.

e) The preheated solution is then directed to the stripper, where CO_2 is desorbed from the amine through an increase in the solution temperature.

f) A mixture of steam and CO_2 leaves the stripper. This mixture is cooled and the steam is condensed to be separated from the CO_2, which is then compressed for storage or further use.

g) The reboiler heats the solution and maintains a high temperature in the stripper to enable the desorption process.

1.3.2 Heat Duty

Following a detailed exploration of the CO_2 capture process stages, the focus will be now shift to the critical final phase: the reboiler. This stage presents one of the most significant challenges associated with these technologies : energy consumption [13].

The function of the reboiler is to heat the solvent employed in capturing CO_2, thereby releasing it in a concentrated and purified form suitable for storage or further utilization. However, this heating process is energy-intensive, about 3 GJ/ton of CO_2 captured are required [14] and the temperature range needed for CO_2 release is typically between 90°C and 130°C and depend on the pressure in the stripper.

Technological advancements and innovations in the field demonstrate that this required amount of energy can be reduced and has already been when compared to the initial post-combustion CO2 capture solutions. However, this reduction has its limits, as illustrated Figure 1.6."

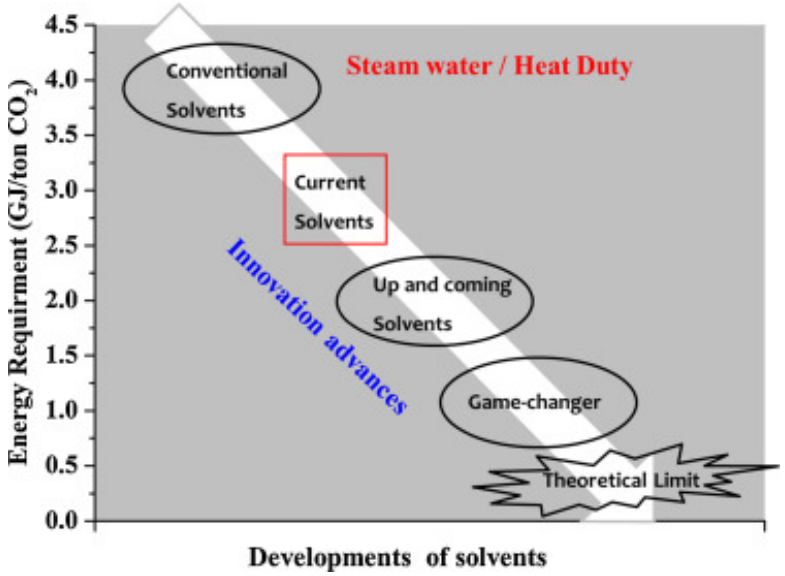

Figure 1.6: Reduction of the process energy requirement [14].

Therefore, to optimize the energy efficiency of the CO_2 capture pilot, it is relevant to explore synergies between research aimed at reducing process energy demands and leveraging established technologies with proven efficacy to provide this energy demand. Among these established technologies lies an interesting and underestimate candidate for CO_2 capture : heat pumps. With its longstanding presence and versatility in various applications, heat pumps offer a promising avenue for enhancing energy efficiency without compromising process performance.

1.4 Structure and objectives of the thesis

1.4.1 Objectives

The primary objective of this thesis is to explore the technical possibilities related to the integration of a high-temperature heat pump into a CO_2 capture pilot project in order to reduce its initial significant energy consumption. The study specifically aims to assess the most effective utilization of the process's various heating and cooling requirements to optimize the integration of the heat pump into the CO_2 capture process. The operational parameters and configurations of the heat pump will be then optimized to enhance its coefficient of performance (COP) and overall energy efficiency. Finally, an initial sizing of the various components of the heat pump, with a primary focus on the required compressors, is provided.

1.4.2 Structure of the Thesis:

This thesis is divided into 7 chapters.

1. **Introduction:** This chapter provides an overview of the context and the different CO_2 capture technologies. The pilot plant project and the associated improvement opportunities are then described, followed by the introduction of the objective of this thesis.

2. **State of the Art:** A comprehensive review of existing literature on heat pump technologies, high-temperature heat pumps (HTHP), and their applications in CO_2 capture processes is realised. This chapter covers the basic principles, performance metrics, cycle improvements, working fluids, and specific components of heat pumps.

3. **Cases Description:** This chapter a detailed description of the initial conditions, including the selection of refrigerants and compressors, and the heat sources available. The two different cases as well as the heat pump configurations studied in this thesis are then described in this chapter.

4. **Modeling:** Explanation of the theoretical models developed for the compressor and heat pump cycles, including the assumptions made and the equations used to simulate their performance are provided in this chapter.

5. **Results:** A presentation and analysis of the simulation results of the first two cases, including model validation, performance evaluation of different heat pump configurations, and optimization outcomes is done. This chapter also includes the energy consumption analysis for full or partial load and the compressors sizing.

6. **Modification of the Process:** Analysis of potential modifications to the CO_2 capture process, such as varying the stripper pressure to enhance heat pump performance and reduce overall energy consumption.

7. **Conclusions and perspectives:** This final chapter presents a conclusion of this work and proposes perspectives for future improvement.

This structured approach ensures a thorough investigation of the integration of high-temperature heat pumps into CO_2 capture processes.

Chapter 2

State of the art

This chapter delves into the current state of heat pump technologies, emphasizing basic principles, performance metrics, cycle improvements, working fluids, and specific components. More attention is then given to high-temperature heat pumps (HTHP), including an industrial overview and recent research developments in this field. Finally, the integration of heat pumps in CO_2 capture processes is discussed, highlighting current innovations and challenges.

2.1 Heat Pumps

In the realm of heat pumps, various operation types exist, as illustrated in Figure 2.1. Firstly, there are open cycles, such as Mechanical Vapor Compression (MVC) and Thermal Vapor Recompression (TVR) cycles. On the other hand, there are closed cycles, among which are absorption heat pumps which employs chemical or thermal reactions to absorb and release heat and finally the compression heat pumps on which this thesis focuses.

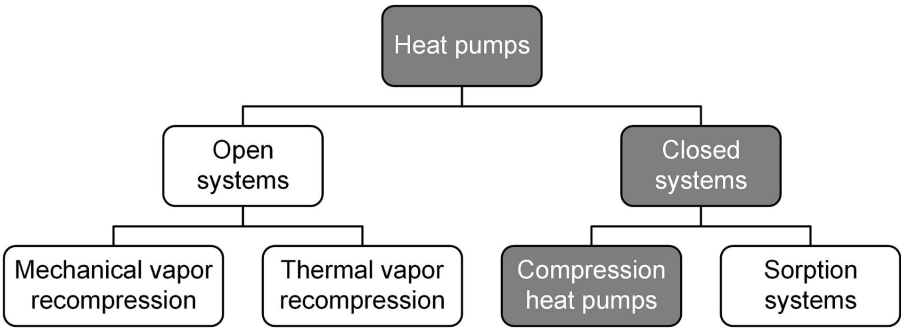

Figure 2.1: Different heat pump operation types[15].

2.1.1 Basic principle

Compression heat pumps are thermodynamic systems used for heating, cooling, and hot water production. Their operation described in Figure 2.2 relies on fundamental thermodynamic principles, leveraging the transfer of heat from a low-temperature environment (the "source") to a high-temperature environment (the "sink") using external work [16]. These can be at constant temperature (Figure 2.2a) or with a temperature glide. (Figure 2.2b).

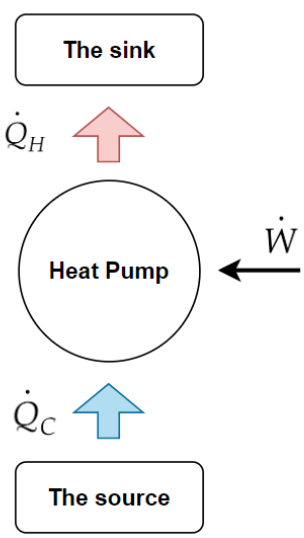

(a) Constant temperature source and sink.

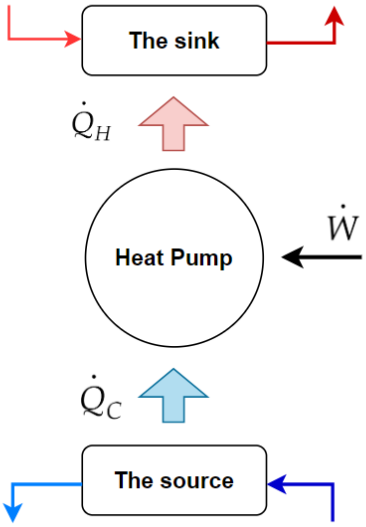

(b) Sources and sink with temperature glide.

Figure 2.2: Heat pump basic principle.

Intuitively, it may seem impossible to transfer heat from a cold body to a hotter body. Heat pumps use mechanical work and two physical properties of the working fluid they use :

1. Firstly, a fluid needs energy to evaporates. This energy, called latent heat of vaporization, is then released when it condenses, thereby releasing heat.
2. Secondly, the evaporation/condensation temperature of a refrigerant increases with pressure. By compressing the fluid, its pressure and temperature increase. Therefore, when the refrigerant condenses at higher pressure, the fluid releases energy at a higher temperature, providing heating power.

The interplay between these two processes, evaporation at low temperature and condensation at higher temperature, forms the thermodynamic cycle that drives the heat pump. The four main steps of the cycle are illustrated in Figure 2.3 and described hereunder :

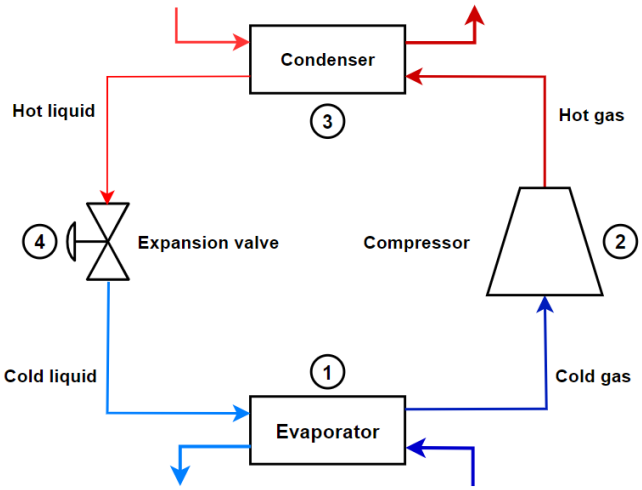

(a) Basic cycle diagram.

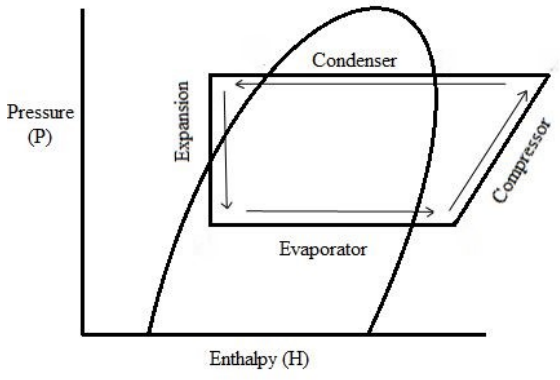

(b) Pressure-enthalpy diagram [17].

Figure 2.3: The four basics steps of a heat pump.

1. **Isothermal evaporation :** The refrigerant, initially at low temperature and pressure, enters the evaporator where it absorbs heat from the low-temperature environment ($\dot{Q}_C$). This heat absorption causes the refrigerant to evaporate, transitioning it from liquid phase to gas phase.

2. **Isentropic compression :** The refrigerant gas is drawn into the compressor and compressed, increasing its pressure and temperature. This process requires an input of energy in the form of mechanical work ($\dot{W}$).

3. **Isothermal condensation :** The compressed refrigerant, now at high temperature and pressure, is directed to the condenser where it releases energy into the high temperature environment ($\dot{Q}_H$). This heat release causes the refrigerant to condense, transitioning it from gas to liquid.

4. **Isenthalpic expansion :** The high-pressure liquid refrigerant passes through the expansion valve, undergoing rapid expansion, which results in a pressure and temperature drop. This process prepares the refrigerant to return to the evaporator to begin the cycle anew.

2.1.2 Performances

To evaluate the maximum efficiency of a heat pump, the Carnot cycle can be used as a theoretical model utilized to assess the highest achievable efficiency when transferring heat between two reservoirs at different temperatures. The Carnot cycle represented in Figure 2.4 consists of four reversible processes : isothermal evaporation, isentropic compression, isothermal condensation, and isentropic expansion.

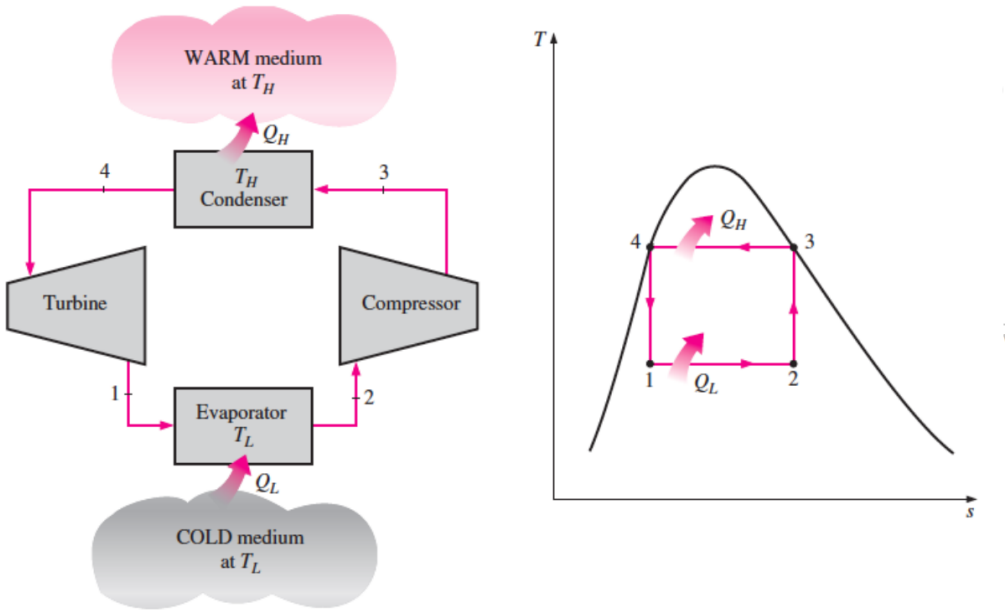

Figure 2.4: Theoretical Carnot's cycle [18].

However, this cycle is not realistic. Indeed, it involves the compression and expansion of a two-phase mixture in an isentropic manner, which is difficult to achieve [18]. The Carnot's cycle is still important for determining the maximum performance that a heat pump can achieve under given source and sink temperature conditions. The coefficient of performances (COP) of that cycle can so be calculated with the following formula :

$$\text{COP}_{Carnot} = \frac{T_{sink}}{T_{sink} - T_{source}} \tag{2.1}$$

Unlike the idealized COP of the Carnot's cycle, the COP of a real heat pump reflects its efficiency under real-world conditions, accounting for irreversibilities (friction losses, ambient losses, ...) and factors such as pressure drop, heat exchanger inefficiencies, fluid properties, ... The COP of the real heat pump is strictly lower than the COP of the Carnot cycle due to these inherent limitations. In general terms, the COP of a heat pump is defined as the ratio of the heat delivered to the sink ($\dot{Q}_H$) to the work input required to achieve that heat transfer ($\dot{W}$). A higher COP signifies that more heat is delivered for a given amount of input energy. Mathematically, it can be expressed as:

$$\text{COP}_{real} = \frac{\dot{Q}_H}{\dot{W}} = \eta_{cycle} \cdot \text{COP}_{Carnot}. \tag{2.2}$$

The parameter η_{cycle} represents the quality factor of the thermodynamic cycle [18]. This factor indicates the extent to which the actual cycle approaches the ideal reversible Carnot cycle. A lower η_{cycle} corresponds to greater irreversibilities within the system, leading to decreased cycle efficiency and suboptimal utilization of available energy. This inefficiency highlights the potential for advancements in system design and operation. In modern heat pumps, this quality factor is usually around 55% [19].

Returning to Equation 2.1, it can be observed that the smaller the difference between T_{sink} and T_{source}, the larger the COP_{Carnot}. This temperature difference is called the temperature lift. Conversely, as the temperature lift increases, both the COP_{Carnot} and consequently the COP_{real} decrease. This effect is double because if the temperature lift increases, the cycle quality factor also η_{cycle} decreases due to higher irreversibilities.

2.1.3 Cycle improvements

As just introduced, the performance of a heat pump will significantly decrease as the temperature lift increases. To maintain it the highest possible, certain elements can be added to the heat pump cycle to enhance its performance. In this subsection, various cycle improvements will be explained, schematized, and compared with the basic cycle using pressure-enthalpy (P-h) and temperature-entropy (T-s) diagrams. These enhancements can then be combined to further improve the cycle, especially when the temperature lift is too high. To facilitate comparisons, Figure 2.5a reminds the basic cycle accompanied by its P-h and T-s diagrams in Figure 2.5b.

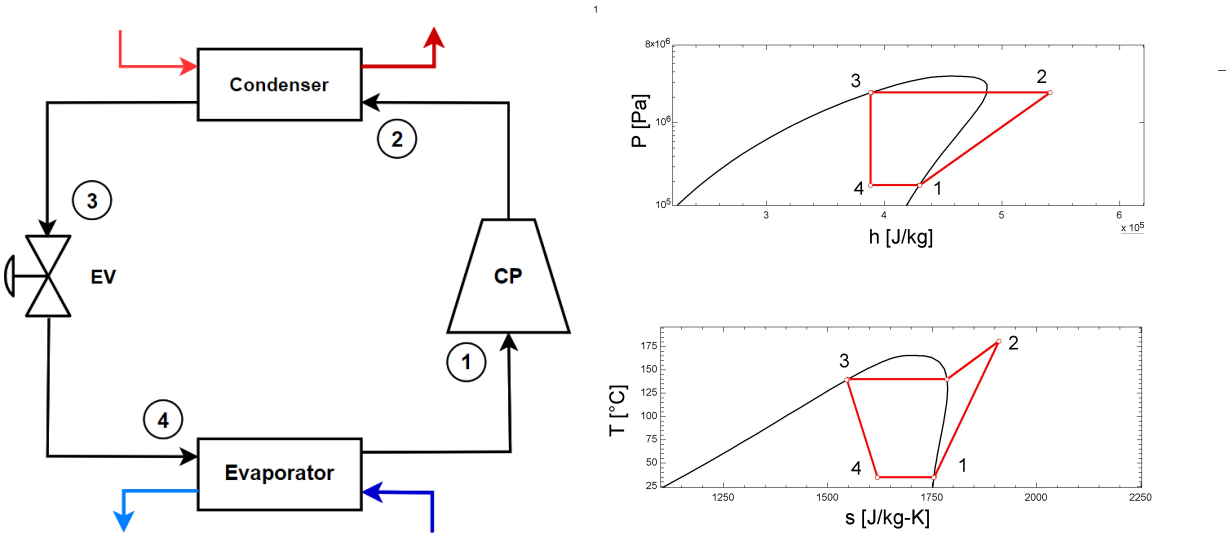

(a) Cycle stages.

(b) P-h (top) and T-s (bottom) diagrams.

Figure 2.5: Basic cycle.

Internal heat exchanger

The first and simplest improvement that can be made to the classic cycle of a heat pump is to add an internal heat exchanger as illustrated in Figure 2.6a . This allows for two things: first, it ensures sub-cooling at the condenser outlet (Figure 2.6b,point 5), which returns the working fluid colder to the evaporator inlet, thereby increasing the quantity of energy that the same mass of refrigerant can absorb at the evaporator [20]. The second effect is to ensure super-heating at the evaporator outlet (Figure 2.6b,point 2), thus ensuring dry compression in the compressor. This superheating is especially necessary in cases where the refrigerant has a saturation curve with a positive slope, requiring more super-heating to avoid wet compression [21].

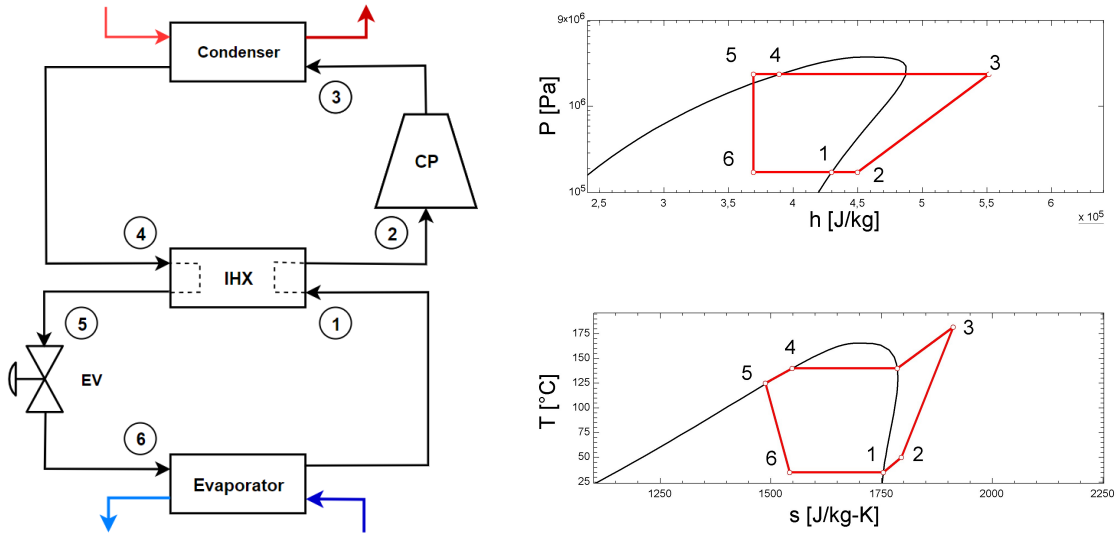

(a) Cycle stages.

(b) P-h (top) and T-s (bottom) diagrams.

Figure 2.6: Internal heat echanger cycle.

Two-stage with economizer

In this context, the economizer is a heat exchanger has two beneficial effect. It allows first to cool the portion of the refrigerant that remains at high pressure (Figure 2.7a, point 5 → point 6) before it is expanded and reaches the evaporator. Secondly, it is used to heat the portion of the refrigerant at medium pressure before mixing it with the refrigerant exiting the low-pressure compressor Figure 2.7a (point 8 to point 9).

This configurations has several positives effects compare to the basic one.

1. High temperature lift means high pressure ratio and therefore lower compressor efficiency. This configuration divides the compression stage into two stages, reducing the pressure ratio for each compressor and increasing their efficiency compared to a single compressor.

2. This injection of refrigerant between the two compressors is beneficial for the high pressure compressor. The injected flow being colder than the flow coming from the first compressor, it cools down the refrigerant before entering the compressor, increasing also its efficiency.

3. Additionally, as the refrigerant mass flow is divided into two parts. The low-pressure compressor will have less refrigerant to compress, decreasing its electricity consumption for the same overall heating capacity, which will also increase the performance of the heat pump.

4. Finally, subcooling at the condenser outlet is also ensured as can be seen on the Pressure-enthalpy diagram in Figure 2.7b (point 6)

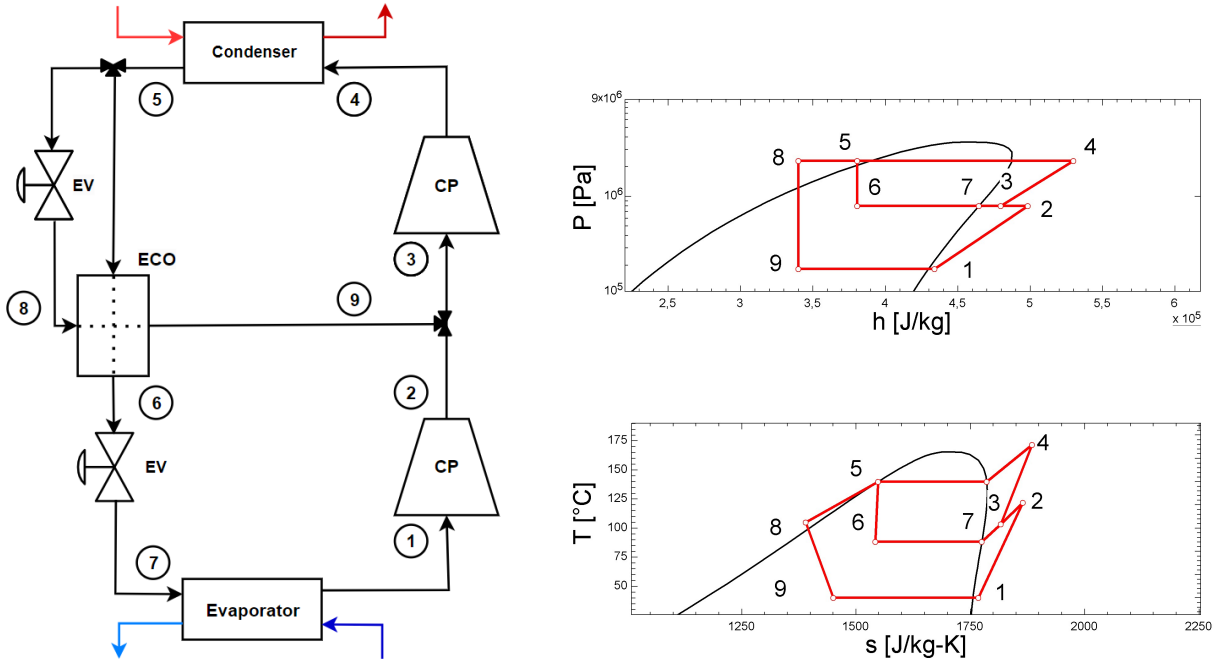

(a) Cycle stages.

(b) P-h (top) and T-s (bottom) diagrams.

Figure 2.7: Two-stage with economizer cycle.

Two-stage with flash tank The flash tank is a separator, it separates the refrigerant into vapor and liquid phases in order to inject the vapor as for the economizer cycle. This configurations present thus the same benefit as the economizer cycle. However, it can be observed in Figure 2.8b (point 3) that the refrigerant remains slightly superheated before entering the compressor. This superheating, necessary to avoid wet compression, depends on the refrigerant used. Additionally, the refrigerant in liquid phase separated by the flash tank, will have a lower enthalpy before entering the evaporator (Figure 2.8b, point 9), thereby increasing its capacity as previously mentioned.

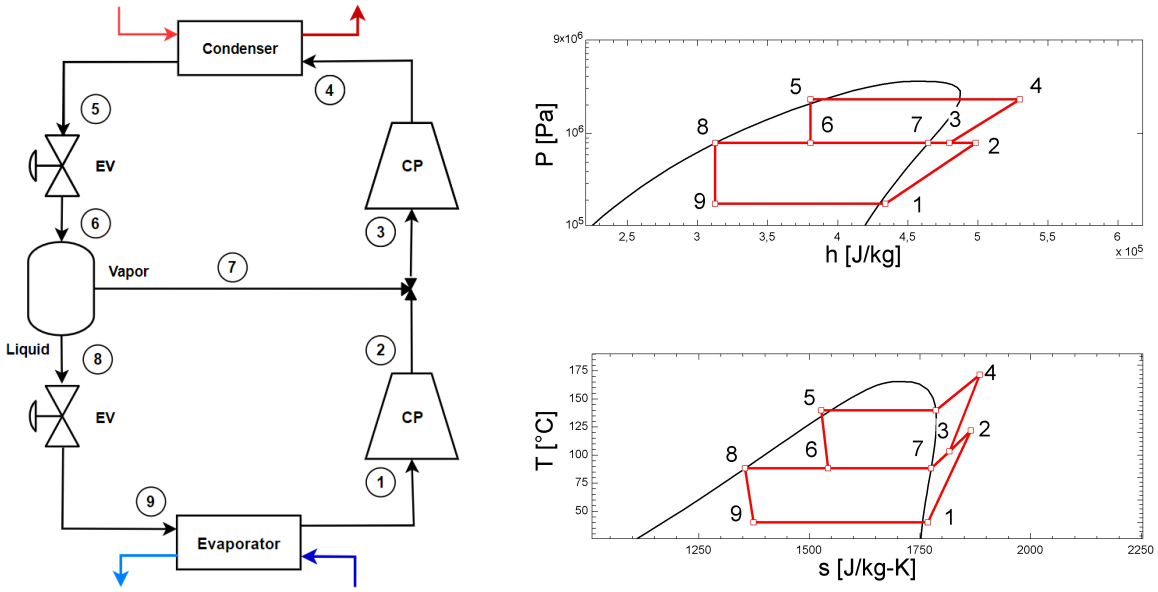

(a) Cycle stages.

(b) P-h (top) and T-s (bottom) diagrams.

Figure 2.8: Two stage with flash tank cycle.

Single stage injection

These two configurations represented in Figure 2.9 share the same advantages as the two-stage vapor injection configurations. However, they are used for lower pressure ratios and temperature lifts that do not require two compressors. Vapor injection is thus done directly into the compressor, which increases its efficiency in the same way as for the two stage configurations and the pressure-enthalpy diagram as well as the temperature-entropy diagram are equivalent to those shown in Figure 2.7b and Figure 2.8b.

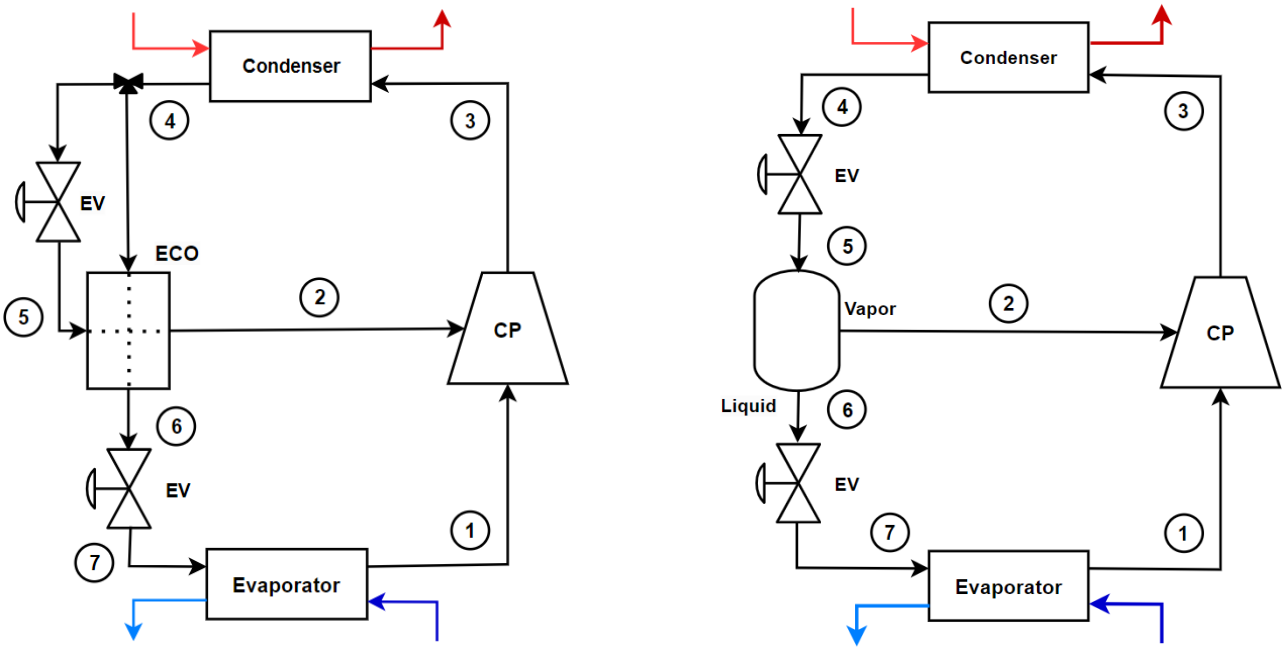

(a) Single stage economizer.

(b) Single stage flash tank.

Figure 2.9: Single stage vapor injection.

Two stage with flash tank and total de-superheating

This configuration is very similar to the simple flash tank configurations, except that in this case, instead of mixing the saturated vapor at the outlet of the low-pressure compressor to cool the fluid, it is the saturated vapor from the flash tank that will directly go to the inlet of the compressor (Figure 2.10a, point 3). The same effects as those mentioned previously are present, but this time the vapor state fluid will not be superheated (Figure 2.10b, point 3). This difference could be a problem for some working fluids, in which case other elements such as an IHX would need to be added to avoid wet compression.

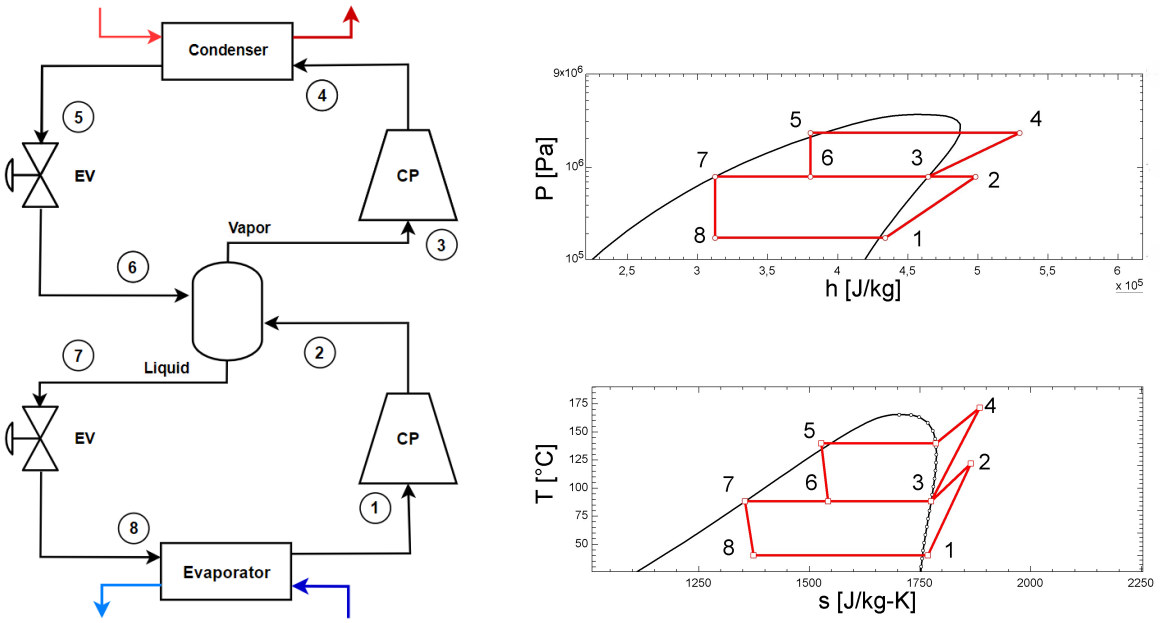

(a) Cycle stages. (b) P-h (top) and T-s (bottom) diagrams.

Figure 2.10: Two-stage with flash tank and total de-superheating cycle.

Cascade

Cascade heat pumps refer to configurations where multiple heat pumps are connected in series. In such setups, the heat available at the condenser of the first heat pump (blue line Figure 2.11b) is used to supply the evaporator of the second heat pump (red line Figure 2.11b). This configuration is employed when the temperature lift becomes too significant, resulting in significant differences in specific volume and pressure [22]. Since the two heat pumps in series are independent, the main advantage of this configuration is the ability to use different working fluids for each heat pump cycle, thus optimizing each stage with the most efficient refrigerant.

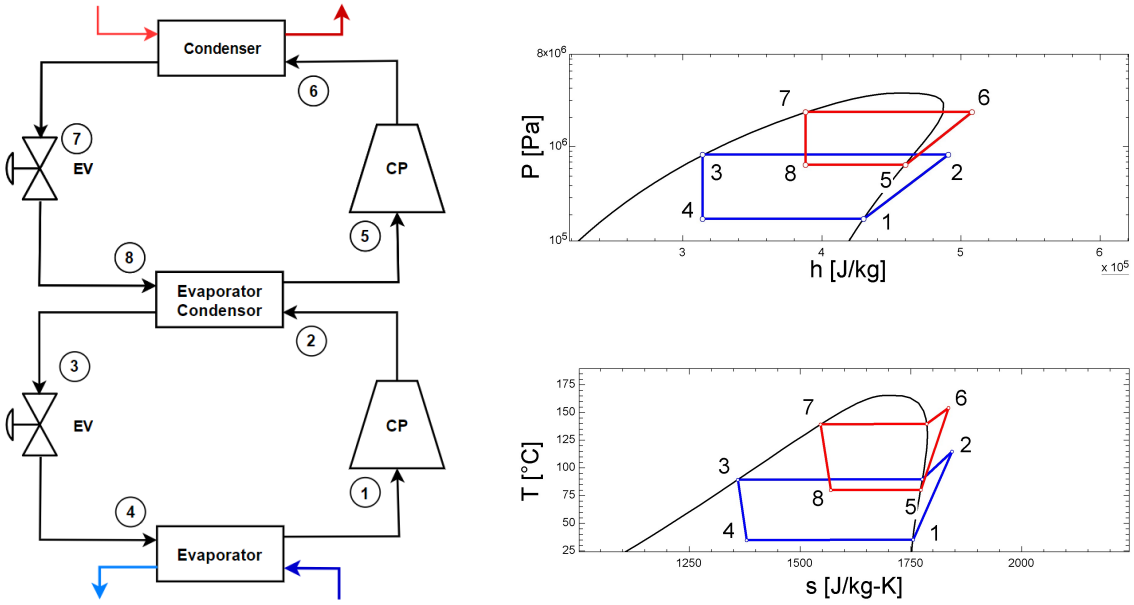

(a) Cycle stages. (b) P-h (top) and T-s (bottom) diagrams.

Figure 2.11: Cascade cycle.

Ejector - transcritical

Unlike subcritical heat pump systems which have just been explained, heat rejection in a transcritical cycle is a cooling process that follows a temperature glide, thereby enhancing the system's performance and heating capacity. However, a transcritical compression cycle exhibits lower thermodynamic performance compared to a subcritical cycle. This is attributed to significant expansion losses during the isenthalpic throttling process, which occurs as the refrigerant transitions from a supercritical to a subcritical state (Figure 2.26b ,point 3 → point 4).

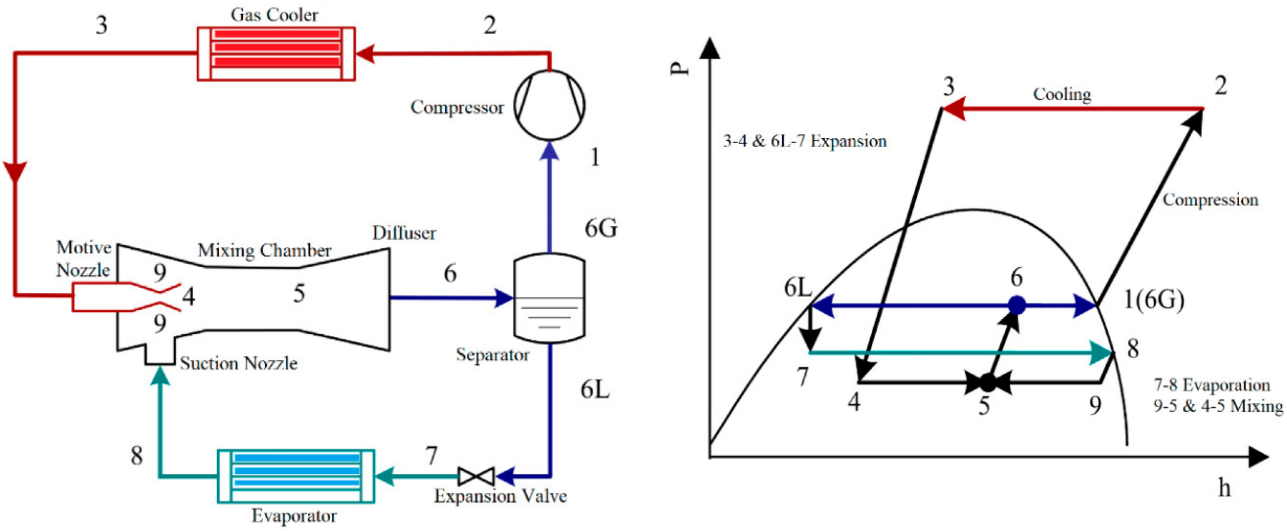

(a) Cycle stages.

(b) Ejector cycle P-h diagram.

Figure 2.12: Transcritical cycle with ejector [23].

An ejector can help reduce losses by recovering a portion of the expansion work loss during the throttling process, thereby enhancing cycle efficiency [24]. This type of cycle is employed in cases of significant temperature lift, especially when there is a considerable difference in temperature glide at the heat sink of the heat pump, such as heating water from 20° to 90°C.

2.1.4 Working fluids - Refrigerant

Characteristics

The choice of working fluid used in a heat pump is crucial. Here are the important characteristics that it must meet :

- *High volumetric heat capacity:* A high volumetric heat capacity allows the fluid to absorb and release a large amount of heat per unit of volume. A smaller volumetric flow rate is thus necessary to achieve the same power and the compressor work is lower.
- *High critical temperature:* The further the heat pump cycle is from the critical temperature, the less refrigerant flow is required at the condenser for a given inlet and outlet temperature. Therefore, it is preferable for the critical temperature to be as high as possible in order to reduce the compressor's workload.
- *Low normal boiling temperature:* If the normal boiling temperature is low, it expands the operating range of the refrigerant. Indeed, if this temperature is above the temperature at the

evaporator, it means that the pressure at the evaporator must be below atmospheric pressure, which is preferable to avoid in a heat pump circuit [22].

- *Low specific volume:* The lower the specific volume of the refrigerant, the smaller the components of the heat pump will be, reducing the costs associated with setting up the cycle.
- *Toxicity and flammability:*

  Heat pumps are not devoid of the risk of leaks, whether during construction or during operation, it is imperative to be aware of the toxic or flammable properties of the fluid used. It is for this purpose that The American Society of Heating, Refrigerating and Air-Conditioning Engineers (ASHRAE) created a reference table, represented in Figure 2.13, to facilitate safety measures.

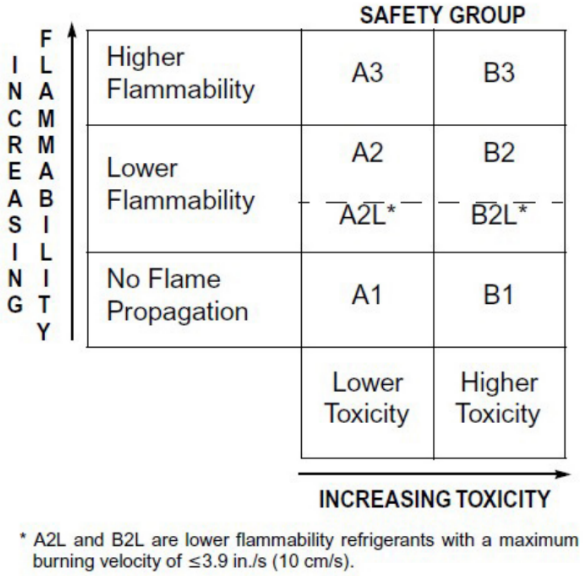

Figure 2.13: Standard 34 tables [25].

- *Availability:* It must be available on the market and at low price
- *Environmental requirements* As discussed in the introduction, it is essential to minimize pollutants as much as possible. Old refrigerants with high ozone depletion potential (ODP) or those with high global warming potential (GWP) are now gradually being replaced with synthetic refrigerants that are more environmentally friendly as well as natural working fluids.

Types of refrigerant

Chlorofluorocarbons (CFCs) are chemical compounds that were once widely used as refrigerants. However, their use has been banned due to their contribution to ozone depletion and huge global warming potential. Hydrochlorofluorocarbons (HCFCs) are less harmful alternatives to CFCs, but they are also gradually being phased out due to their very high GWP by the following refrigerants [26], [27], [28],[29]:

1) **Hydrofluorocarbons (HFCs):**
   - Fluorinated organic compounds containing hydrogen and carbon atoms.
   - Non-halogenated refrigerants, meaning they do not contribute to ozone depletion, but they have a high global warming potential (GWP)

- Widely used for a long time but is gradually phasing out and being replaced by alternatives with much lower Global Warming Potential (GWP)

2) **Hydrofluoroolefins (HFOs):**

- Class of organic compounds derived from hydrocarbons by substituting hydrogen functional groups with fluorine atoms.
- They have been developed as alternatives to HFCs due to their reduced GWP and lesser impact on climate change.
- Exhibit similar thermodynamic properties to HFCs and are widely used in modern refrigeration and air conditioning applications.

3) **Hydrochlorofluoroolefins (HCFOs):**

- Category of organic compounds containing chlorine, fluorine, hydrogen, and oxygen.
- Exhibit similar thermodynamic properties to HFCs but have lower GWPs.

4) **Hydrocarbons (HCs):**

- Organic compounds consisting solely of carbon and hydrogen atoms.
- They are used as refrigerants due to their low environmental impact, as they contain no chlorine or fluorine and have a low GWP but they are flammable.

5) **Natural Refrigerants:**

- Natural refrigerants are substances that occur naturally in the environment and are used as refrigerants.
- They include gases such as carbon dioxide (CO_2) and ammonia (NH_3), which are environmentally friendly due to their low GWP and ODP.

However per- and polyfluoroalkyl substances (PFAS) pose a contemporary threat to humanity, as highlighted by recent research [30]. PFAS are categorized as "persistent chemicals" due to their inherent chemical stability, resulting in their widespread presence as environmental pollutants [31]. Despite being produced for over 70 years, public awareness of PFAS remains relatively recent. The latest proposal from the European Chemicals Agency (ECHA) regarding PFAS regulation suggests that many current alternative refrigerants HFC/HFO could face prohibition [32].

2.1.5 Compressor

The essential component that makes the heat pump cycle possible is the compressor. It increases the pressure, the temperature, and thus the enthalpy of the working fluid. The multiple types of compressors available are represented in Figure 2.14, so it is important to choose the most suitable one for each situation.

First, the **dynamic compressor**, also known as a flow compressor or centrifugal compressor. This type of compressor increases the kinetic energy of the fluid which is then converted into pressure. They are often used in applications requiring high volumetric flow rate with a compact design and quiet operation, but may require sophisticated control mechanisms to maintain constant pressure. Among them are ejectors, axial compressors, and radial compressors.

Secondly, the **reciprocating compressor** compresses gas using pistons that move back and forth inside cylinders. Gas is drawn in during the intake stroke, compressed during the compression stroke, and expelled during the exhaust stroke, creating a continuous flow of compressed gas.

Finally the **rotating compressor** uses rotating elements, such as screws, vanes, or impellers, to compress gas. As the rotating elements spin, they draw in gas and then compress it before expelling it at a higher pressure. This process is continuous, allowing for a steady flow of compressed gas.

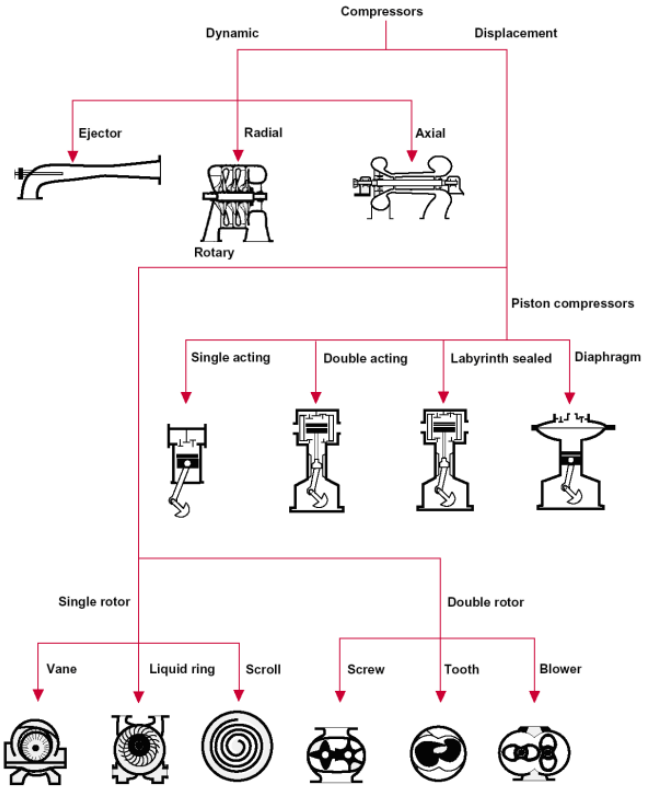

Figure 2.14: Compressors types [18].

In general, a compressor is chosen for a heat pump based on its operating range, i.e., its heating capacity (and therefore its volumetric flow rate). Figure 2.15 illustrates the operating ranges of the different types of compressors

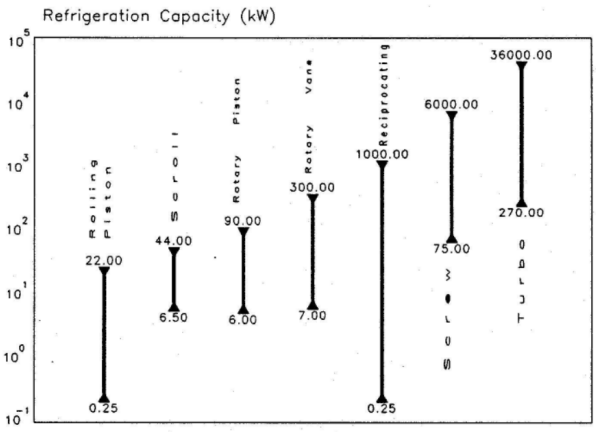

Figure 2.15: Compressors operating range [18].

2.1.6 Other components

Expansion valve

After transferring its accumulated energy in the condenser, the working fluid must be brought back to low pressure before entering the evaporator to restart the cycle. Recovering the energy it contains at high pressure by bringing it back to low pressure is technically feasible but remains complicated. As introduced at the beginning of this section, recovering energy from a two-phase expansion remains difficult and costly. Additionally, the available energy is relatively low. For these reasons, throttling valves are predominantly installed in heat pump cycles, involving irreversibilities.

Heat exchangers

Among the various types of heat exchangers, the most well-known and commonly used are the shell and tube, coaxial, plate, and spiral plate heat exchangers. Figure 2.16 summarize their different characteristics. These can be used as internal heat exchangers, economizers, condensers, and evaporators. Modeling and further details regarding their performance will be elaborated in Chapter 3

	Shell-and-tube	Co-axial	Plate	Spiral plate
Max Temperature	1100°C	500 °C	260°C	500°C
Max Pressure	1000 bar	40 bar	30 bar	250 bar
Compactness	Voluminous (approx. 100 m^2/m^3)	Voluminous	Very compact (120- 660 m^2/m^3)	Slightly more compact than shell and tube
Tightness	All these types of heat exchanger can be designed tight			

Figure 2.16: Heat exchangers operating range [18].

2.2 High Temperature Heat Pump

The heat requirements of the CO2 capture process correspond to what are called high-temperature heat pumps and refers to heat pumps with a sink temperature above 100°C in this study. The solutions that are already commercialized will be highlighted, whether it be their configurations, refrigerants, or the compressor used. Furthermore, the various research projects that have already been conducted will be grouped together, including both simulations and experiments.

2.2.1 Industry overview

The interest for high-temperature heat pumps is undergoing substantial expansion. Indeed, a wide array of potential uses across diverse sectors exist [33]. As a result, several companies have already developed and commercialized various high-temperature heat pumps, as shown in Figure 2.17 . Details regarding the refrigerant, compressor, and configuration used are specified, as well as the different temperatures of the heat sources, sinks, temperature lift and COP. Configurations vary, ranging from simple models using a single compressor to enhanced versions of the cycle described in the previous section.

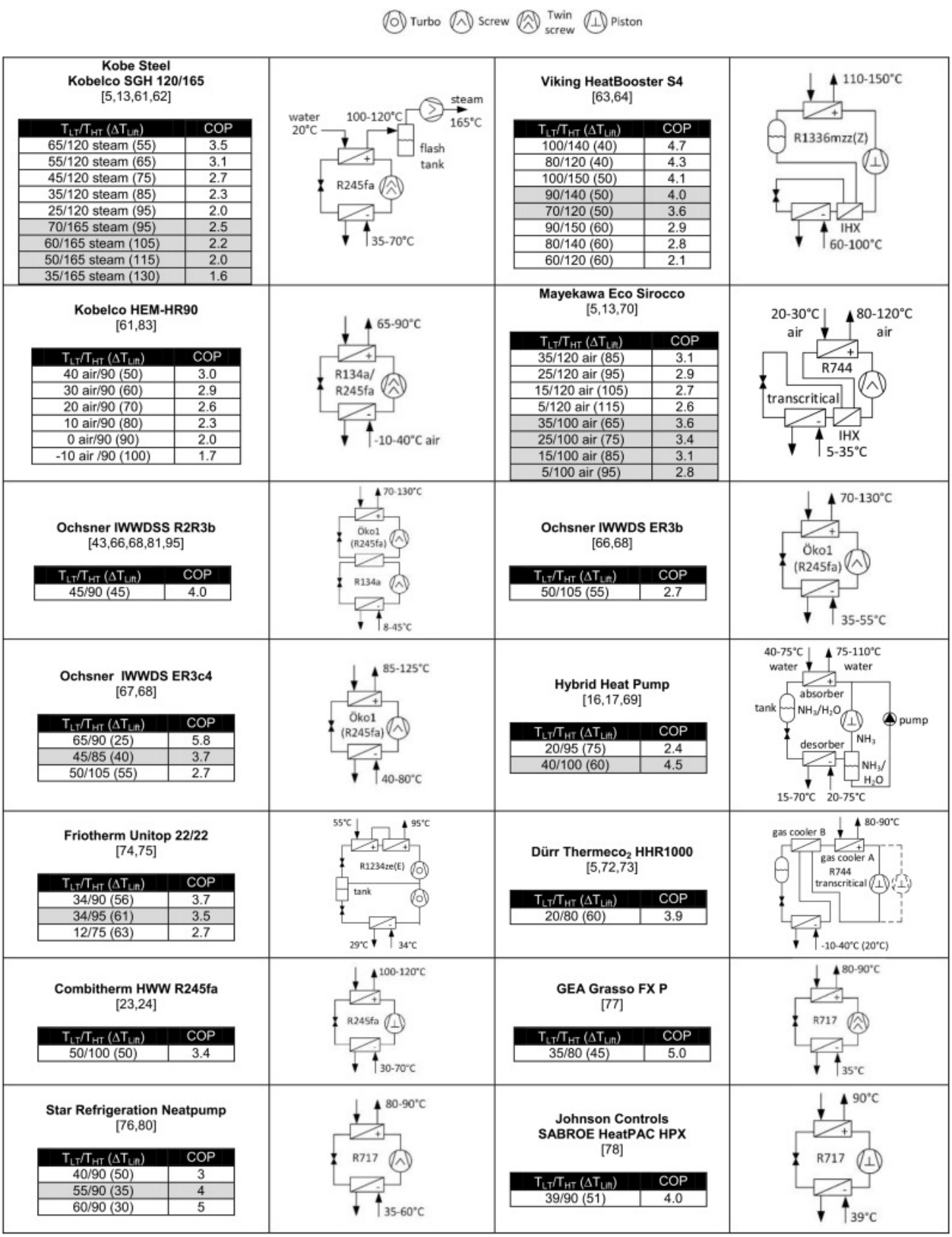

Figure 2.17: Industrial overview [15].

2.2.2 HTHP research project

In addition to these commercially available heat pumps, many research projects are underway and are included in Figure 2.18. Some of these research projects use even more advanced heat pump configurations, combining multiple possible enhancements to optimize the COP in the case of high temperature lift.

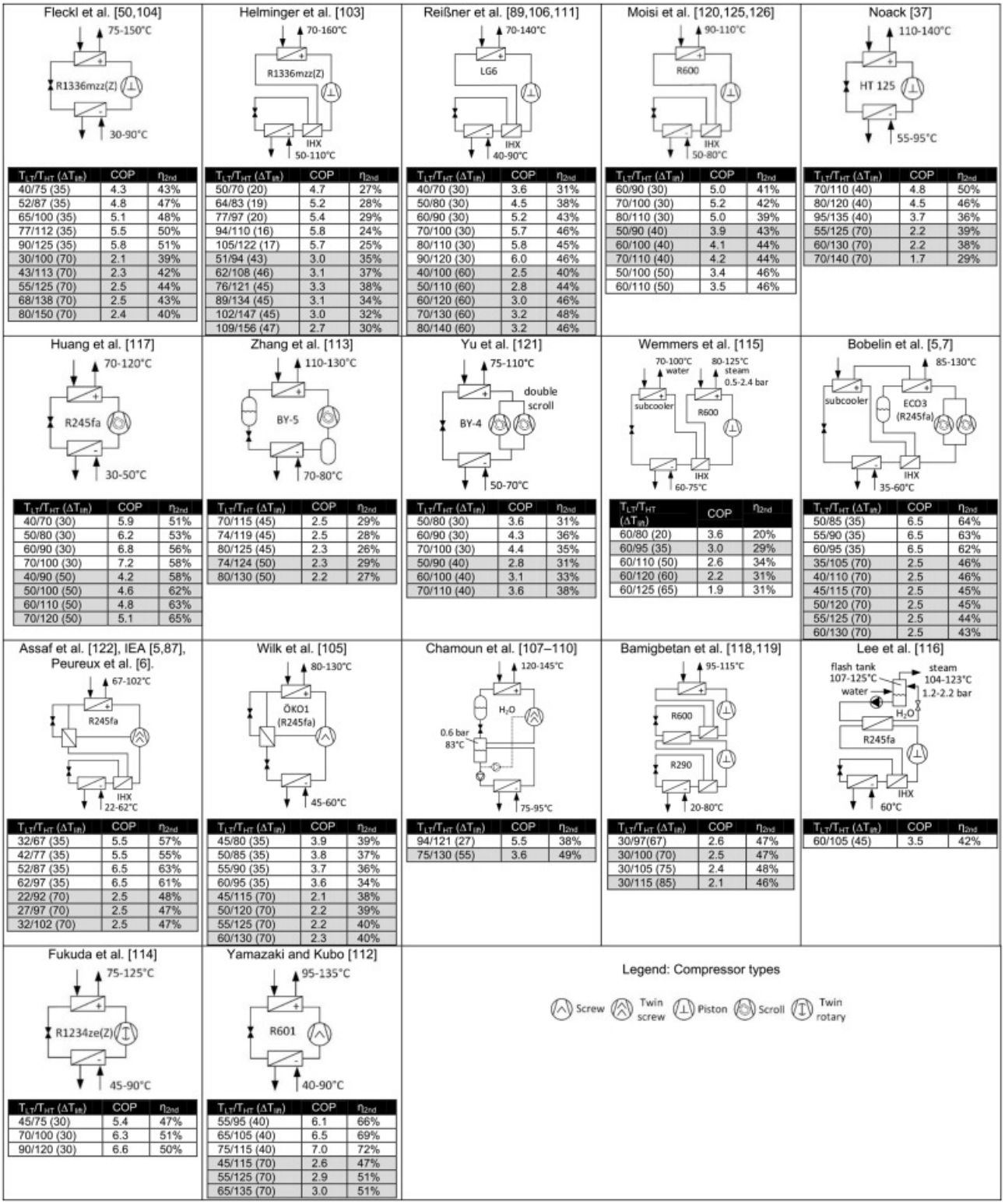

T_{LT}/T_{HT} (ΔT_{lift})	COP	η_{2nd}
40/75 (35)	4.3	43%
52/87 (35)	4.8	47%
65/100 (35)	5.1	48%
77/112 (35)	5.5	50%
90/125 (35)	5.8	51%
30/100 (70)	2.1	39%
43/113 (70)	2.3	42%
55/125 (70)	2.5	44%
68/138 (70)	2.5	43%
80/150 (70)	2.4	40%

T_{LT}/T_{HT} (ΔT_{lift})	COP	η_{2nd}
50/70 (20)	4.7	27%
64/83 (19)	5.2	28%
77/97 (20)	5.4	29%
94/110 (16)	5.8	24%
105/122 (17)	5.7	25%
51/94 (43)	3.0	35%
62/108 (46)	3.1	37%
76/121 (45)	3.3	38%
89/134 (45)	3.1	34%
102/147 (45)	3.0	32%
109/156 (47)	2.7	30%

T_{LT}/T_{HT} (ΔT_{lift})	COP	η_{2nd}
40/70 (30)	3.6	31%
50/80 (30)	4.5	38%
60/90 (30)	5.2	43%
70/100 (30)	5.7	46%
80/110 (30)	5.8	45%
90/120 (30)	6.0	46%
40/100 (60)	2.5	40%
50/110 (60)	2.8	44%
60/120 (60)	3.0	46%
70/130 (60)	3.2	48%
80/140 (60)	3.2	46%

T_{LT}/T_{HT} (ΔT_{lift})	COP	η_{2nd}
60/90 (30)	5.0	41%
70/100 (30)	5.2	42%
80/110 (30)	5.0	39%
50/90 (40)	3.9	43%
60/100 (40)	4.1	44%
70/110 (40)	4.2	44%
50/100 (50)	3.4	46%
60/110 (50)	3.5	46%

T_{LT}/T_{HT} (ΔT_{lift})	COP	η_{2nd}
70/110 (40)	4.8	50%
80/120 (40)	4.5	46%
95/135 (40)	3.7	36%
55/125 (70)	2.2	39%
60/130 (70)	2.2	38%
70/140 (70)	1.7	29%

T_{LT}/T_{HT} (ΔT_{lift})	COP	η_{2nd}
40/70 (30)	5.9	51%
50/80 (30)	6.2	53%
60/90 (30)	6.8	56%
70/100 (30)	7.2	58%
40/90 (50)	4.2	58%
50/100 (50)	4.6	62%
60/110 (50)	4.8	63%
70/120 (50)	5.1	65%

T_{LT}/T_{HT} (ΔT_{lift})	COP	η_{2nd}
70/115 (45)	2.5	29%
74/119 (45)	2.5	28%
80/125 (45)	2.3	26%
74/124 (50)	2.3	29%
80/130 (50)	2.2	27%

T_{LT}/T_{HT} (ΔT_{lift})	COP	η_{2nd}
50/80 (30)	3.6	31%
60/90 (30)	4.3	36%
70/100 (30)	4.4	35%
50/90 (40)	2.8	31%
60/100 (40)	3.1	33%
70/110 (40)	3.6	38%

T_{LT}/T_{HT} (ΔT_{lift})	COP	η_{2nd}
60/80 (20)	3.6	20%
60/95 (35)	3.0	29%
60/110 (50)	2.6	34%
60/120 (60)	2.2	31%
60/125 (65)	1.9	31%

T_{LT}/T_{HT} (ΔT_{lift})	COP	η_{2nd}
50/85 (35)	6.5	64%
55/90 (35)	6.5	63%
60/95 (35)	6.5	62%
35/105 (70)	2.5	46%
40/110 (70)	2.5	46%
45/115 (70)	2.5	45%
50/120 (70)	2.5	45%
55/125 (70)	2.5	44%
60/130 (70)	2.5	43%

T_{LT}/T_{HT} (ΔT_{lift})	COP	η_{2nd}
32/67 (35)	5.5	57%
42/77 (35)	5.5	55%
52/87 (35)	6.5	63%
62/97 (35)	6.5	61%
22/92 (70)	2.5	48%
27/97 (70)	2.5	47%
32/102 (70)	2.5	47%

T_{LT}/T_{HT} (ΔT_{lift})	COP	η_{2nd}
45/80 (35)	3.9	39%
50/85 (35)	3.8	37%
55/90 (35)	3.7	36%
60/95 (35)	3.6	34%
45/115 (70)	2.1	38%
50/120 (70)	2.2	39%
55/125 (70)	2.2	40%
60/130 (70)	2.3	40%

T_{LT}/T_{HT} (ΔT_{lift})	COP	η_{2nd}
94/121 (27)	5.5	38%
75/130 (55)	3.6	49%

T_{LT}/T_{HT} (ΔT_{lift})	COP	η_{2nd}
30/97(67)	2.6	47%
30/100 (70)	2.5	47%
30/105 (75)	2.4	48%
30/115 (85)	2.1	46%

T_{LT}/T_{HT} (ΔT_{lift})	COP	η_{2nd}
60/105 (45)	3.5	42%

T_{LT}/T_{HT} (ΔT_{lift})	COP	η_{2nd}
45/75 (30)	5.4	47%
70/100 (30)	6.3	51%
90/120 (30)	6.6	50%

T_{LT}/T_{HT} (ΔT_{lift})	COP	η_{2nd}
55/95 (40)	6.1	66%
65/105 (40)	6.5	69%
75/115 (40)	7.0	72%
45/115 (70)	2.6	47%
55/125 (70)	2.9	51%
65/135 (70)	3.0	51%

Figure 2.18: Research project overview.

2.2.3 Configurations comparison

Some research compare differents configurations for different temperature lifts to find the best combinaison. First, [34] delves into the energy efficiency of five distinct system configurations designed for high-temperature heat pumps, employing low Global Warming Potential (GWP) alternatives to HFC-245fa. They investigates both single-stage and two-stage cycles, with and without internal heat exchangers (IHX) positioned differently, while considering the optimal intermediate pressure for each setup. For applications necessitating moderate to high temperatures and low temperature lifts, a single-stage cycle incorporating IHX demonstrates notable COP enhancement. In scenarios requiring higher temperature lifts, a two-stage cycle featuring IHX emerges as the configuration with the most favorable energy performance.

[35] compare the theoretical performance of one and two-stage heat pump cycles with internal heat exchanger, economizer, flash tank and cascade configuration at different temperature levels. They conclude by recommending the incorporation of an internal heat exchanger to ensure dry compression, along with a two-stage configuration for high temperature lift and a cascade heat pump for temperature lifts exceeding 70K.

Another study evaluates the efficiency of a vapor-injection scroll compressor (SCVI) versus a two-stage scroll compressor (TSSC) under high pressure ratios with R290 refrigerant [36]. Semi-empirical models, fine-tuned with experimental data, are applied. The findings indicate that the SCVI is more efficient for pressure ratios below 5, whereas the TSSC excels at higher ratios, achieving a lower discharge temperature. The TSSC's heating capacity can be enhanced by 7% compared to the SCVI by adjusting the swept volume of the high-pressure compressor, with minimal effect on COP and discharge temperature.

Furthermore [37] compare eight innovative cycle designs alongside nine refrigerants with low global warming potential (GWP) across energetic, economic, and environmental criteria. The aim is to identify the most suitable combination for various high-temperature, high-pressure (HTHP) applications. Initially, a range of single-stage and two-stage compression cycles are proposed, each incorporating different elements such as ejectors, economizers, parallel compressors, flash tanks, and additional evaporators and condensers. Additionally, all configurations feature an internal heat exchanger (IHX). The results indicate that a two-stage with flash tank/IHX, a two stage with economizer/IHX and a two cascade/IHX becomes the most appropriates configurations for high temperature lifts (60 K and above). In contrast, single-stage cycles with economizer, parallel compression and IHX are suitable for low temperature lifts (50 K and below).

Moreover, [38] conducted a study on six different cycles, among which the two-stage flash tank and the two-stage flash tank with complete desuperheating stood out. These two configurations demonstrated significantly higher COP and exergetic efficiency, as well as a shorter payback period. Finally, a three-stage compression cycle is investigated by [39], comparing single, double, and triple-stage heat pumps. Their findings reveal a non-linear but significant enhancement in both COP and exergetic efficiency.

2.2.4 Refrigerants

To easily visualize the different refrigerants that meet the important characteristics mentioned in the previous section, the Annex 58's team, part of the IEA's HPTTCP (Heat Pumping Technologies Technology Collaboration Programme) [21], has grouped them into two tables. The first table Figure 2.19 summarizes the various important characteristics, and the second, Figure 2.20, illustrates the possibilities of using each fluid based on the required source and sink temperatures, assuming a temperature difference of 15K between the critical temperature and the condensation temperature, in order to avoid entering the transcritical region.

Type	Working fluid	Description	T_{crit} (°C)	p_{crit} (bar)	ODP (-)	GWP (-)	SG
Natural	R-718	Water	373.9	220.6	0	0	A1
	R-717	Ammonia	132.3	113.3	0	0	B2L
	R-744	Carbon dioxide	31.0	73.8	0	1	A1
HC	R-601	n-Pentane	196.6	33.7	0	5	A3
	R-601a	Isopentane	187.8	33.8	0	4	A3
	R-600	n-Butane	152.0	38.0	0	4	A3
	R-600a	Isobutane	134.7	36.3	0	3	A3
	R-290	Propane	96.7	42.5	0	3	A3
HFO	R-1336mzz(Z)	1,1,1,4,4,4-Hexafluoro-2-butene	171.3	29.0	0	2	A1
	R-1234ze(Z)	cis-1,3,3,3-Tetrafluoro-1-propene	150.1	35.3	0	<1	A2L
	R-1336mzz(E)	trans-1,1,1,4,4,4,-Hexafluoro-2-butene	130.4	27.8	0	18	A1
	R-1234ze(E)	trans-1,3,3,3-Tetrafluoro-1-propene	109.4	36.4	0	<1	A2L
	R-1234yf	2,3,3,3-Tetrafluoro-1-propene	94.7	33.8	0	<1	A2L
HCFO	R-1233zd(E)	1-chloro-3,3,3-Trifluoro-propene	166.5	36.2	0.00034	1	A1
	R-1224yd(Z)	1-chloro-2,3,3,3-Tetrafluoro-propene	155.5	33.3	0.00012	<1	A1
HFC	R-365mfc	1,1,1,3,3-Pentafluorobutane	186.9	32.7	0	804	A2
	R-245fa	1,1,2,2,3-Pentafluoropropane	154.0	36.5	0	858	B1
	R-134a	1,1,1,2-Tetrafluoroethane	101.1	40.6	0	1'300	A1

Figure 2.19: Available and suitable refrigerant [21].

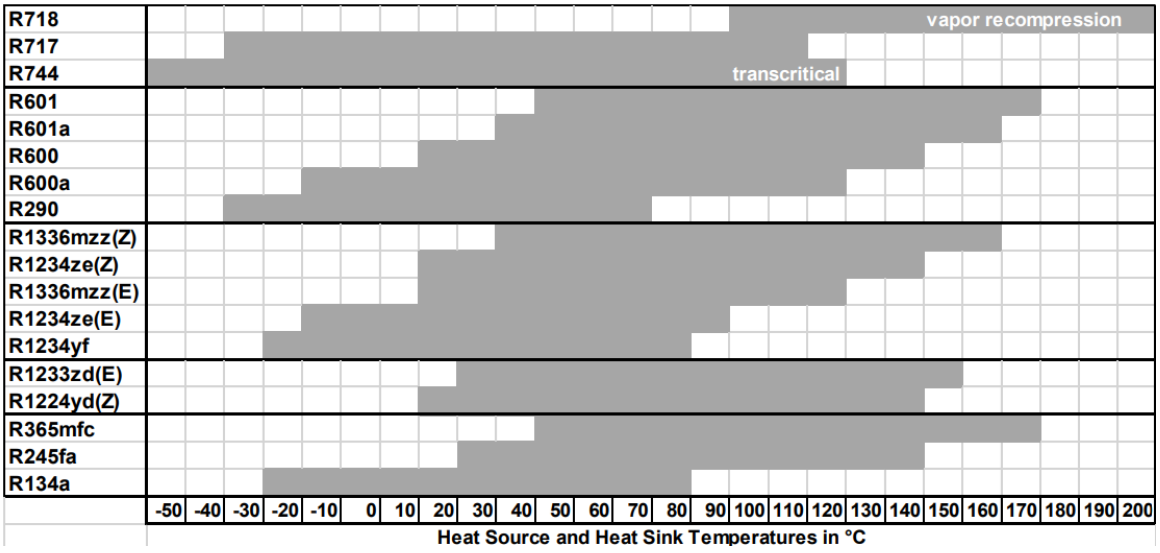

Figure 2.20: Temperature range [21].

Although these refrigerants are all available and suitable for high-temperature heat pumps, they each possess unique characteristics. Therefore, it is important to study which refrigerants are best suited, which ones yield the highest COP based on the chosen heat pump configuration, the best efficiency, and the highest volumetric heating capacity. Hence, numerous studies have been undertaken, employing either theoretical simulations or experimental approaches, to compare these various working fluids.

Initially, the thermodynamic attributes of the low GWP refrigerants R-1234ze(E) and R-1234ze(Z) were comprehensively assessed by [40]. Through a combination of thermodynamic analysis, numerical simulations, and experimental validation, the study revealed that the theoretical coefficients of performance (COP) reach their maximum values when the condensation temperature is approximately 20 K below the critical temperatures for each refrigerant.

Following that, [41] delved into simulating a high-temperature heat pump (HTHP) cascade system employing internal heat exchangers (IHXs) and utilizing low GWP refrigerants in both the high-stage

(HS) and low-stage (LS) cycles. The HS cycle featured R-1233zd(E), R-1336mzz(Z), R-1224yd(Z), and pentane, while the LS cycle included R-1234yf, R-1234ze(E), butane, isobutane, and propane. Their findings revealed that butane and isobutane emerged as the most favorable LS working fluids in terms of coefficient of performance (COP). Moreover, the highest system performance was achieved with pentane and HFO-1336mzz(Z) in the HS cycle. Comparatively, a marginal COP enhancement was observed using R-1233zd(E) and R-1224yd(Z) when compared to third-generation refrigerants such as R-245fa and R-134a.

[42] theoretically investigates the environmentally friendly R-1336mzz(Z) and R-1234ze(Z), as well as the R-1233zd(E) and R-1224yd(Z), comparing their coefficient of performance (COP) and volumetric heating capacity (VHC) with the HFC refrigerants R-365mfc and R-245fa at various condensation temperatures and temperature lifts. The theoritical simulation shows that a trade-off between performance (COP) and volumetric heating capacity (VHC) must be done and it is confirmed by [43]. R-1336mzz(Z) was found to be the next drop-in replacement for R-365mfc. The performance figures of R-1224yd(Z), R-1234ze(Z), and R-1233zd(E) were closer to those of R-245fa.

They proceeded with experimental testing of R-1233zd(E) and R-1336mzz(Z) [44]. Performance data were gathered across temperature lifts of 30, 50, and 70 K (40 to 80°C for the heat source, 80 to 150°C for the heat sink). Findings revealed that for a evaporation temperature of 60°C and condensation temperature of 110°C, the COP for R-1233zd(E) stood at 2.8 for the basic cycle and increased to 3.1 with IHX integration. Meanwhile, R-1336mzz(Z) yielded COP values of 2.4 and 3.0, respectively. As temperatures rose, the differences in COP between R-1336mzz(Z) and R-1233zd(E) fell within the measurement uncertainty. Furthermore, R-1336mzz(Z) demonstrated the potential for higher condensing temperatures due to its elevated critical temperature.

[45] add the hydrocarbons R-600, R-600a, R-601 and R-601a to the theoretical analysis and comparison. Among them, R600 and R-1233zd(E) showed the highest potential for immediate future implementation in HTHPs. R-1233zd(E) exhibits a high COP and favorable low auto-ignition temperature (A1 ASHRAE classification).

[46] confirmed the previous results and add an analysis of Total Equivalent Warming Impact (TEWI) to assess the environmental impact of each refrigerant. The TEWI analysis reveals a substantial reduction in equivalent CO_2 emissions for each low GWP alternative. Among them, R-1233zd(E) exhibits the most significant reduction in all simulation cases, followed by R-1224yd(Z) and R-1336mzz(Z).

[47] proposed to include R-718 in the comparison. They first evaluated it theoretically against hydrocarbons (R-600 and R-601), HFOs (R-1234ze(Z), R-1336mzz(Z)), and HFCs (R-245fa). Simulations revealed that R-718 exhibited the best system performance and Carnot efficiency. Subsequently, the experimental comparison between R-718 and R-1336mzz(Z)/R-600/R-245fa demonstrated that R-718 had unique advantages in HTHP applications. The only issue lies in its high normal boiling temperature, requiring a decrease below atmospheric pressure if the source temperature is below 100°C.

More recently, [48] revisited the working fluids included in the ANSI/ASHRAE Standard 34 since 2015, such as R-1130(E), R-1336mzz(Z), R-1336mzz(E), R-1233zd(E), R-1224yd(Z), R-13I1, and R-1132a. Additionally, they examined other molecules identified in recent studies but not yet added to that standard, including R-1123, R-1243zf, R-1225ye(Z), R-1132(E), R-1252ye, R-1261ze, and R-1141. The thermodynamic characteristics of R-1233zd(E) and R-1224yd(Z) were thoroughly investigated, confirming their suitability for high-temperature heat pump (HTHP) and Organic Rankine Cycle (ORC) systems through experimental validation. R-1336mzz(Z), R-1336mzz(E), and R-1132a were also identified as promising candidates for HTHP applications.

2.3 Heat pumps and CO_2 capture

As introduced in chapter 1, one of the main drawbacks of the post-combustion CO_2 capture process based on absorption/desorption using amine is the high heating demand at the regeneration column. Heat pumps are a proven and accessible technology but only a few research have integrated a heat pump into the CO_2 capture process. This is due to the relatively high temperature (90°C-130°C) required for the stripper. However, high-temperature heat pumps are currently in full development, as explained previously. Additionally, the CO_2 capture process by post-combustion using amines has several cooling demands that could be used as a heat source for a heat pump circuit. Therefore, integrating high temperature heat pump to this carbon capture process is becoming increasly attractive. Here is a summary of the previous study on this topic.

Initially, [49] focused on optimizing heat supply for the capture process in terms of cost-effectiveness. They evaluated five distinct heat supply options using an energy market scenario tool alongside variations in specific heat demand (reboiler duty). Among these options were three standalone choices (natural gas combined cycle, natural gas boiler, and biomass boiler) and two options involving excess heat with heat pump (utilization of current excess heat and optimal utilization of excess heat, Figure 2.21). The most favorable alternatives were those leveraging excess heat in conjunction with a heat pump. Given the typically high process integration potential within the process industry and anticipating substantial future CO_2 charges, these options hold potential for profitability.

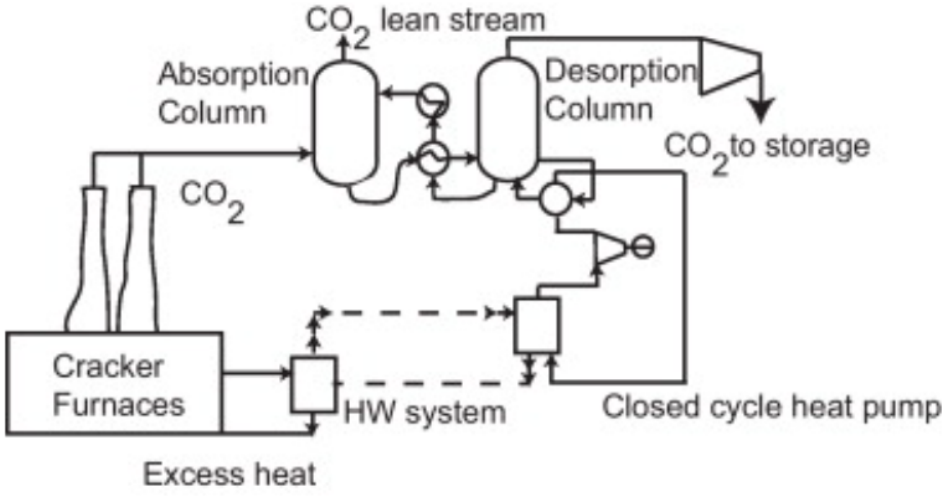

Figure 2.21: Use of excess heat from steam cracker plant with heat pump [49].

Several years later, [50] explored the possibility of integrating a heat pump directly into the process through pinch analysis. They concluded that the most effective approach would be to integrate a heat pump across the pinch point. However, they deemed this challenging, if not impossible, as high-temperature heat pumps were not yet widely popular, and the heat demand of the regenerator exceeded what heat pumps could provide at that time. At the same time, seven configurations of heat pumps integrated with the CCS plant were meticulously evaluated and compared by [51] against the base case of steam utilization from the power plant. The proposed heat pump design represented Figure 2.22 harnesses the various cooling demands of the system to provide heat to the evaporator of the heat pump. Additionally, the study explored the use of expanders to recover expansion losses. Furthermore, a cascade heat pump configuration was devised, enabling the utilization of water in the top cycle. Another innovative concept involved the development of a dual-evaporator heat pump, enabling solvent regeneration, CO_2 liquefaction, and process cooling within a single unit. Incorporating heat pump cooling and heating capacities into efficiency calculations revealed a remarkable efficiency improvement of up to 13,6%.

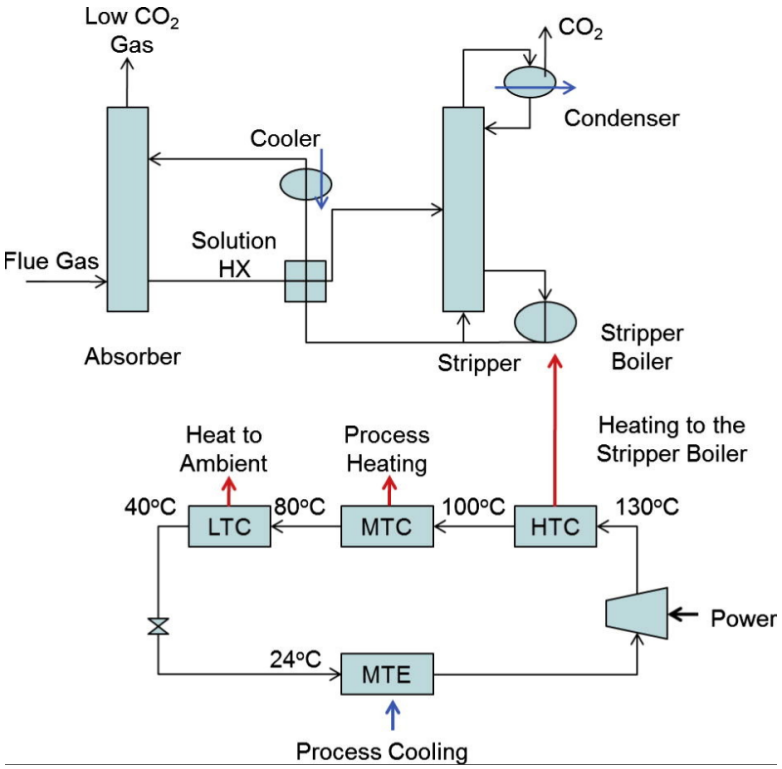

Figure 2.22: Integrated heat pump design [51].

More recently [52] opted to merge a high-temperature heat pump (HTHP) with direct air capture (DAC) of CO2, which entails a similar absorption-desorption process and also entails significant heat demand at the reboiler. They proposed three distinct thermal integration strategies that combine an HTHP with solid adsorbent-based DAC. Among these strategies, the deeply integrated DAC-HTHP system (I-DAC) illustred Figure 2.23 harnesses low-grade adsorption heat and waste heat to provide direct heating and cooling energy to the DAC system. This innovative approach yields a remarkable 69,5% reduction in energy consumption compared to traditional DAC systems operating under identical conditions.

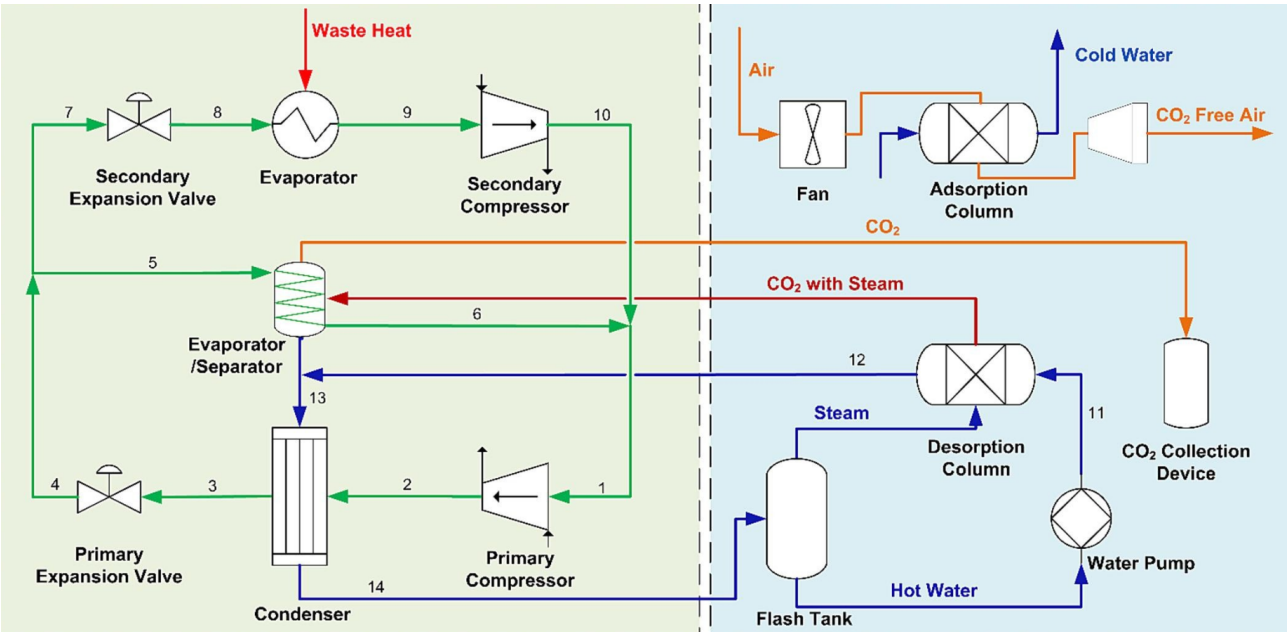

Figure 2.23: Integrated DAC-HTHP system (I-DAC) [52].

In addition [53] delved into an in-depth examination of the process itself, focusing on solely recovering heat within it. They developed several theoretical models and compared them to determine the most suitable heat sources and heat sinks, along with achievable energy savings, operational costs, and investments. Four stationary models with different heat sources were compared. The first model utilized only cooling at the condenser, the second relied solely on the necessary cooling of the amine at the absorber inlet, the third employed two heat pumps, respectively at the condenser and absorber inlet Figure 2.24, and finally, the fourth model connected a single heat pump to the process cooling circuit Figure 2.25. Interestingly, while the fourth solution has the greatest energy savings, it was the third model that present the lowest operational and investment costs.

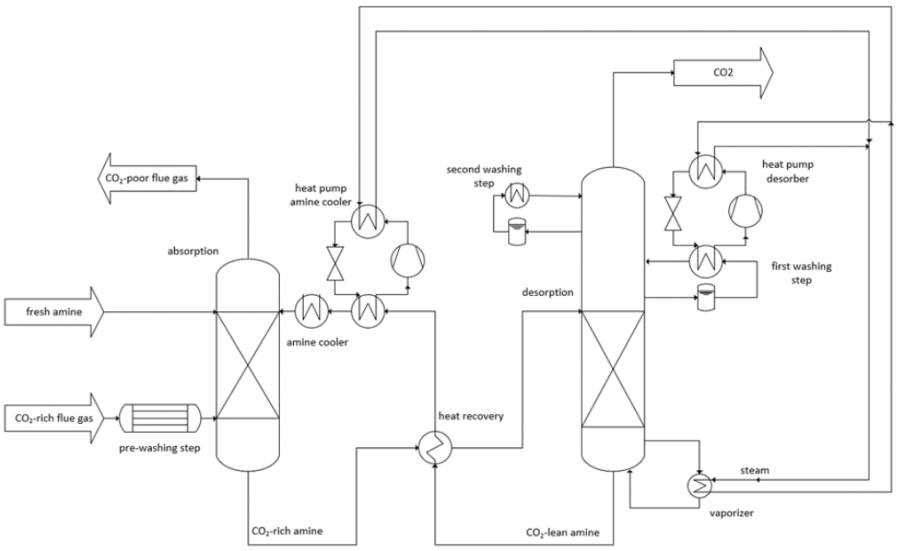

Figure 2.24: Two heat pump model [52].

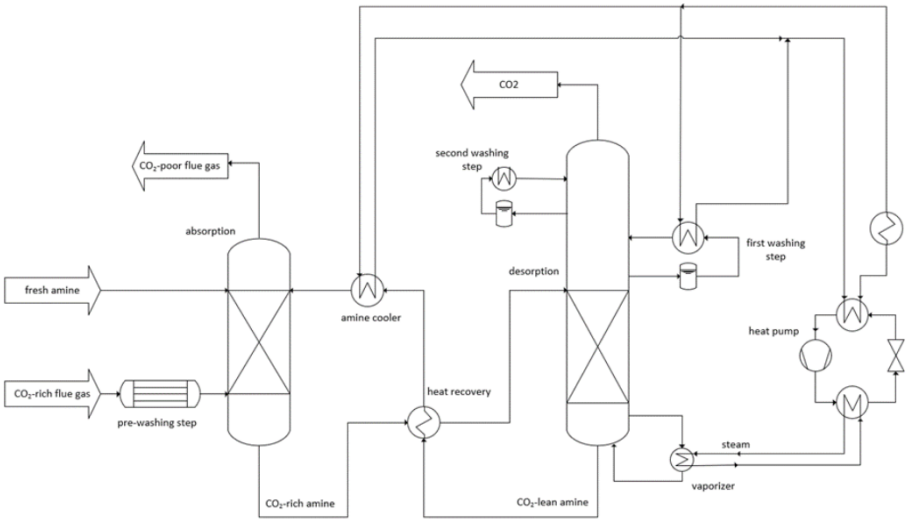

Figure 2.25: Cooling system connected to the heat pump model[52].

Finally [54] try to integrate a heat pump system aimed at electrifying an amine CO_2 capture unit for a biogas upgrading process employing aqueous monoethanolamine. They uses a two stage evaporator heat pump using the cooling demand of the process, as can be seen Figure 2.26. The study analyses the overall energy consumption across a spectrum of stripper pressures ranging from 0.313 to 1.813 bara. Indeed, as the pressure decreases, the required high temperature in the stripper decreases but the heating power increase. It is therefore crucial to found the optimal conditions. The most optimal heat pump scenario entailed a vacuum-operated stripper operating at 0.513 bara, yielding a remarkable 68% reduction in overall energy consumption compared to a conventional amine scrubbing unit.

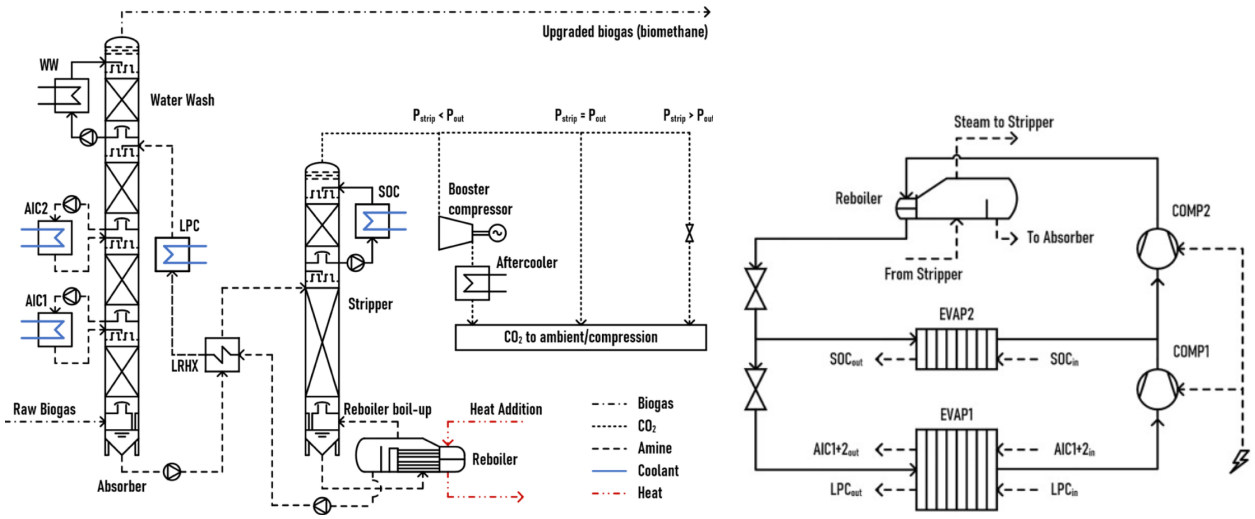

(a) Heating demand (red) and cooling demand (blue). (b) Two-stage evaporator HTHP.

Figure 2.26: HTHP integration [54].

Chapter 3

Cases Description

3.1 Initial Conditions

The simulations in this work are conducted using Aspen Plus software [55], in steady-state conditions corresponding to the nominal conditions of the CO_2 capture process. These simulations allow to determine two crucial parameters:

1. The required reboiler power, which is 36,728 kW.
2. The operating temperature of the stripper, set at 125°C.

3.1.1 Condensation temperature

The amine used in the capture process is corrosive, which prevents the direct implementation of the heat pump condenser in the stripper. Therefore, it is necessary to use an intermediate working fluid to transfer the heat from the condenser to the stripper. Regardless of the working fluid used, to maintain the stripper at 125°C, it needs to be heated to 135°C to avoid requiring an excessively high flow rate. Consequently, assuming an approach temperature of 5K, the condensation temperature of the heat pump is set at 140°C.

3.1.2 Choice of refrigerant

The refrigerant used in the heat pump will be R-1233zd(E). This choice is motivated by the following advantages highlighted in chapter 2:

- Low Global Warming Potential (GWP) and ozone depletion potential (ODP).
- High Critical Temperature of 166°C.
- High volumetric heating capacity.
- High COP.
- No flammability (A1 category Figure 2.13)

This last characteristic is one of the conditions imposed by the safety requirements of the carbon capture pilot plant project.

3.1.3 Choice of compressor

The reboiler power lies within the operational range of scroll compressors (Figure 2.15). As they are known for their high efficiency, offer high reliability and require minimal maintenance, this type of compressor is chosen.

3.2 Available heat

Once the initial conditions are defined, it is important to clearly understand the potential heat sources that can be used at the evaporator of the heat pump. Figure 3.1 represents the cooling power required by the carbon capture process, as well as the available flow rates and temperatures.

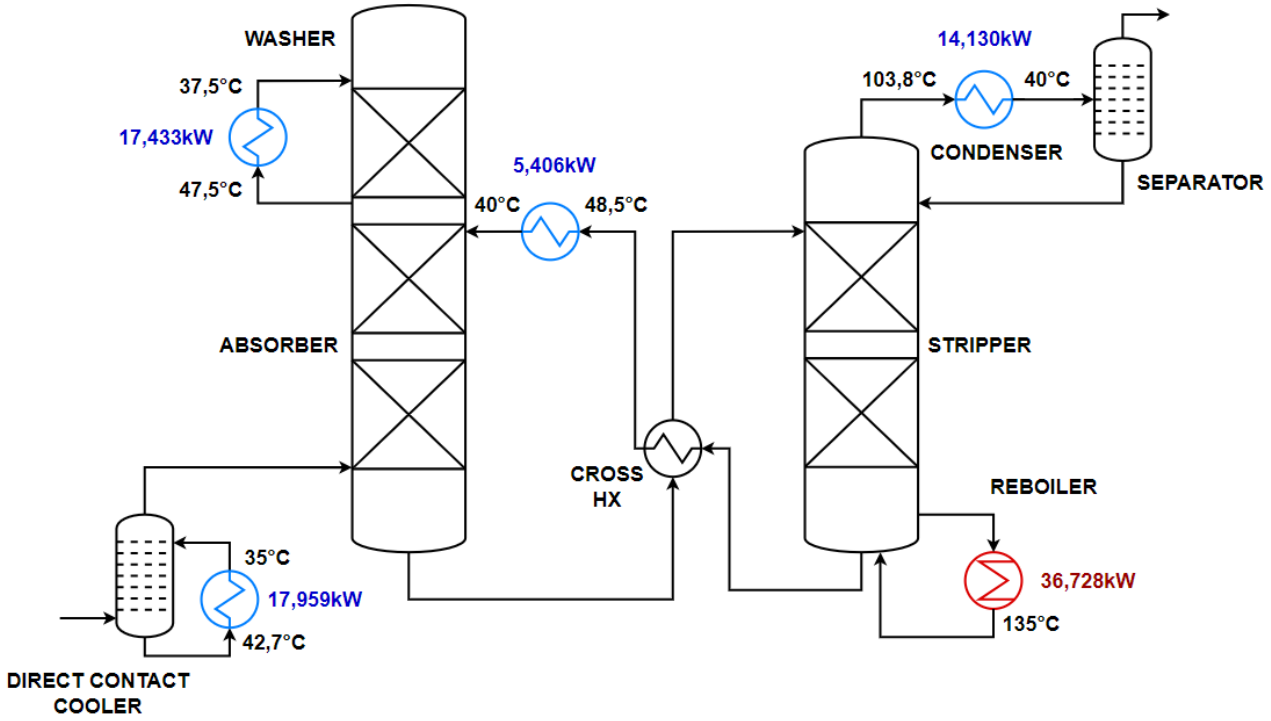

Figure 3.1: Heating and cooling demand of the process.

To begin with, regarding the flue gas, it is cooled by a direct contact cooler (DCC). The water that has been in direct contact with the flue gas must then be cooled from 42,7°C to 35°C, requiring a cooling power of 17,959 kW. Once the flue gas are rid of CO_2, they must be cooled and washed again in the washer (WASH) with a power of 17,433 kW. The water that has been in contact with the flue gas needs to be cooled from 47,5°C to 37,5°C. The lean amine mixture, although it has already transferred some of its heat to the rich amine mixture in the "CROSS HX" heat exchanger, still needs to be cooled from 48,5 to 40°C, requiring a power of 5,406 kW. Finally, the CO2, desorbed in the stripper, is evacuated from the stripper mixed with water vapor. In order to separate the two substances, the mixture must be cooled from 103,8°C to 40°C in the condenser (CD) to condense all the water and allow the separation of the vapor CO_2 from the liquid water in the separator.

Lead by the literature and these various heat sources, this thesis will initially investigate two different case :

The first involves collecting the different cooling waters into a single circuit and then using it in the evaporator of the heat pump. It is the most practical solution to implement for a pilot installation.

The second will investigates a two-evaporator heat pump at different pressure and temperature to uses the high temperature of the CO_2-water mixture exiting the stripper. This solution could improve the performance of the heat pump but increases the complexity of the process.

3.3 Case 1 : Single evaporator

To facilitate understanding the description of this first case, Figure 3.2 illustrates the integration of the heat pump into the cooling circuit, replacing the reboiler in the CO2 capture process.

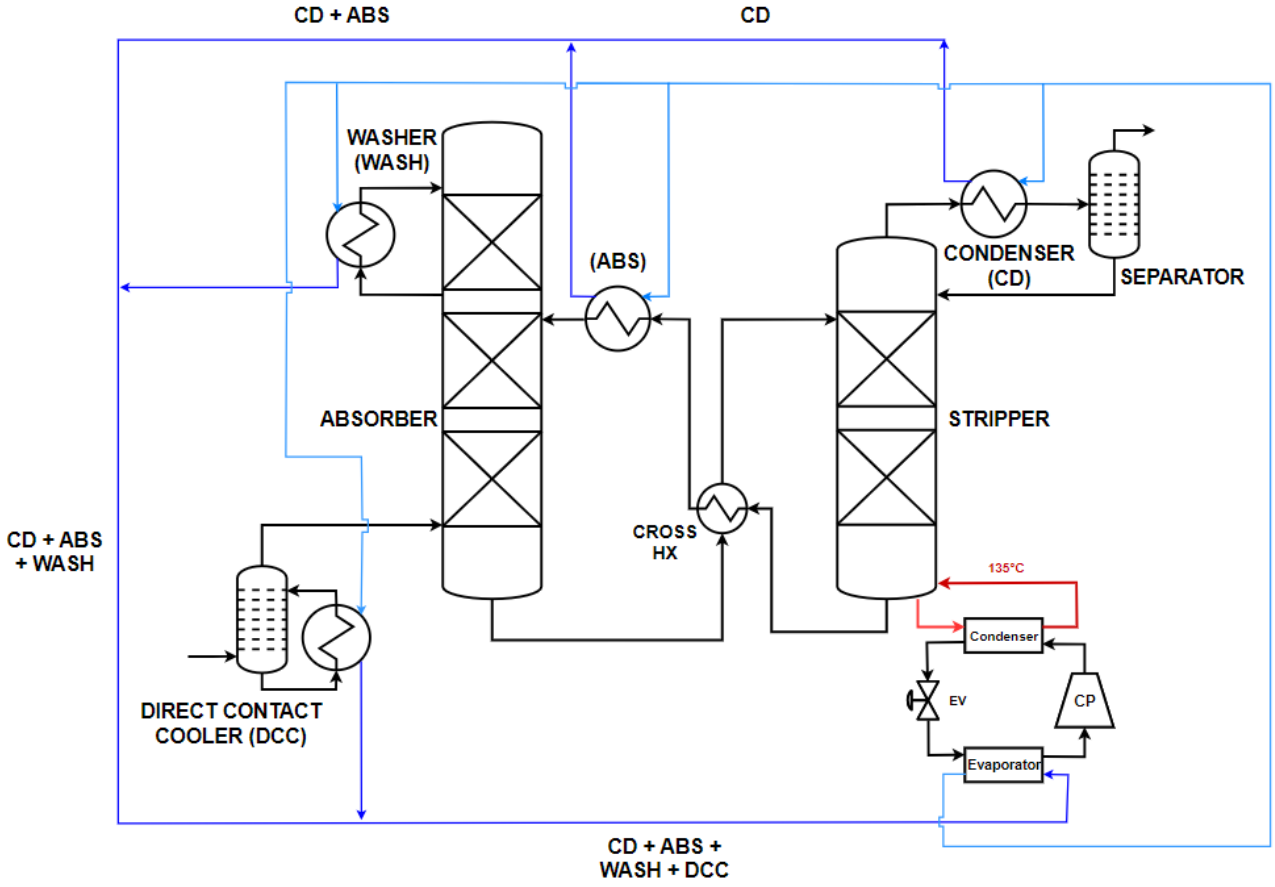

Figure 3.2: Heat pump single evaporator integration to the cooling circuit.

3.3.1 Preliminary study

As already discussed, the temperature of the cold source will influence the pressure required at the evaporator and therefore the operating conditions of the heat pump. These operating conditions will be essential in the selection of the refrigerant and the configurations of the heat pump studied in this work. It is therefore crucial to determine the temperature of the mixture once they are combined.

Firstly, The use of indirect contact heat exchangers results in a temperature difference. Indeed, due to the imperfect efficiency of these exchangers, the hot fluid exits at a higher temperature than the

cold fluid. The temperature difference between these these two fluid is the approach temperature is set to 5K.

Secondly, it is important to determine whether all cooling waters should be used or only selected ones among them. Since they do not all have the same temperature, the warmer ones will be prioritized, while the cooler ones will be used only if necessary. Using the thermodynamic function, the temperature and the pressure of each cooling water, each enthalpy (h) of each flow before mixing can be found :

$$\begin{aligned} h_{CD} &= h(T = 98.8\,^{\circ}C; P = P_{atm}), \\ h_{ABS} &= h(T = 43.5\,^{\circ}C; P = P_{atm}), \\ h_{DCC} &= h(T = 42.5\,^{\circ}C; P = P_{atm}), \\ h_{WASH} &= h(T = 37\,^{\circ}C; P = P_{atm}), \end{aligned}$$

Then, with mass and energy balance, the enthalpy and therefore the temperature of the mixture can be found :

$$\dot{M}_{total} = \sum(\dot{M}) \tag{3.1}$$

$$h_{total} = \frac{\sum(\dot{M} \cdot h)}{\dot{M}_{total}} \quad \Rightarrow \quad T_{total} = T(h_{total}; P_{atm}) \tag{3.2}$$

As the evaporator is also a indirect heat exchanger, the available temperatures are further reduced by another 5K. Here is a summary of the temperature truly exploitable and the flow rate of each mixture :

$$\begin{aligned} \text{CD} &: \dot{M}_{total} = 0.05\ kg/s \quad \text{and} \quad T_{total} = 93.8\,^{\circ}C \\ \text{CD + ABS} &: \dot{M}_{total} = 0,20\ kg/s \quad \text{and} \quad T_{total} = 52.79\,^{\circ}C \\ \text{CD + ABS + WASH} &: \dot{M}_{total} = 0,62\ kg/s \quad \text{and} \quad T_{total} = 42,54\,^{\circ}C \\ \text{CD + ABS + WASH + DCC} &: \dot{M}_{total} = 1,18\ kg/s \quad \text{and} \quad T_{total} = 37,89\,^{\circ}C \end{aligned}$$

The aim of this preliminary study is to determine the temperature at which the working fluid would evaporate, and therefore to establish the pressure level at the evaporator. A basic cycle of a heat pump working with the R-1233zd(E) has been implemented on the Engineering Equation Solver (EES) software [56] to quantify the heat requirements $\dot{Q}_{ev}$ at the evaporator and to determine which mixture will allow the highest evaporation temperature. As a reminder, for an ideal heat pump without losses, it follows :

$$\dot{Q}_{cd} = \dot{Q}_{ev} + \dot{W}_{cp}. \tag{3.3}$$

This means that for a constant power at the condenser, if the power required by the compressor decreases, the amount of heat required at the evaporator increases. This compressor power being proportional to the pressure ratio [22], if the pressure, and thus the temperature at the evaporator, increases, the amount of heat required at the same evaporator also increases. It implies that a compromise between the evaporator pressure in function of the available heat is required.

Figure 3.3 represents, on one hand, the amount of heat available for each mixture as a function of the chosen evaporation temperature and on the other hand, the amount of heat required at the heat pump evaporator for this same chosen evaporation temperature.

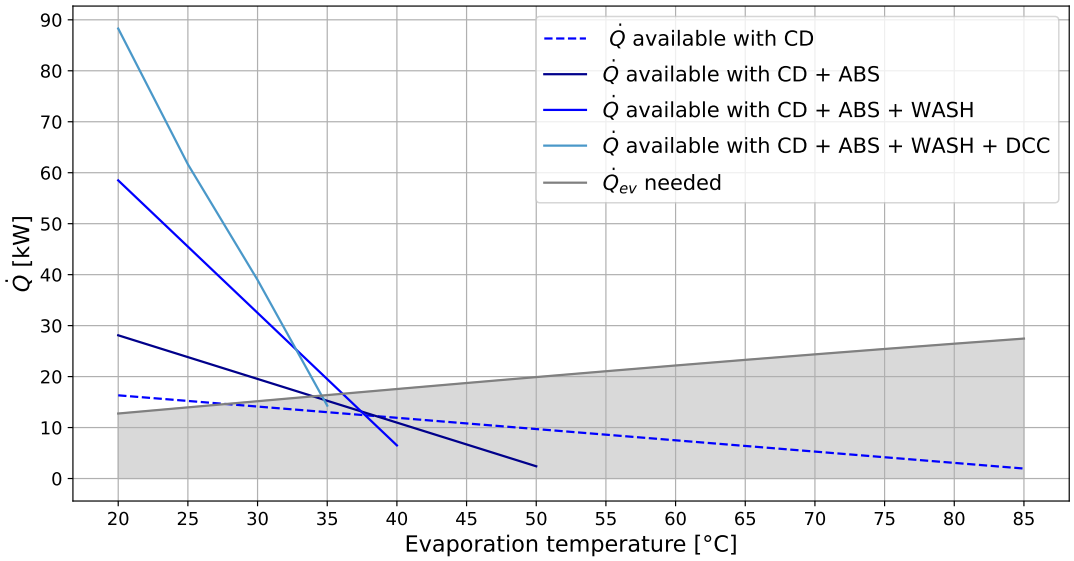

Figure 3.3: Evaporator heat duty in function of the evaporation temperature.

The maximal evaporation temperature correspond to the first intersection between the heat requirements and the available heating quantity. This temperature corresponds to the use of the cooling water from the condenser, the heat exchanger cooling the lean amine mixture before it enters the absorber, and the cooling water from the second washing section (CD + ABS + WASH). As this is a preliminary study without consideration of a specific and optimized heat pump model, the evaporation temperature is rounded to 35°C and will be revised after the optimization of the heat pump.

3.3.2 Optimization

The preliminary study identified the operating conditions for the heat pump. These conditions are summarized below :

- Refrigerant : R-1233zd(E).
- Nominal heating power : Q_{cd} = 36,728kW.
- Condensation temperature/pressure : T_{cd} = 140°C / P_{cd} = 22,92 bar.
- Evaporation temperature/pressure : T_{ev} = 35°C / P_{ev} = 1,83 bar.
- Temperature lift : 105°C
- Pressure ratio : r_p = 12,52.

The temperature lift and the pressure ratio are huge. As explained in chapter 2, such a temperature difference and pressure ratio implies a two-stage cycle with two compressors to conserve good performance. Based on the literature reviewed chapter 2, four advanced heat pump configurations will be considered and compared to the basic configuration with no amelioration :

1. Two-stage (TS) with flash tank (FT) and IHX (Figure 3.4a).
2. Two stage (TS) with economizer (ECO) (Figure 3.4b).
3. Two stage (TS) with flash tank (FT), total desuperheating and two IHX (Figure 3.4c).
4. Cascade with two internal IHX (Figure 3.4d).

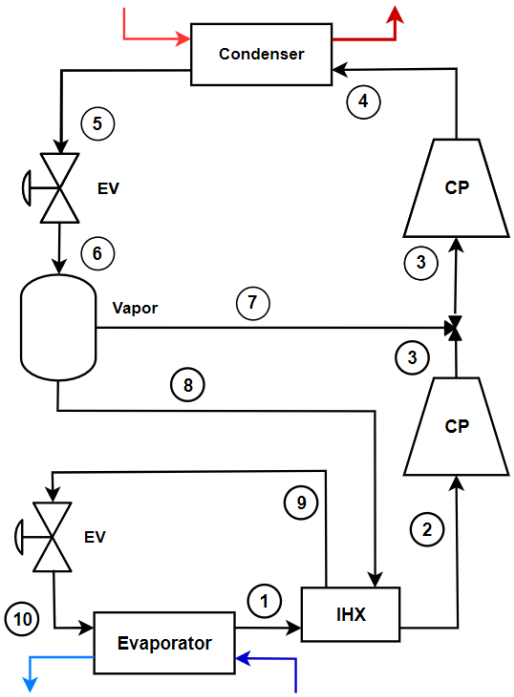

(a) Flash tank + IHX.

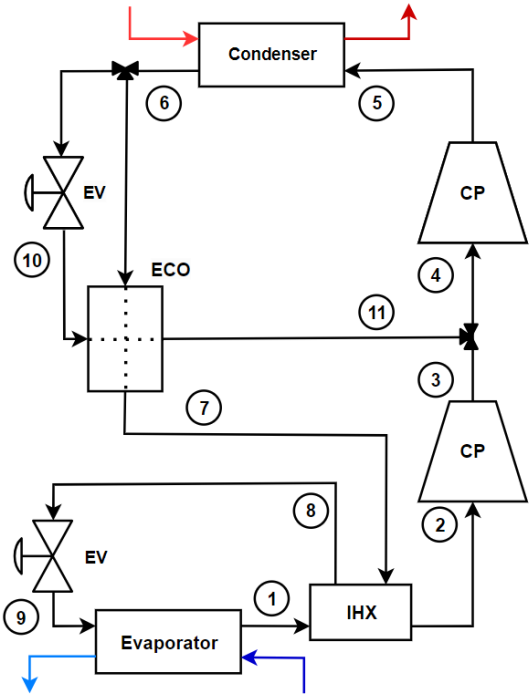

(b) Economizer + IHX.

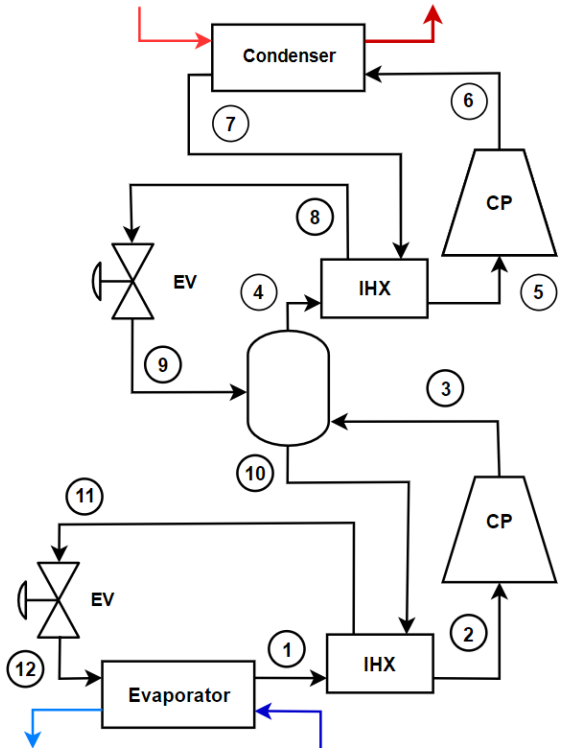

(c) Flash tank with total desuperheating + IHX.

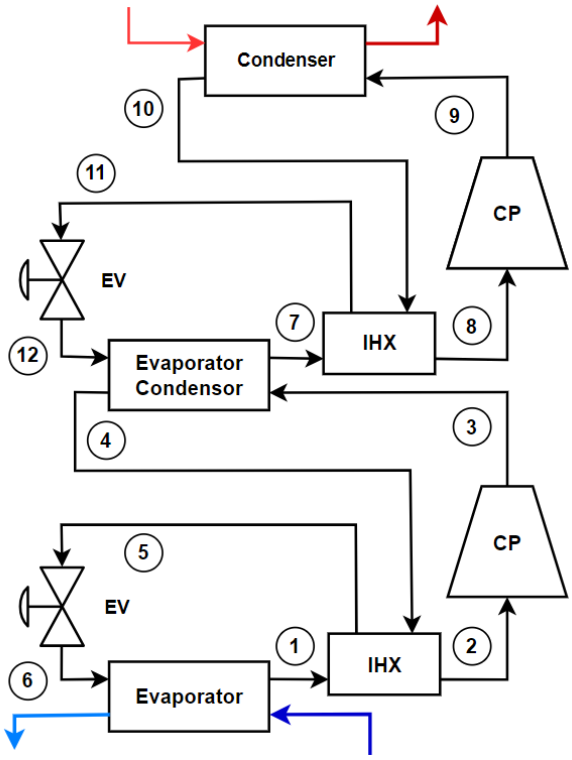

(d) Cascade + IHX.

Figure 3.4: Studied configurations, case 1.

3.4 Case 2 : Two evaporator

As for the first case, a representation of the integration of the heat pump is illustrated in Figure 3.5 to facilitate understanding of the heat pump integration.

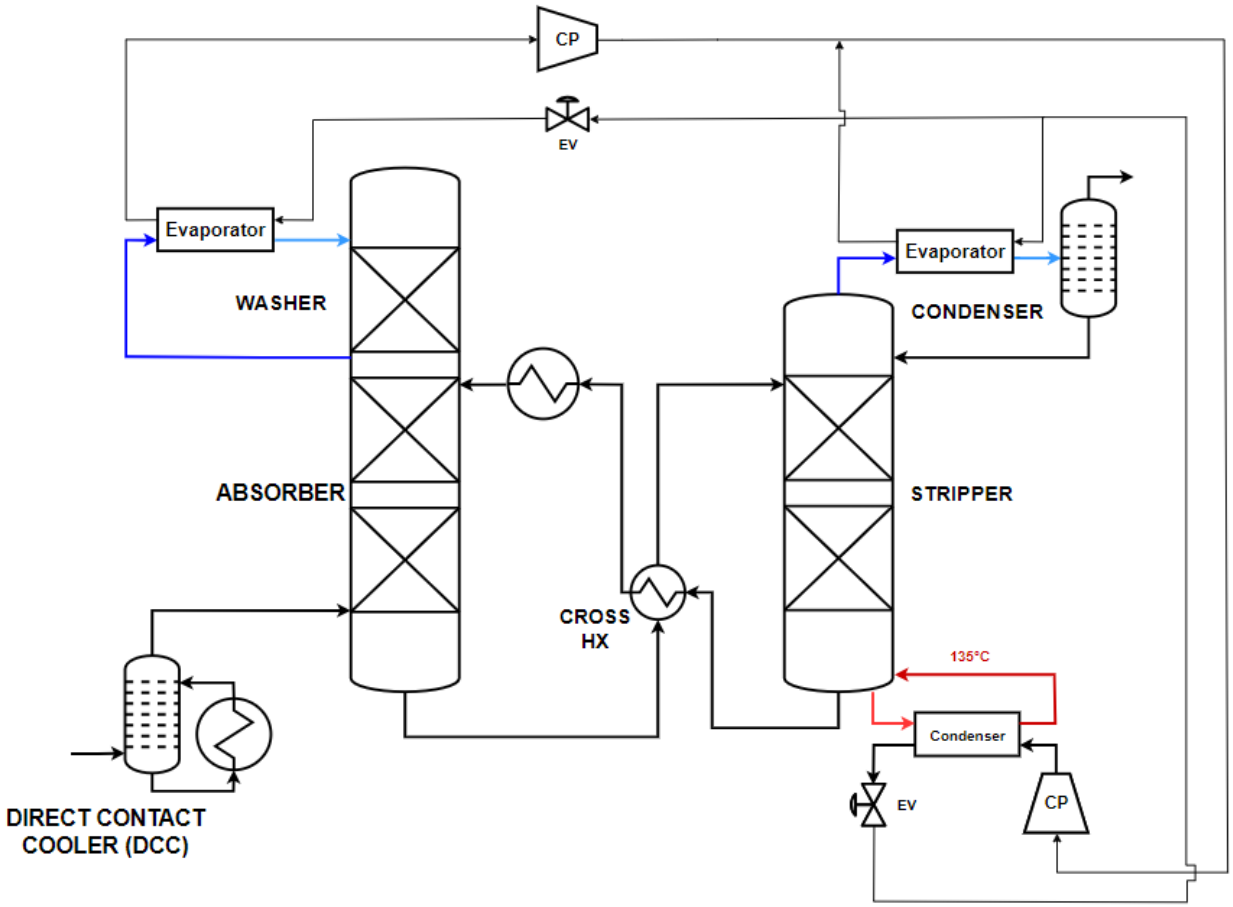

Figure 3.5: Heat pump with two evaporators integration.

In this case study, the high temperature of the mixture exiting from the stripper is harnessed. To do so, the condensation process has to be separated (Figure 3.6). The mixture will exit the first condenser at an intermediate temperature T_{int} exceeding 40°C, this higher temperature allows for an higher pressure within the evaporator. Depending on the power available when cooling down the fluid from 103°C to T_{int}, the entirety or a portion of the refrigerant will not need to be expanded to lower pressure, thereby limiting the irreversibilities occurring within the expansion valve and reducing the power required by the low-pressure compressor, which will need to compress less fluid.

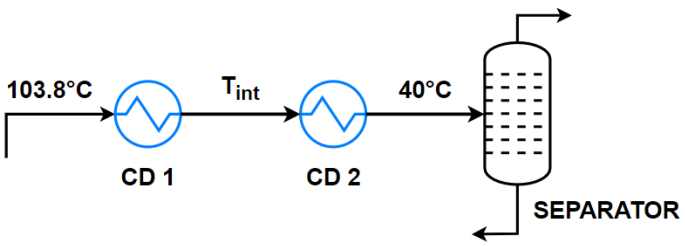

Figure 3.6: Condenser process separation.

3.4.1 Preliminary study

The first step for this case is to verify that the high temperature of the mixture at the stripper outlet is not misleading. Just because the fluid is at a high temperature when entering the condenser does not mean that this temperature will be usable. It will depend on the amount of energy required to lower the temperature of the mixture of one degree, which can be qualitatively observed using a T-$\dot{Q}$ curves (Figure 3.7), calculated using AspenPlus [55]. This figure represent the temperature profile of the mixture in relation to the cooling power at the condenser. The small negative slope of the curves at high temperature indicates that a lot of power is needed to cool down the fluid by one degree at high temperature, confirm that the high temperature of the mixture can be used.

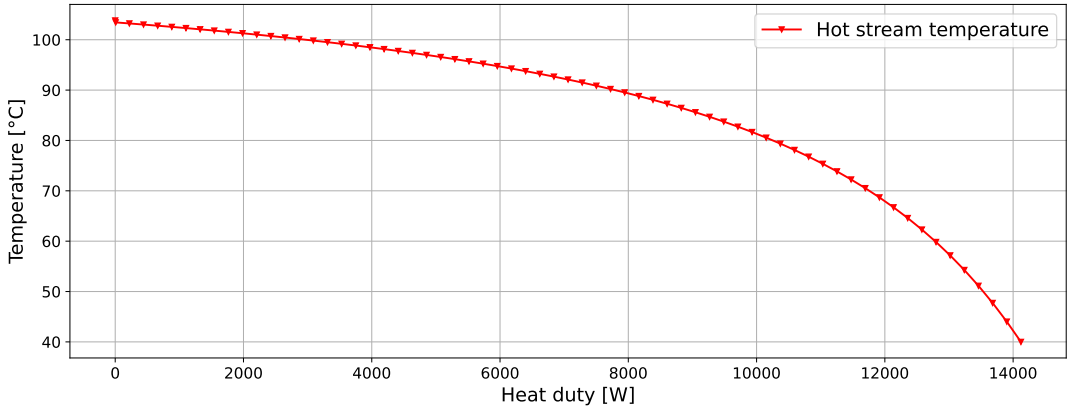

Figure 3.7: T-$\dot{Q}$ curve of the condenser hot stream.

However, it is still necessary to determine to what extent this temperature can be used, therefore, it is important to find the ideal intermediate temperature T_{int}. To achieve this, a heat pump cycle using two evaporators was implemented. This cycle (Figure 3.8) was simplified with a basic scheme without cycle improvements, as it is only used to evaluate the intermediate temperature that will provide the best COP.

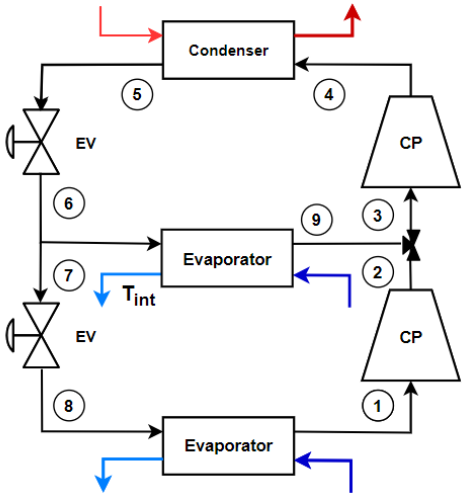

Figure 3.8: Basic two-evaporator heat pump cycle.

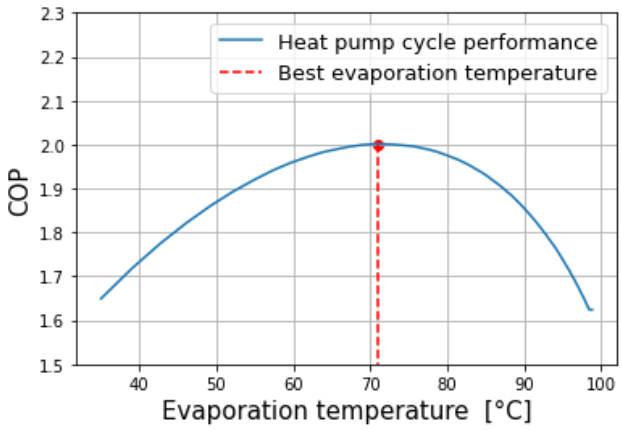

Figure 3.9: Medium pressure evaporator's evaporation temperature influence on the COP.

This allows us to determine the operating conditions and requirements of the necessary heat pump. As in the first case, the approach temperature at the two evaporators is 5K. However, it is assume

that they are directly connected to the cooling demand of the process as illustrated in Figure 3.5. Therefore, there is no intermediate cooling water and no additional 5K temperature difference, which increase the available temperature. The low pressure evaporator is fixed to the pressure corresponding to an evaporation temperature of 35°C, as for the case 1.

The evaporation temperature of the medium pressure evaporator was gradually increased. Fixing the corresponding cooling duty of the condenser as the heating power avalaible at the evaporator, it was possible to evaluate which of these temperatures allowed for the best COP. The various points have been plotted Figure 3.9, where the peak of the curve is easily noticeable and corresponds to an evaporation temperature of 71°C. This evaporation temperature correspond to a intermediate temperature T_{int} = 71 + 5 = 76°C.

The initial condensation process is therefore separated into two condensers (Figure 3.10). The first is the heat pump's evaporator and cools the mixture from 103.8°C to the intermediate temperature of 76°C, representing a cooling power of 10.930 kW. This cooling demand is therefore the available heating source of the medium pressure evaporator of the heat pump. The second condenser cools the mixture from 76°C to the desired temperature of 40°C.

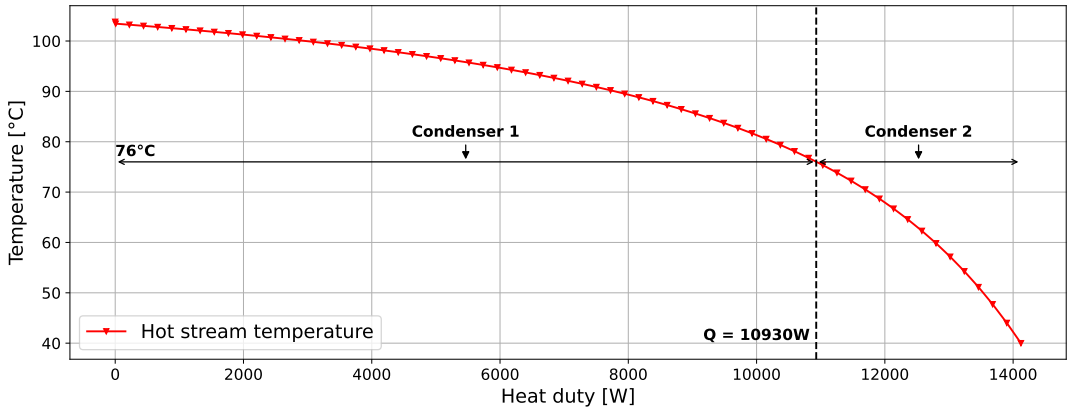

Figure 3.10: Condensation process separation.

In this simplified model, The remaining required power for the low pressure evaporator is 7,440 kW, this quantity will be re-evaluated after the best configurations and optimized cycle will be found, in order to determine if the washer can effectively be used to meet this demand.

3.4.2 Optimization

Similarly to the first case, this preliminary study identified the operating conditions for the heat pump. These conditions are summarized below :

- Refrigerant : R-1233zd(E).
- Nominal heating power : Q_{cd} = 36,728kW.
- Condensation temperature/pressure : T_{cd} = 140°C / P_{cd} = 22,92 bar.
- Middle pressure evaporator temperature/pressure : T_{ev} = 71°C / P_{ev} = 5,246 bar
- Heating power avalaible at medium pressure : $\dot{Q}_{ev,1}$ = 10,930 kW
- Low pressure evaporator temperature/pressure : T_{ev} = 35°C / P_{ev} = 1,83 bar.
- Middle to high temperature lift/pressure ratio : $T_{lift,H}$ = 69°C / $r_{p,H}$ = 4,369.
- Low to middle temperature lift/pressure ratio : $T_{lift,L}$ = 36°C / $r_{p,L}$= 2,867.
- Total pressure ratio : r_p = 12,52.

These operating conditions show a low temperature lift and a low pressure ratio for the part of the cycle comprising the low-pressure evaporator. The literature tells us in chapter 2 that for this value of pressure ratio, a simple internal heat exchanger is recommended to increase performance. However, the operating conditions for the high-pressure part of the cycle, comprising the medium-pressure evaporator and the condenser, allow several improvements to be envisaged. The temperature lift is 69°C, which is still high, and the pressure ratio of 4,369 means that several compressors can be used in series with a flash tank or economiser. The configurations studied for this second case are therefore all using an internal heat exchanger for the low pressure part, and the improvements compared for the high pressure part are the following :

1. No improvement
2. Two stage (TS) with flash tank (FT)
3. Two stage (TS) with flash tank (FT) and total desuperheating
4. Two stage (TS) with economizer (ECO)

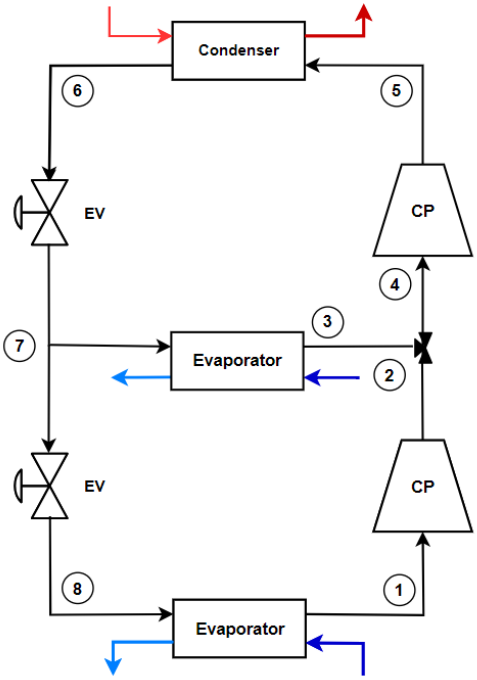

(a) No improvement.

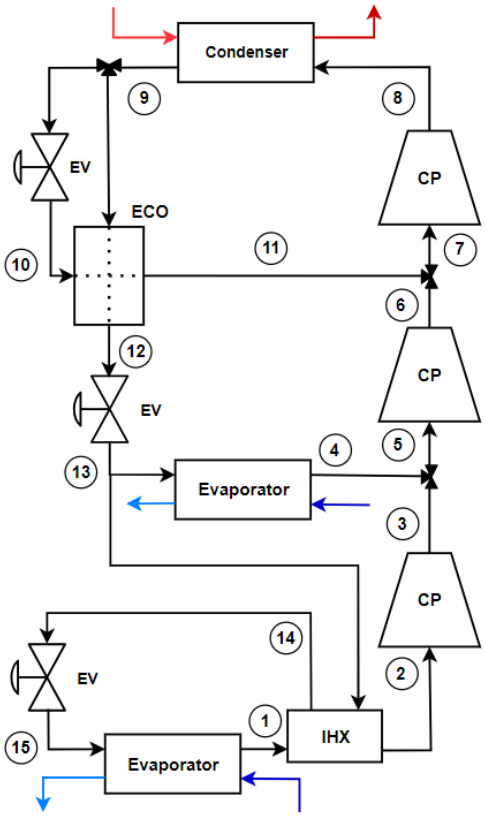

(b) TS with ECO.

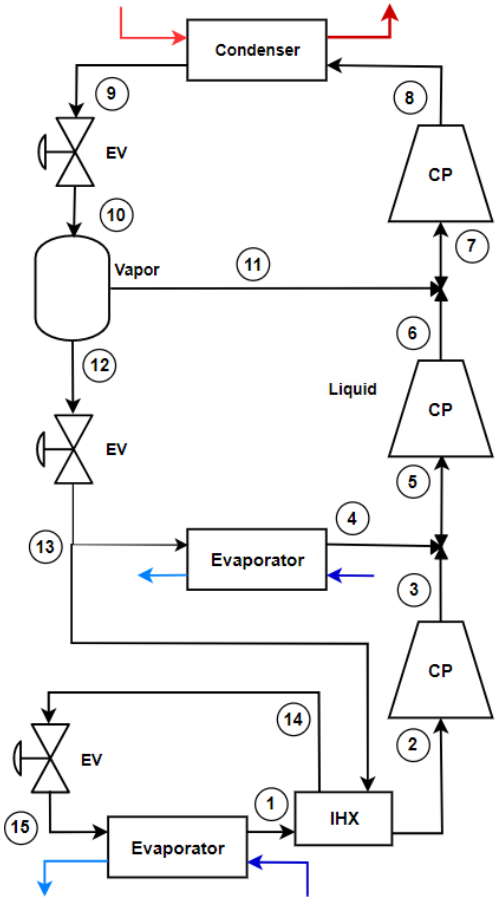

(c) TS with FT.

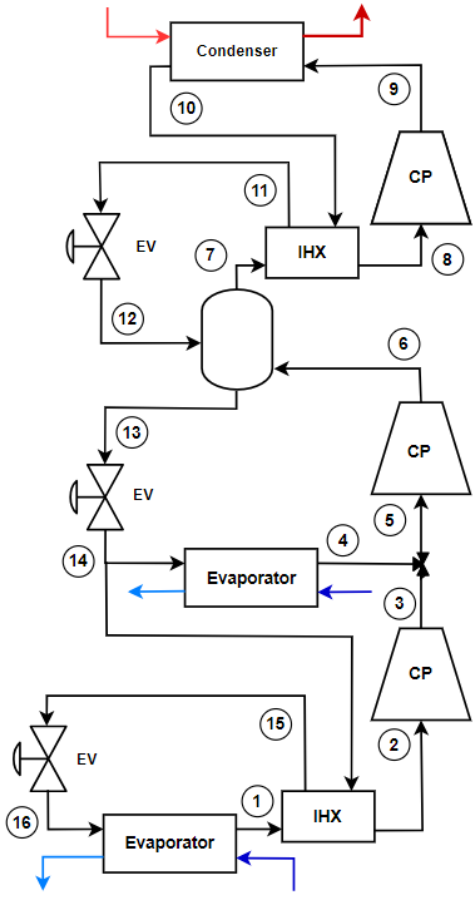

(d) TS with FT and total desuperheating.

Figure 3.11: Studied configurations, case 2.

Nevertheless, [36] shown that a configuration using a single compressor with vapor injection offers better performance than a configuration with two compressors at a pressure ratio smaller than 5. Therefore, two configurations using a flash tank and an economizer but with a single stage and a vapor injection compressor are added :

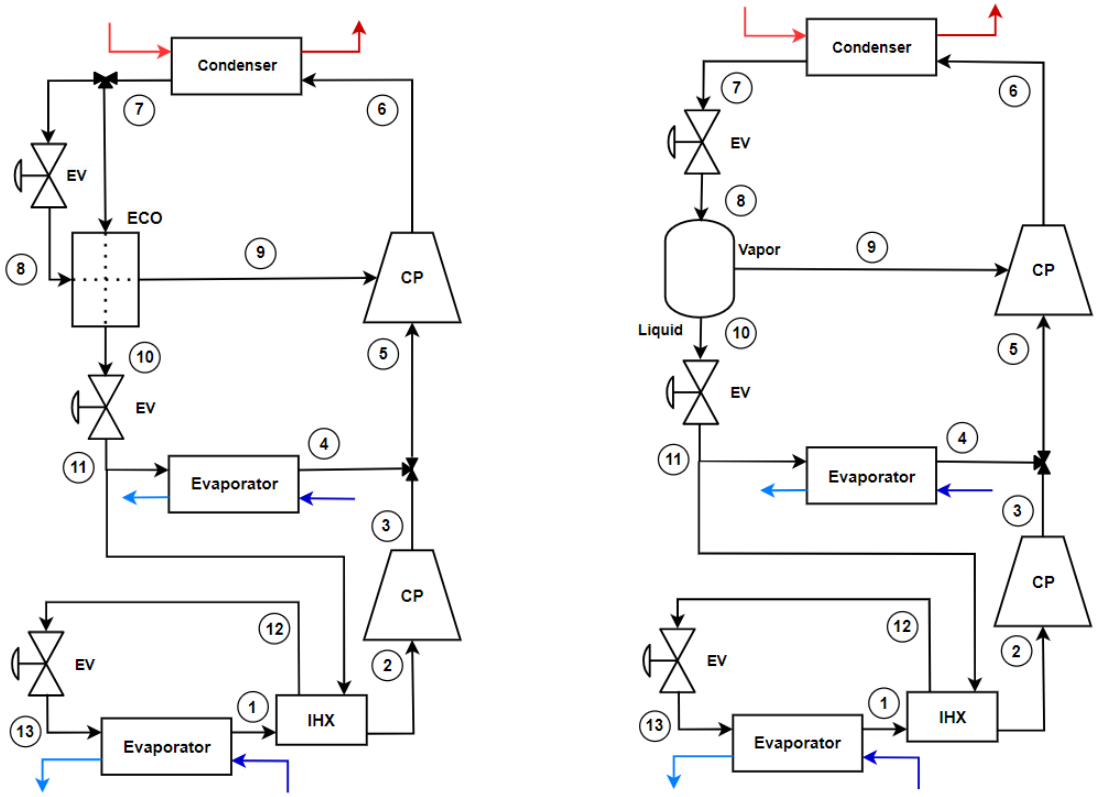

(a) SS with VI and ECO.

(b) SS with VI and FT.

Figure 3.12: Configurations with vapor injection compressor, case 2.

Chapter 4

Modeling

This chapter presents the models of the various components used in heat pump configurations. The general assumptions made for these models are as follows: there are no ambient losses, except for the compressor, and there are no pressure drop. These assumptions simplify the analysis while allowing for a focus on comparing the performance of each configuration. The modeling and simulations will be done using the Engineering Equation Solver (EES) software [56].

4.1 Compressor

The compressor is the essential component of the heat pump cycle. Indeed, its performance (i.e., its efficiency) will largely influence the cycle's performance. Therefore, properly modeling this element is particularly important to assess a relevant analysis. This modeling is developed, explained and justify in this section.

4.1.1 Compressor without injection

To analyze the performance of the heat pump on full and partial load conditions, it is essential to develop an accurate model of the compressor. This model should include various potential losses, such as leakage losses, ambient losses, heat transfer during suction and discharge, and the electromechanical losses of the compressor. The model is based on the one proposed by [57] for a hermetic scroll compressor as well as the leakage losses model by [58]. This model, represented Figure 4.1, is divided into several steps.

1. Suction pressure drop : su $\rightarrow$ su,1
2. Isobaric heating-up : su,1 $\rightarrow$ su,2
3. Internal leakages : su,2 $\rightarrow$ su,3
4. Isentropic compression : su,3 $\rightarrow$ in
5. Constant volume compression : ad $\rightarrow$ ex,2
6. Isobaric cooling down : ex,2 $\rightarrow$ ex,1
7. Discharge pressure drop : ex,1 $\rightarrow$ ex

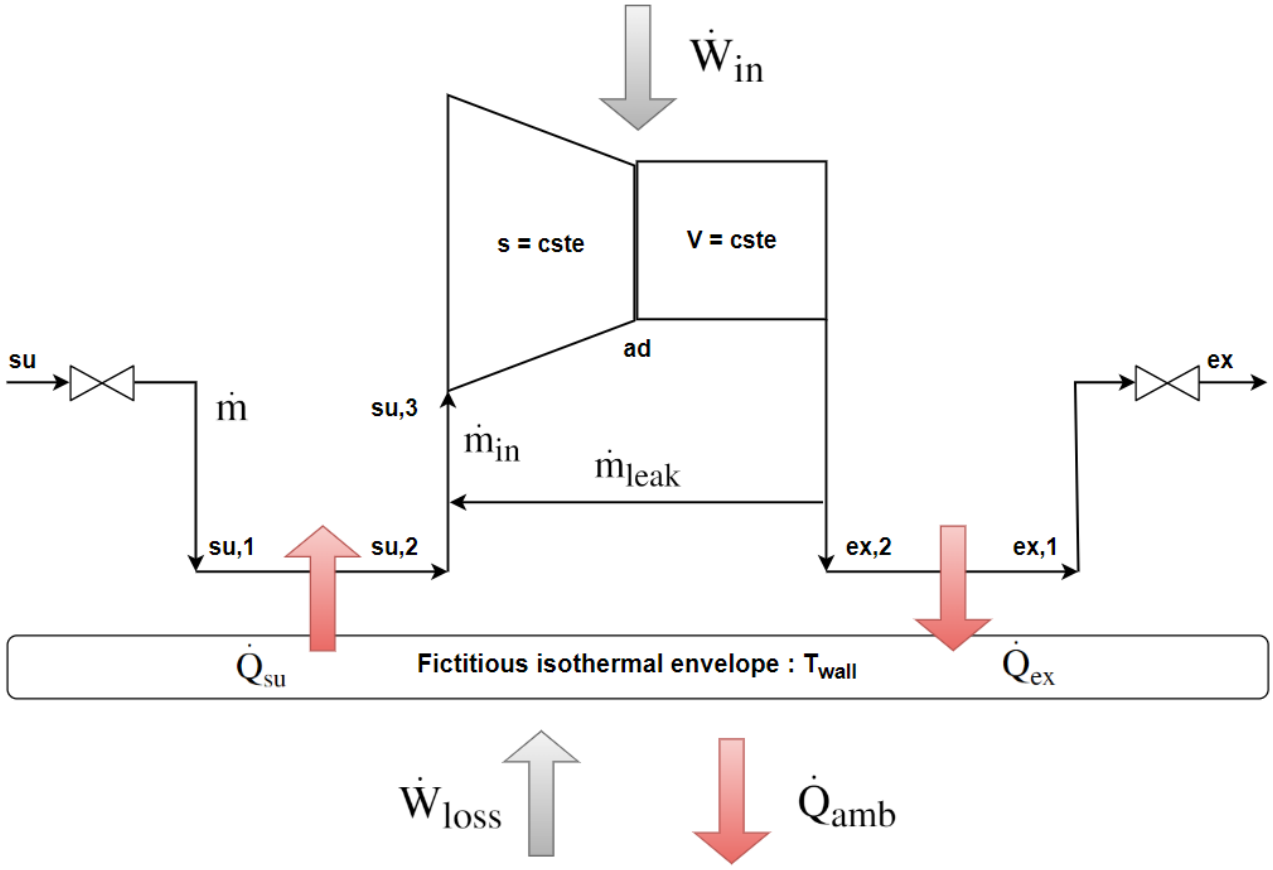

Figure 4.1: Hermetic scroll compressor diagram.

Suction/Discharge pressure drop

In this study, pressure drops at the suction and discharge are neglected. This decision is based on several factors. Firstly, preliminary analysis conducted by [57]. found that these pressure losses were very low, approaching zero. Secondly, it is common practice in scientific and technical literature to discard these pressure losses in similar scenarios due to their minimal impact on the overall outcomes [59],[60],[61].

Isobaric heating-up

The employed model facilitates the regrouping of various heat transfers encountered within a compressor. These heat transfers are represented by a hypothetical envelope with a temperature T_{wall}. The equations governing the suction heat transfer with a constant wall temperature are:

$$\dot{Q}_{su} = \dot{M} \cdot (h_{su,2} - h_{su,1}). \tag{4.1}$$

With

$$\dot{Q}_{su} = \epsilon_{su} \dot{C}_{su} \cdot (T_{wall} - T_{su,1}). \tag{4.2}$$

And ϵ is found with the ϵ-NTU method :

$$\epsilon = 1 - exp(-NTU_{su}), \tag{4.3}$$

with

$$NTU_{su} = \frac{AU_{su}}{\dot{C}_{su}} = \frac{AU_{su}}{\dot{m} \cdot cp_{su}}. \tag{4.4}$$

Internal leakages losses

Internal leakage represents a source of performance degradation in compressors. It occurs whenever there is a gap between the high pressure regions and the low pressure regions.The leakage flow rate is determined by referencing the isentropic flow through a simple convergent nozzle and the fictitious leakage area A_{leak} , which is a parameter of the model, is treated as the nozzle throat [62]. The pressure at the nozzle inlet is calculated with :

$$P_{\text{crit, leak}} = \max\left(P_{\text{su, 3}}, P_{\text{crit, leak}}\right). \tag{4.5}$$

Where $P_{crit,leak}$ is introduced to consider the possible choked flow that could occur in the nozzle throat. This critical pressure $P_{\text{crit, leak}}$ is computed by considering the refrigerant vapor as a perfect gas:

$$P_{\text{crit, leak}} = P_{\text{ex, 2}} \cdot \left[\left(\frac{2}{\gamma+1}\right)^{\frac{\gamma}{\gamma-1}}\right] \tag{4.6}$$

The equations of continuity and conservation of enthalpy between the nozzle supply and throat are combined to express the leakage mass flow rate:

$$\dot{m}_{\text{leak}} = \frac{A_{\text{leak}}}{v_{\text{thr, leak}}} \cdot \sqrt{2(h_{\text{ex, 2}} - h_{\text{thr, leak}})} \tag{4.7}$$

The specific enthalpy $h_{\text{thr, leak}}$ and the specific volume $v_{\text{thr, leak}}$ at the throat are computed assuming that the expansion from $P_{\text{ex, 2}}$ to $P_{\text{thr, leak}}$ is isentropic. The internal mass flow rate of the compressor is calculated with:

$$\dot{m}_{\text{in}} = \frac{\dot{V}_{\text{s,cp}}}{v_{\text{su,3}}}, \tag{4.8}$$

where $\dot{V}_{\text{s,cp}}$ is the compressor displacement volume. In this model, the process is assumed to be isobaric but not adiabatic, mass and energy balance yields to

$$\dot{m} + \dot{m}_{leak} = \dot{m}_{in} \tag{4.9}$$

$$\dot{m} \cdot h_{su,2} + \dot{m}_{leak} \cdot h_{ex,2} = \dot{m}_{in} \cdot h_{su,3}. \tag{4.10}$$

The effects of internal leakage on compressor performance are quantified by the volumetric efficiency, denoted by

$$\eta_{vol} = \frac{\dot{m}}{\dot{m}_{Theoretical}}. \tag{4.11}$$

Where η_v represents the ratio of the actual mass of refrigerant in the first compression pocket to the mass that would enter the pocket from the suction reservoir in the absence of internal leakage. The re-expansion and re-compression associated with the leakage process also further diminish the compressor's isentropic efficiency.

Isentropic and isochoric compression

One of the particularities of the scroll compressor is its fixed geometry and associated internal volume ratio. It is defined during design and is calculated as the ratio between the initial volume V_i and the final volume V_f within the compression chamber . This internal volume ratio $r_{v,in}$, combined with the specific operating conditions of the refrigerant fluid, determines the internal pressure ratio of the compressor. If the internal and external pressure ratios are equal, compression occurs without additional losses and the compressor is adapted Figure 4.2a. However, when the external pressure ratio differs from the fixed internal pressure ratio, it indicates that the compressor is not suited to these specific conditions. This generate power losses in the form of heat and can occur in two cases :

1. Over-compression (P2>Pad) where the external pressure exceeds the adapted internal pressure Figure 4.2b.
2. Under-compression (P2<Pad) where the external pressure is lower than the adapted internal pressure Figure 4.2c.

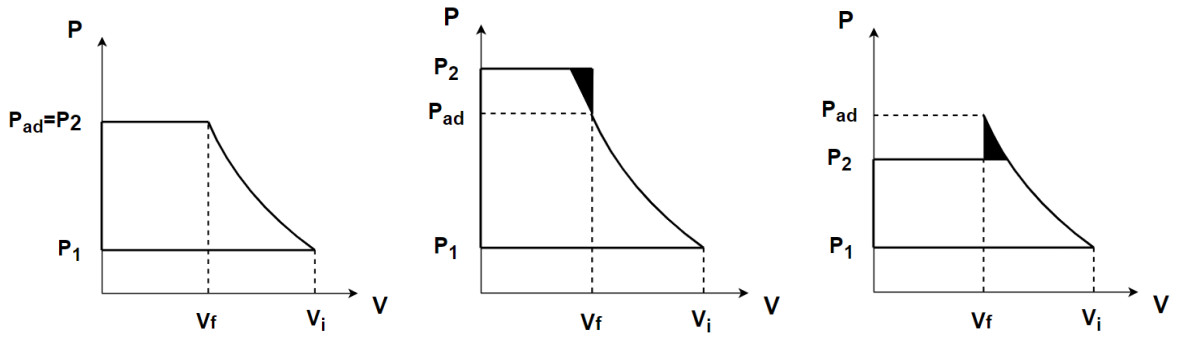

(a) Adapted compression. (b) Over-compression. (c) Under-compression.

Figure 4.2: Influence of internal volume ratio on the compression process.

The compression process is therefore divided into two parts: firstly, an adiabatic reversible compression, hence isentropic and requiring the following work :

$$w_{in,1} = (h_{ad} - h_{su,3}). \tag{4.12}$$

With,

$$h_{ad} = h(s_{su,3}; v_{ad}). \tag{4.13}$$

And

$$v_{ad} = \frac{v_{su,3}}{r_{v,in}}. \tag{4.14}$$

Secondly, an isochoric compression, correspondings to the opening of the compression chamber to the discharge plenum [57] and requiring the following work:

$$w_{in,2} = v_{ad} \cdot (P_{ex,2} - P_{ad}). \tag{4.15}$$

With,

$$P_{ad} = P(s_{su,3}; v_{ad}). \tag{4.16}$$

Finally, the total internal power of the compressor is :

$$\dot{W}_{in} = \dot{m}_{in} \cdot (w_{in,1} + w_{in,2}). \tag{4.17}$$

Compressor real electrical power

The actual electrical power of a hermetic compressor is generally formulated by the followings equations :

$$\dot{W}_{real} = \dot{W}_{in} + \dot{W}_{loss} \tag{4.18}$$

$$= \dot{W}_{in} + \dot{W}_{loss,0} + \alpha \cdot \dot{W}_{in}. \tag{4.19}$$

Where, $\dot{W}_{in}$ is the internal power, $\dot{W}_{loss,0}$ represents the total power losses, which can be divided into two parts. Firstly, the constant electro-mechanical losses $\dot{W}_{loss,0}$ and secondly the electromechanical losses proportionnal to the internal compressor power $\alpha \cdot \dot{W}_{in}$ [22]. For an hermetic compressor, these losses are directly injected as heat to the wall [57].

Discharge cooling down

As for the suction heating up, the refrigerant transfer heat to the fictitious wall at the discharge. The calculation procedure is therefore the same as for the isobaric suction heating up.

Power balance

Finally, conducting a steady-state power balance on the uniform temperature fictitious wall yields :

$$W_{loss} + Q_{ex} - Q_{su} - Q_{amb} = 0 \tag{4.20}$$

This allows to find the temperature of the fictitious wall T_{wall}

Isentropic efficiency

Once all the compressor losses are modeled, its isentropic efficiency can be calculated :

$$\eta_{is} = \frac{\dot{W}_{is}}{\dot{W}_{real}} \tag{4.21}$$

$$= \frac{\dot{m} \cdot (h_{ex,s} - h_{su})}{\dot{W}_{real}} \tag{4.22}$$

4.1.2 Compressor with vapor injection

The model used for a compressor with vapor injection is build upon the one developed in the previous section. Vapor injection is integrated using the models established by [63] and [64]. The various steps are represented Figure 4.3 and are as follows:

1. Suction pressure drop : su $\rightarrow$ su,1

2. Isobaric heating-up : su,1 → su,2
3. Internal leakages : su,2 → su,3
4. Isentropic compression : su,3 → inj,1
5. Isobaric injection : inj,1 → in,2
6. Second isentropic compression : inj,2 → ad
7. Constant volume compression : ad → ex,2
8. Isobaric cooling down : ex,2 → ex,1
9. Discharge pressure drop : ex,1 → ex

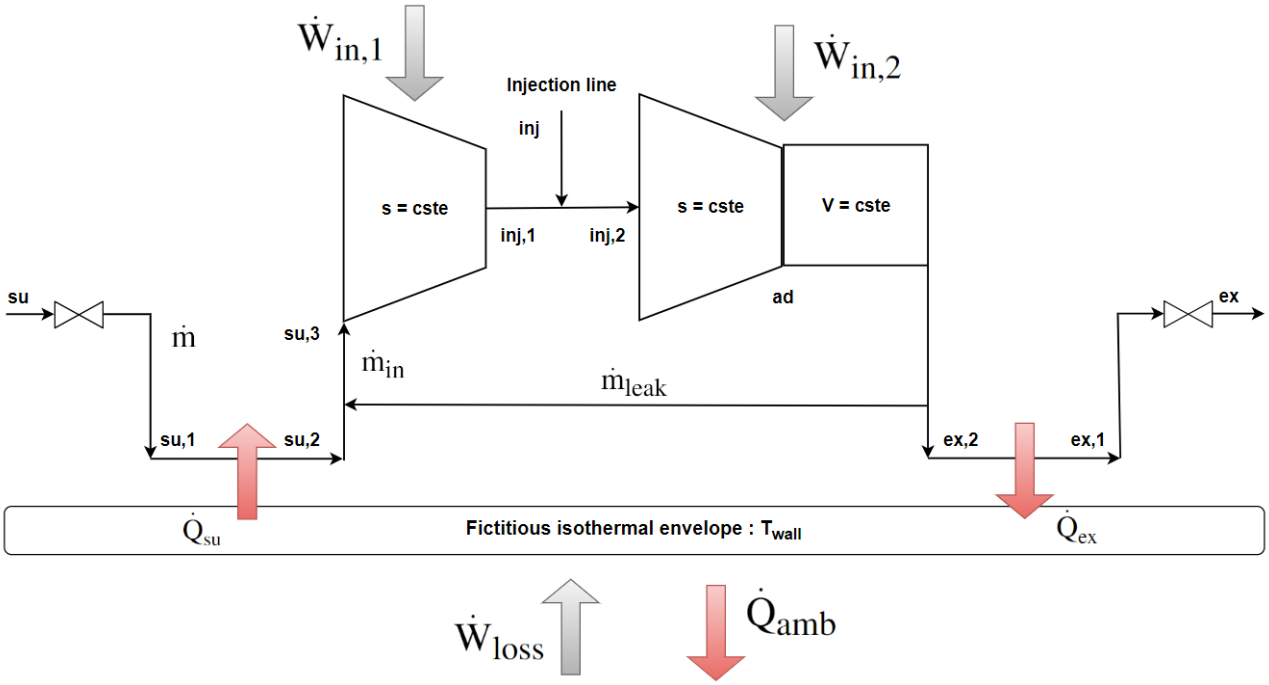

Figure 4.3: Vapor injection compressor diagram.

The heating at the suction, cooling at the discharge, leakage flux, as well as pressure drops at the inlet and outlet, have already been developed for the model without injection. Only the steps specific to vapor injection will be addressed in this subsection.

First isentropic compression

The first step involves isentropic compression up to an assumed appropriate pressure. Neither under-compression nor over-compression occurs. The intermediate pressure is assumed to be equal to the absolute pressure of the vapor injected into the compressor. The work corresponding to this process is as follow :

$$w_{in,1} = (h_{inj,1} - h_{su,3}). \tag{4.23}$$

With,

$$h_{inj,1} = h(s_{su,3}; v_{inj,1}). \tag{4.24}$$

And

$$v_{inj,1} = \frac{v_{su,3}}{r_{v,in,1}}. \tag{4.25}$$

Injection process

The injection process is assumed to be instantaneous and isobaric, where the injection flow and the flow from the first isentropic compression are mixed. This increases the flow rate within the compressor and reduces the refrigerant temperature. With mass and energy balance, it comes :

$$\dot{m}_{in} \cdot h_{inj,1} + \dot{m}_{inj} \cdot h_{inj} = (\dot{m}_{in} + \dot{m}_{inj}) \cdot h_{inj,2} \tag{4.26}$$

Second isentropic compression and isochoric compression

This part is the same as for the compressor without injection. First an isentropic compression requiring the following work :

$$w_{in,3} = (h_{ad} - h_{inj,2}). \tag{4.27}$$

With,

$$h_{ad} = h(s_{inj,2}; v_{ad}). \tag{4.28}$$

And

$$v_{ad} = \frac{v_{inj,2}}{r_{v,in,2}}. \tag{4.29}$$

Secondly, an isochoric compression :

$$w_{in,4} = v_{ad} \cdot (P_{ex,2} - P_{ad}). \tag{4.30}$$

With,

$$P_{ad} = P(s_{inj,2}; v_{ad}). \tag{4.31}$$

Finally, the total internal power of the compressor is :

$$\dot{W}_{in,total} = \dot{W}_{in,1} + \dot{W}_{in,2} = \dot{m}_{in} \cdot w_{in,1} + (\dot{m}_{in} + \dot{m}_{inj}) \cdot (w_{in,3} + w_{in,4}). \tag{4.32}$$

And the corresponding real electrical power :

$$\dot{W}_{real} = \dot{W}_{in} + \dot{W}_{loss} \tag{4.33}$$

$$= \dot{W}_{in} + \dot{W}_{loss,0} + \alpha \cdot \dot{W}_{in}. \tag{4.34}$$

Isentropic efficiency

The isentropic efficiency is calculated using Equation 4.21 but the isentropic power has to take into account the injected mass flow :

$$\dot{W}_{is} = \dot{m} \cdot (h_{in,1,is} - h_{su,3}) + (\dot{m} + \dot{m}_{inj}) \cdot (h_{ex,is} - h_{in,2}) \tag{4.35}$$

4.1.3 Asumptions

Since the heat pump model is purely theoretical, some parameters had to be estimated and assumed in order to create a realistic model despite the absence of experimental data.

First, the nominal rotational speed of each comppressor is assumed to be 3000 rpm.

Secondly, the heat transfer coefficients AU_{su}, AU_{ex}, and AU_{amb} has to be estimated based on previous research [57], [59], [60], [61],[65],[66]. Despite little differences in each study, the values obtained are never very far apart. The values assume for this thesis are as follows:

$$AU_{su} = 50WK^{-1}, \quad AU_{ex} = 35WK^{-1} \quad \text{and} \quad AU_{amb} = 10WK^{-1}$$

Moreover, the constant electromechanical losses of the compressor $\dot{W}_{loss,0}$ and the coefficient α modeling the losses proportional to the internal power of the compressor also had to be estimated. Using the availables studies [[57]], [59], [60], [61], [67],[68],[69], the most common values and the ones chosen for this study are :

$$\dot{W}_{loss,0} = 0,05 \cdot \dot{W}_{nominal} \quad \text{and} \quad \alpha = 0,4 \tag{4.36}$$

Finally, as explained in chapter 2, a key feature of scroll compressors is the internal volume ratio determined during design. This parameter significantly influences compressor performance, and setting it arbitrarily could bias the results. Therefore, the value of this parameter will be varied from 2 to 5, which are the respectively the minimal and maximal values for scroll compressors on the market.

4.2 Heat exchangers

4.2.1 Condenser/evaporator

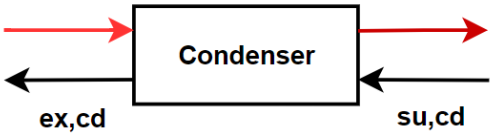

Figure 4.4: Condenser.

Figure 4.5: Evaporator.

A subcooling of 5K is fixed for the condenser and a superheating of 5K is fixed at the evaporator. The amount of heat transferred respectively at the condenser and at the evaporator are given by the equations :

$$\dot{Q}_{cd} = \dot{m}_{cd} \cdot (h_{\text{su,cd}} - h_{\text{ex,cd}}). \tag{4.37}$$

And

$$\dot{Q}_{ev} = \dot{m}_{ev} \cdot (h_{\text{ex,ev}} - h_{\text{su,ev}}). \tag{4.38}$$

4.2.2 Internal Heat echanger

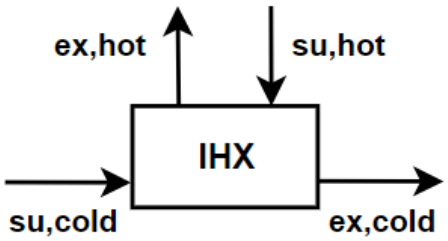

Figure 4.6: Internal heat exchanger.

The efficiency of the internal heat exchangers is not fixed to a unique value in this model but is adjusted so that the compressor outlet temperature does not exceed 156°C, thus providing a 10°C margin before reaching the fluid's critical temperature of 166°C. However, the maximum efficiency of the heat exchangers is limited to 0,9 to avoid excessively large heat exchangers. The amount of heat transfered is therefore calculated with :

$$\dot{Q}_{IHX} = \epsilon_{IHX} \cdot \dot{m} \cdot cp_{min} \cdot (T_{su,cold} - T_{su,hot}) \tag{4.39}$$

$$\dot{Q}_{IHX} = \dot{m} \cdot (h_{su,hot} - h_{ex,hot}) \tag{4.40}$$

$$\dot{Q}_{IHX} = \dot{m} \cdot (h_{ex,cold} - h_{su,cold}). \tag{4.41}$$

With cp_{min} the lower specific heat capacity between the hot and the cold flow.

4.2.3 Economizer

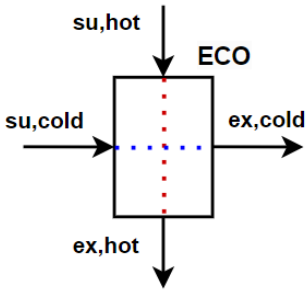

Figure 4.7: Economizer.

For the economizer heat exchanger, two variables need to be specified. The first is the efficiency ϵ_{ECO}, which is set at 0,9 to achieve significant heat transfer while keeping the exchanger relatively small. The second variable in this model is the outlet temperature of the cold fluid, which will be set to achieve a superheat of 1K. This ensures that the injected vapor will be slightly superheated, preventing wet compression. The quantity of heat transfered is calculated with

$$\dot{Q}_{ECO} = \epsilon_{ECO} \cdot \dot{C}_{min} \cdot (T_{su,cold} - T_{su,hot}) \tag{4.42}$$

$$\dot{Q}_{ECO} = \dot{m} \cdot (h_{su,hot} - h_{ex,hot}) \tag{4.43}$$

$$\dot{Q}_{ECO} = \dot{m} \cdot (h_{ex,cold} - h_{su,cold}). \tag{4.44}$$

Where ,

$$\dot{C}_{min} = min(\dot{C}_{hot}; \dot{C}_{cold}) \quad \text{and} \quad \begin{cases} \dot{C}_{hot} & = \dot{m}_{hot} \cdot cp_{hot} \\ \dot{C}_{cold} & = \dot{m}_{cold} \cdot cp_{cold} \end{cases} \tag{4.45}$$

4.2.4 Cascade condenser/evaporator

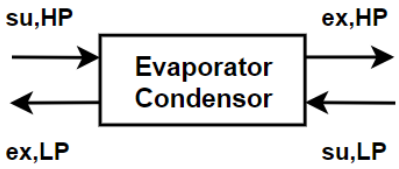

Figure 4.8: Cascade heat exchanger.

The difference between the condensation temperature of the low pressure cycle and the evaporation temperature of the high pressure cycle (i.e. the approach temperature) assumed to be 5K:

$$T_{ev,HP} = T_{cd,LP} - 5 \tag{4.46}$$

Moreover, the high pressure cycle evaporator overheating as well as the low pressure cycle condenser subcooling are fixed to 0K. Indeed, the superheating and subcooling will be ensured by the internal heat exchangers present in both low-pressure and high-pressure cycles. The quantity of heat trasnfered is calculated with the same equation as for the other condenser and evaporator :

$$\dot{Q} = \dot{m}_{cold} \cdot (h_{ex,cold} - h_{su,cold}) \tag{4.47}$$

$$\dot{Q} = \dot{m}_{hot} \cdot (h_{su,hot} - h_{ex,hot}) \tag{4.48}$$

4.3 Specific components

4.3.1 Flash tank

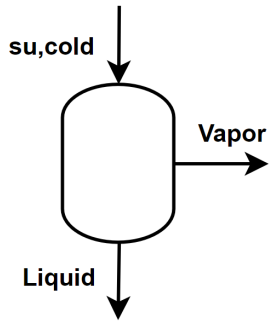

(a) Vapor injection.

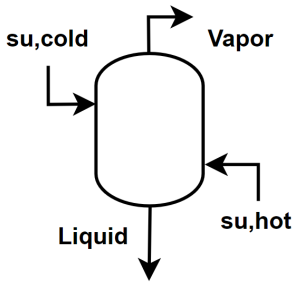

(b) Total de-superheating.

Figure 4.9: Flash tank

Mass and energy balance are used to calculate mass flow rates :

$$\dot{m}_{su,cold} + \dot{m}_{su,hot} = \dot{m}_{vapor} + \dot{m}_{liquid}. \tag{4.49}$$

$$\dot{m}_{su,cold} \cdot h_{su,cold} + \dot{m}_{su,hot} \cdot h_{su,hot} = \dot{m}_{vapor} \cdot h_{vapor} + \dot{m}_{liquid} \cdot h_{liquid}. \tag{4.50}$$

Obviously, when the heat pump is in vapor injection configuration (Figure 4.9a), both $h_{su,hot}$ and $\dot{m}_{su,hot}$ are zero.

4.3.2 Mixer

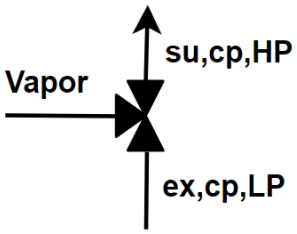

Figure 4.10: Mixer.

This process is assumed to be instantaneous and isobaric. The mass flow rates and the enthalpy are calculated using mass and energy balance :

$$\dot{m}_{su,HP} = \dot{m}_{ex,LP} + \dot{m}_{vapor}, \tag{4.51}$$

$$\dot{m}_{su,HP} \cdot h_{su,HP} = \dot{m}_{ex,LP} \cdot h_{ex,LP} + \dot{m}_{vapor} \cdot h_{vapor}. \tag{4.52}$$

4.3.3 Expansion valve

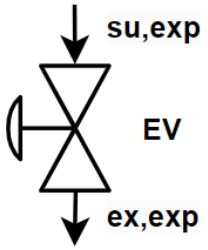

Figure 4.11: Expansion valve.

The expansion is assumed to be isenthalpic.

$$\mathrm{h_{su,exp}} = \mathrm{h_{ex,exp}} \tag{4.53}$$

4.4 Performances

The coefficient of performance (COP) will be calculated for each cycle using the following formulas :

- Single stage configurations :

$$COP = \frac{\dot{Q}_{cd}}{\dot{W}_{real}} \tag{4.54}$$

- Two-stage configurations :

$$COP = \frac{\dot{Q}_{cd}}{\dot{W}_{real,LP} + \dot{W}_{real,HP}} \tag{4.55}$$

The volumetric heating capacity (VHC) of the fluid will also be evaluated :

- Single stage configurations :

$$VHC = \frac{\dot{Q}_{cd}}{\frac{\dot{m} \cdot v_{su}}{\eta_{vol}}} \tag{4.56}$$

- Two-stage configurations :

$$VHC = \frac{\dot{Q}_{cd}}{(\frac{\dot{m}_{LP} \cdot v_{su,LP}}{\eta_{vol,LP}} + \frac{\dot{m}_{HP} \cdot v_{su,HP}}{\eta_{vol,HP}})} \tag{4.57}$$

Chapter 5

Results

5.1 Model validation

The models developed in the previous section depend on several parameters and assumptions. Since these parameters and assumptions are mostly approximations or results from various studies, it is crucial to verify whether the compressor and heat pump models are realistic and align with what has been previously established in the literature. Given that this study focuses on a purely theoretical and general model, a traditional model validation is not performed. However, the results obtained are compared qualitatively to assess their relevance.

5.1.1 Compressor models

The isentropic and volumetric efficiencies of a compressor are among its most critical characteristics. Their variations directly impact compressor performance, the required electrical power, and thus the overall performance of the heat pump. It is therefore crucial to verify that the compressor models, whether with or without injection, are relevant.

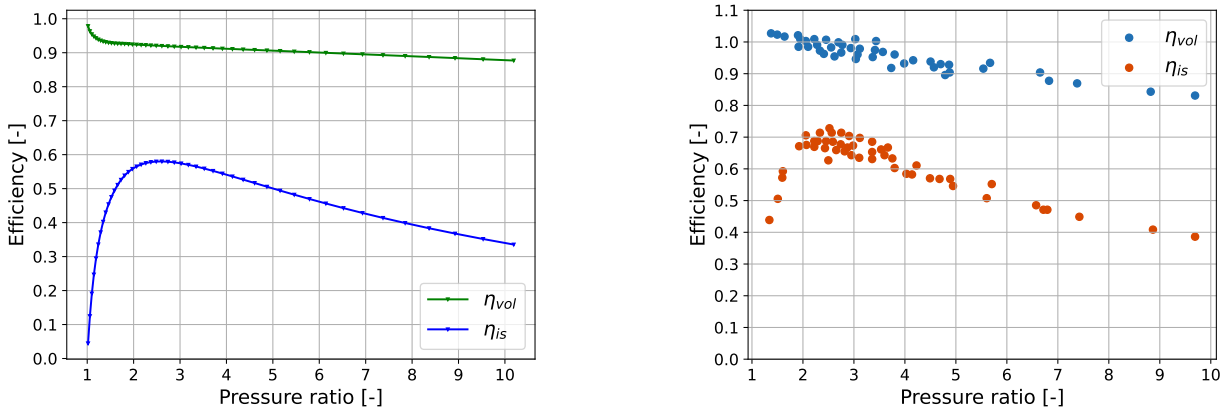

(a) Results from the model.

(b) Experimental results [60].

Figure 5.1: Isentropic and volumetric efficiency without vapor injection.

First, the compressor model without injection is compared to the experimental results obtained during the characterization of a scroll compressor [60]. In this initial comparison, the internal volume ratio is arbitrarily fixed to $r_{v,in}$ = 3. The results obtained from the model (Figure 5.1a) show that both curves, for isentropic and volumetric efficiencies, are very similar to the experimental results(Figure 5.1b) and for scroll compressor in general. Indeed, scroll compressors exhibit higher efficiency when operating near their optimal internal volume ratio and this efficiency can decline rapidly if the compressor operates under pressure or temperature conditions that deviate from its design specifications. This particularity of the scroll compressor is well represented in both Figure 5.1a and Figure 5.1b.

For the compressor with vapor injection, the results obtained experimentaly by [70] are used to compare the variation of the volumetric and isentropic efficiency. As for the compressor without injection, the internal volume ratio is fixed to $r_{v,in}$ = 3.

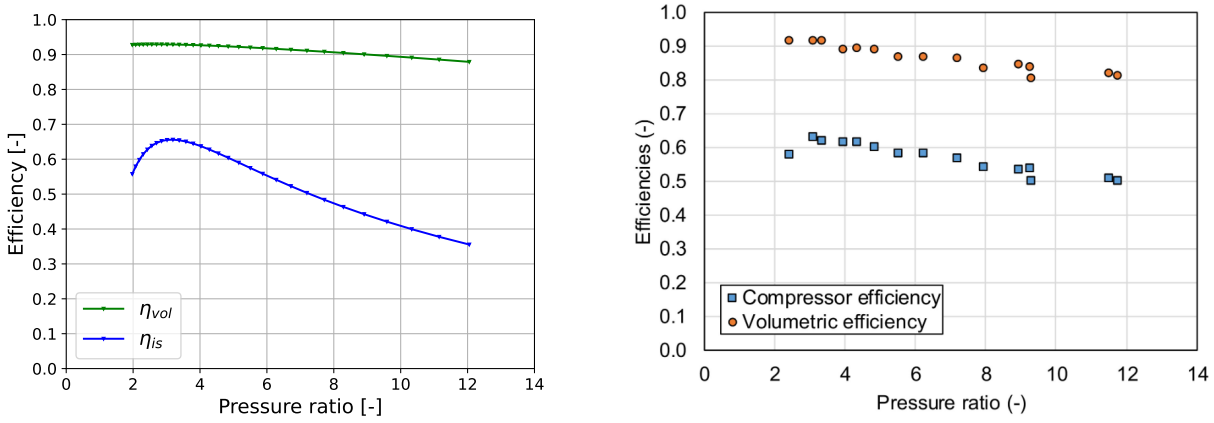

(a) Results from the model.

(b) Experimental results [70].

Figure 5.2: Isentropic and volumetric efficiency with vapor injection.

Both Figure 5.2a and Figure 5.2b show that volumetric efficiency remains relatively stable as the pressure ratio increases, although the experimental data presents a slight decrease at higher pressure ratios. However, there is a notable difference in the trend of isentropic efficiency. The model shows a rapid decline after the initial peak, while the experimental data indicates a more gradual decrease which is not surprising as the vapor injection compressor are specifically design for high pressure ratio. These results from the model suggest that it accurately captures the stability of volumetric efficiency but may underestimate the consistency of isentropic efficiency at higher pressure ratio for scroll injection compressor.

Despite the differences observed between the model predictions and experimental data, both models provide valuable qualitative results. Given the primary qualitative nature of the comparisons, these models are sufficiently reliable to be used for this thesis.

5.1.2 Heat pump cycles

The compressor is one of the main components of a heat pump, but the other components are also important. Therefore, it is crucial to ensure that the different configurations models are coherent and relevant.

Configurations without vapor injection compressor :

A recent study [37] will be used for comparison purposes. They investigates several configurations of heat pumps and compare their theorical performances based on the temperature lift. To obtain a relevant comparison, the model was subjected to the same operating conditions as the experimentally tested cycles. Although these conditions are not the ones in which the heat pump modeled in this work will operate, they allow us to visualize the behavior of the model based on the variation of several parameters. The simulation conditions are as follows:

- Refrigerant : R245fa
- Internal volume ratio : 2,45
- Condensation temperature : 130°C
- Temperature lift : [30;80]

Given that these illustrations are solely for the purpose of qualitatively comparing the model developed in this work, it is important to note that the curves are similar. Indeed, in all the figures, the performance of each cycle tends to decrease proportionally with the temperature lift.

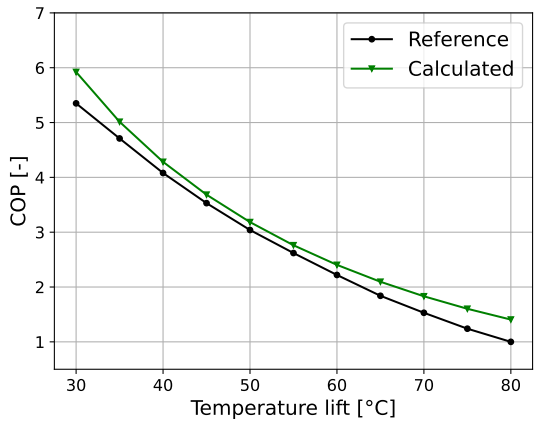

Figure 5.3: Single stage with IHX.

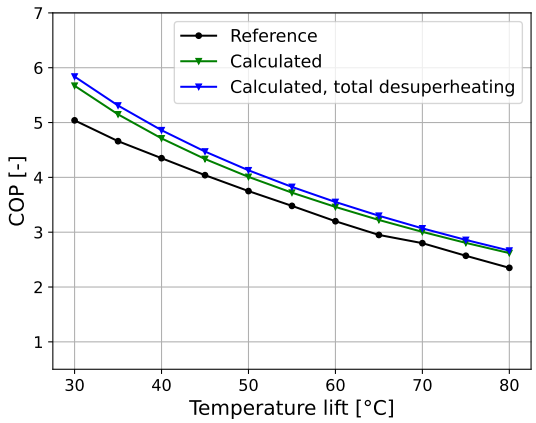

Figure 5.4: FT with IHX and desuperheating.

It is interesting to highlight the more pronounced gap between the curves Figure 5.3 and Figure 5.4. The model tends to overestimate the performance of the cycles compared to the reference. However, as shown Figure 5.3, the reference achieved a very low COP of 1 for a temperature lift of 80°C. This low performance can be attributed to the formula they used to calculate the volumetric efficiency, which more significantly reduces the compressor's volumetric efficiency with high pressure ratio.

The results obtained from the model for the economizer (Figure 5.5 and cascade (Figure 5.6) cycles appear to be closer to those found in the literature. However, it is important to note that the cascade cycle was simulated using the same fluid for both the high and low-pressure sections due to a lack of information on the second refrigerant used by the reference. This can possibly explain the lower performances at high temperature lift.

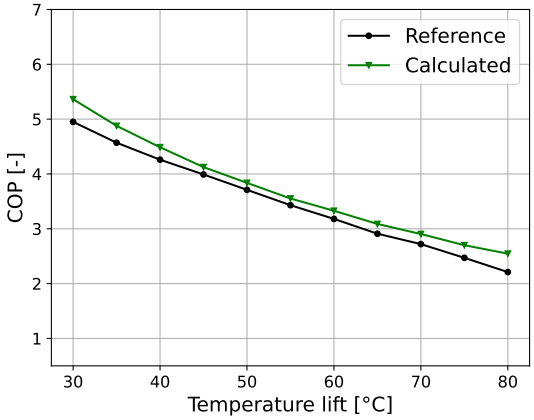

Figure 5.5: Economizer with IHX.

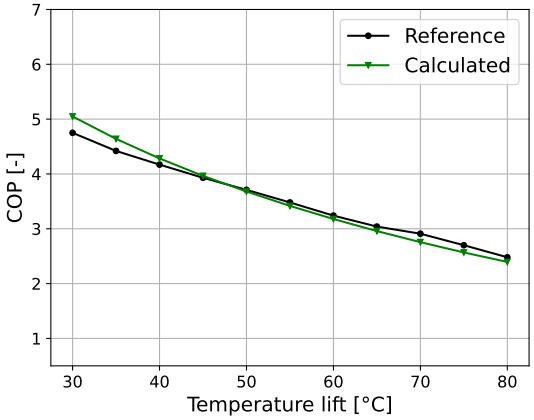

Figure 5.6: Cascade with two IHX.

Configurations with vapor injection compressor :

Although the vapor injection compressor heat pump model is based on the same model as the one without injection, it relies on additional assumptions that need to be verified for relevance. To do this, the results of an semi-empirical model study using a economizer will be used as a reference [36]. As for the configurations without vapor injection compressor, the model was subjected to the same operating conditions as the experimentally tested cycles. The simulation conditions are as follows:

- Refrigerant : R290
- Configuration : Single stage vapor injection compressor with economizer and IHX.
- Internal volume ratio for the VI compressor : 2,98
- Condensation temperature : 50°C and 80°C
- Evaporation temperature : [-30;20]

With the condensation temperature fixed, the only way to vary the temperature lift and pressure ratio is by adjusting the evaporation temperature. This temperature will be increased from -30°C to 20°C, and the corresponding coefficient of performance for each conditions is calculated. The results obtained by the model are illustrated with the experimental results Figure 5.7.

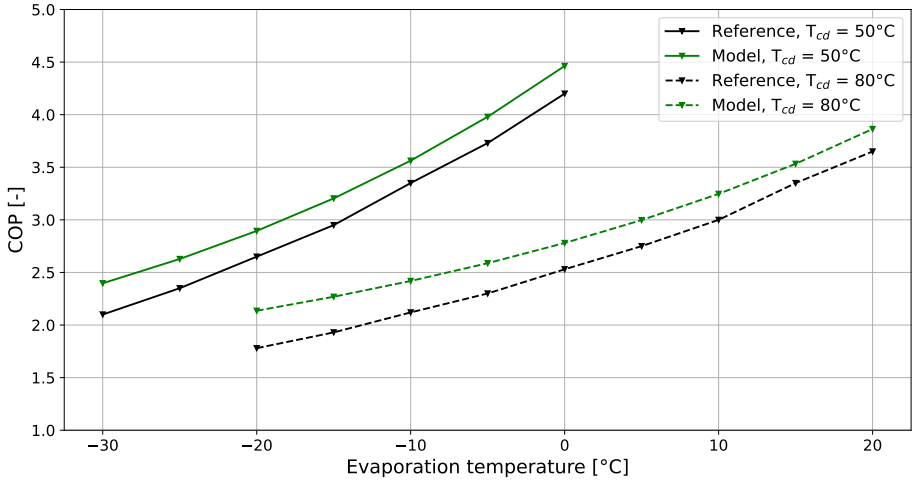

Figure 5.7: Theoretical model comparison to the semi-empirical model reference [36].

Two observations can be made. First, the evolution of the coefficient of performance (COP) with respect to the evaporation temperature is consistent with the experimental results. However, when analyzing a specific operating condition, a significant difference between the actual COP calculated with the semi-empirical model and the COP obtained from the theoretical model is clearly visible. This overestimation of the performances can be explained by the assumptions made in the model. Indeed, heat losses to the surroundings and pressure drops through the pipes and heat exchangers used in the various configurations are neglected. Additionally, vapor injection and mass flow of injection into the compressor is assumed to be instantaneous and isobaric. While these assumptions are relevant, they do not perfectly represent the actual process [71].

It is evident that the developed models, whether for compressors or heat pump configurations, are not perfect and remain theoretical estimations of reality. Nevertheless, none of them show too significant difference or inconsistent variations compared to real-world data, making them sufficiently reliable for further analysis.

5.2 Case 1 : Single evaporator connected to the cooling circuit

Here is a summary of the operating conditions for the heat pump :

- Refrigerant : R-1233zd(E)
- Nominal heating power : $\dot{Q}_{cd}$ = 36,728kW
- Condensation temperature/pressure : T_{cd} = 140°C / P_{cd} = 22,92 bar
- Evaporation temperature/pressure : T_{ev} = 35°C / P_{ev} = 1,83 bar
- Pressure ratio : r_p = 12,52

5.2.1 Intermediate pressure

To make the variation of the internal volume ratio relevant for the two-stage configurations, the initial assumption of setting the intermediate pressure as the geometric mean of the low and high pressures was modified because the external volume ratios of the two compressors were not equal, and adjusting each internal volume to optimize the efficiency of each compressor made the process too complicated. Therefore, the intermediate pressure is set so that the external volume ratios of the two compressors are equal. It allows the internal volume ratio of each compressor to become a single unique parameter in the model, so that its variation affects both compressors in the same way. The COP of the different two-stage cycles for these two intermediate pressure values were compared, with the same arbitrarely fixed values of the internal volume ratio $r_{v,in}$ = 2,5 and the results shown in Figure 5.8 demonstrate that this new method of determining the intermediate pressure not only simplifies the comparison but also slightly improves the performance of each cycle. The new intermediate pressure calculation method is thus preferred to the old one.

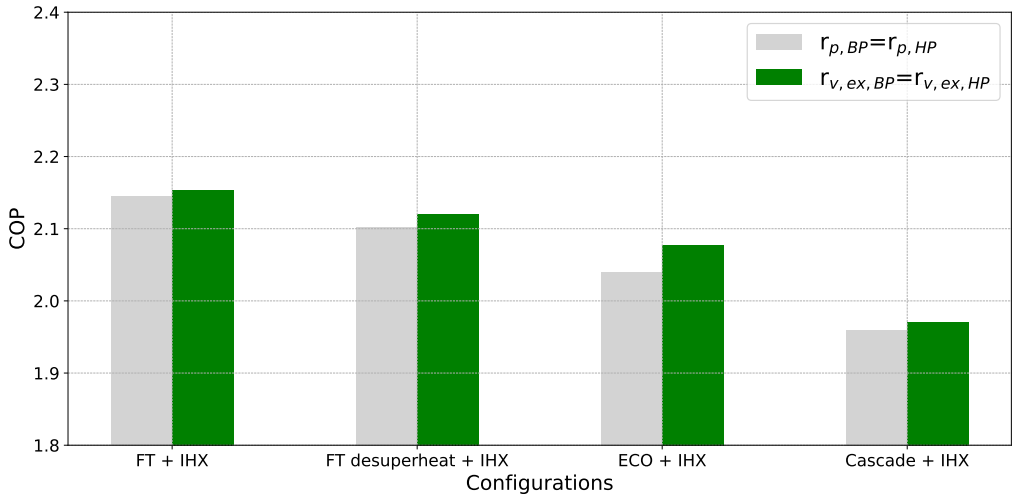

Figure 5.8: Intermediate pressure performance comparison.

5.2.2 Performances

Once the intermediate pressure is fixed, the comparison of the COPs of the different configurations while varying the internal volume ratio can be done and the results are illustrated in Figure 5.9. It demonstrates the low coefficient of performance of the single-stage configuration, particularly, it shows a COP of 1,267 for an internal volume ratios of 2. This can be attributed to the significant difference between the internal and external volume ratios, which implies a lot of under-compression and therefore reduces the isentropic efficiency of the compressor. Additionally, the compressor's volumetric efficiency is significantly reduced due to the particularly high pressure ratio. These combined effects result in a substantial decrease in the cycle's performance. Given that the performance with small internal volume ratio are close to the one that could give a simple electrical heater (COP of 1), it would not be pertinent and practical to use a compressor with a small internal volume ratio for this configurations of the heat pump.

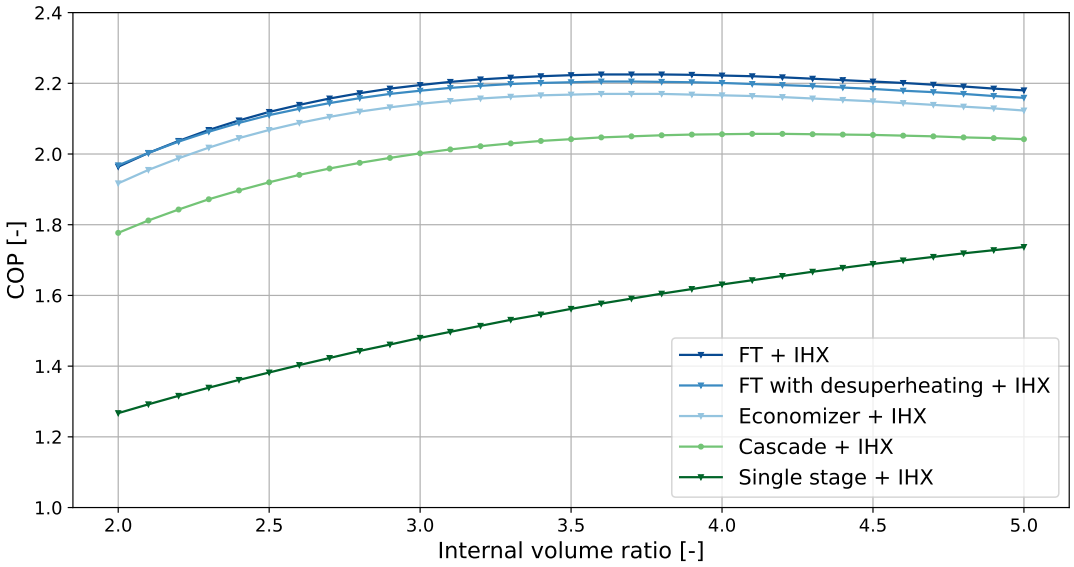

Figure 5.9: Influence of the $r_{v,in}$ and the configurations on the COP.

Then, it can be seen from this figure that the configuration with the best COP, regardless of the internal volume ratio, is the one using the flash tank + IHX. It performs slightly better than the configuration with the flash tank with full desuperheating, which itself slightly outperforms the economizer + IHX configuration. The cascade configuration shows a lower COP compared to the other two-stage configurations, which may be surprising. Typically, this configuration is recommended for high pressure ratios like those present in the operating conditions of the studied heat pump. These bad results are not surprising as the refrigerant used for the low pressure and high pressure cycle is the same one. Therefore, it does no take advantage of the main benefit of the cascade configuration, which is to optimize each cycle with the refrigerant that offers the best performance.

The use of the same refrigerant for both cycles is not a trivial choice. Indeed, the conditions imposed by the pilot project only allow the use of refrigerants classified in the ASHRAE [25] A1 category. The three refrigerants belonging to this category that have at the same time a low ODP and GWP, and a sufficiently high critical temperature to bu used in the low pressure cycle are the R-1336mzz(Z), R-1336mzz(E), and R-1224yd(E). Unfortunately, the refrigerant R-1336mzz(E) is not listed in EES. Therefore, an analysis of the performance of the cascade configuration with only the R-1336mzz(Z) and R-1224yd(E) in the low pressure cycle was conducted.

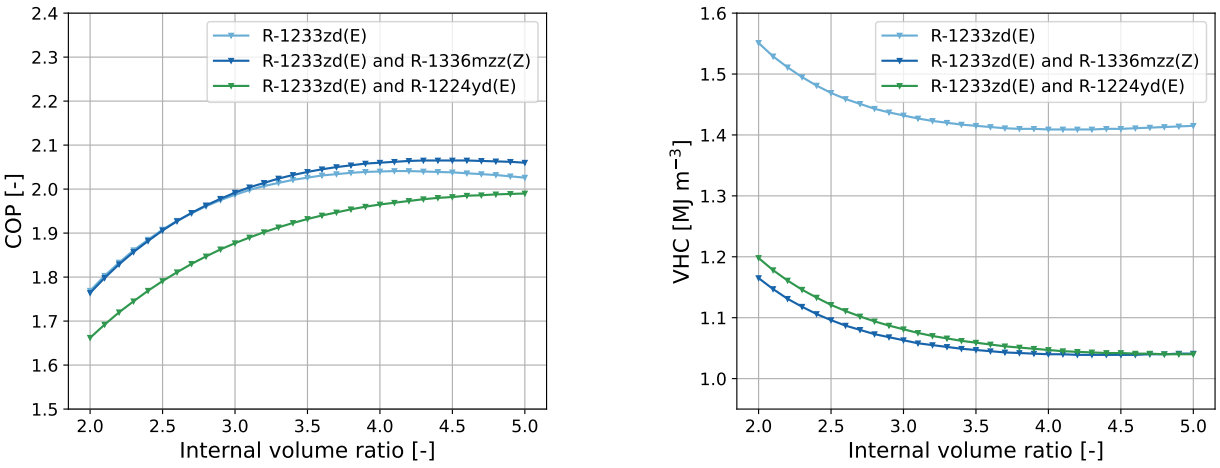

(a) COP with different refrigerants.

(b) VHC with different refrigerants.

Figure 5.10: Performances comparison with different refrigerants.

The results illustrated in Figure 5.10 clarify the choice of using R-1233zd(E) for both cycles. Indeed, it can be observed from Figure 5.10a that only the refrigerant R-1336mzz(Z) offers a better COP, increasing it by 1,2% for an internal volume ratio of 4,5. This increase could be interesting if R-1336mzz(Z) did not have such a large specific volume. Observing Figure 5.10b, it is evident that the configuration using only R-1233zd(E) has a volumetric heating capacity significantly (approximately 30%) higher than the other two refrigerants. This property can significantly reduces the size of the various components of the heat pump and thus significantly reduces its cost. The small COP increase when using the R-1336mzz(Z) refrigerant is therefore not sufficiently interesting and the best option is to use R-1233zd(E) for both the low and high-pressure cycles.

5.2.3 Evaporator available heating power

In Chapter3, a basic cycle of heat pump was used to fixe the operating conditions and specifically the evaporation temperature of the heat pump to 35°C. However, with the optimization of the heat pump,

the two-stage with flash tank configuration exhibits a higher COP, necessitating greater heating power at the evaporator. This required heating power at the evaporator is 22.533 kW and can no longer be met if the evaporation temperature remains at 35°C. Therefore, a new analysis of the evaporator's heating requirements as a function of the evaporation temperature must be realised.

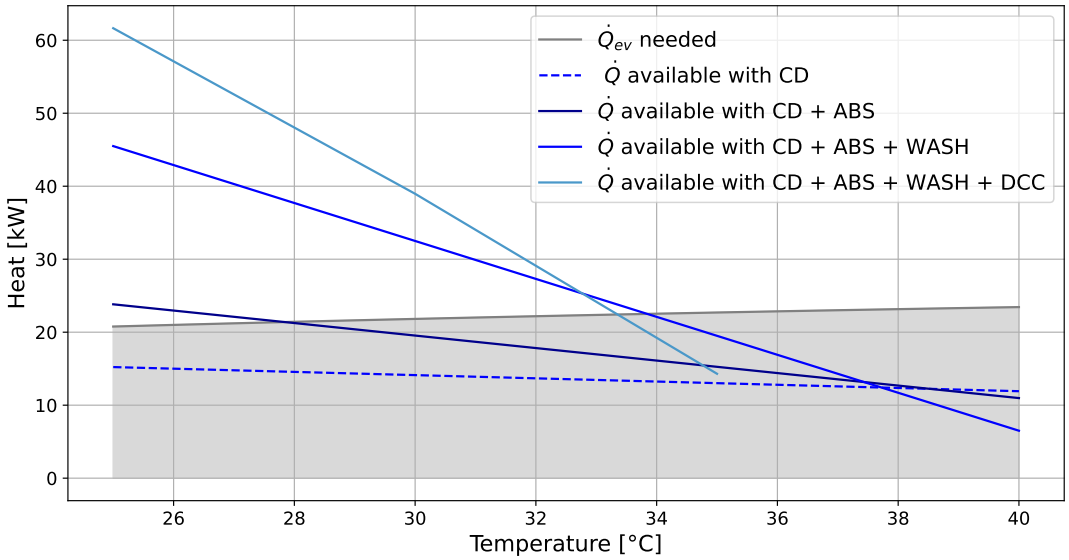

Figure 5.11: Evaporator heat duty in function of the evaporation temperature.

The results, illustrated in Figure 5.11, show that the highest evaporator temperature that can be used to meet the heating power required at the evaporator is 33,83°C which can be rounded to 33°C.

This new evaporator temperature leads to a small decrease of the performances that are illustrated in Figure 5.12. The configuration using two compressors and a flash tank with IHX remains the best and presents a maximal COP of 2,18 with an internal volume ratio of 3,7.

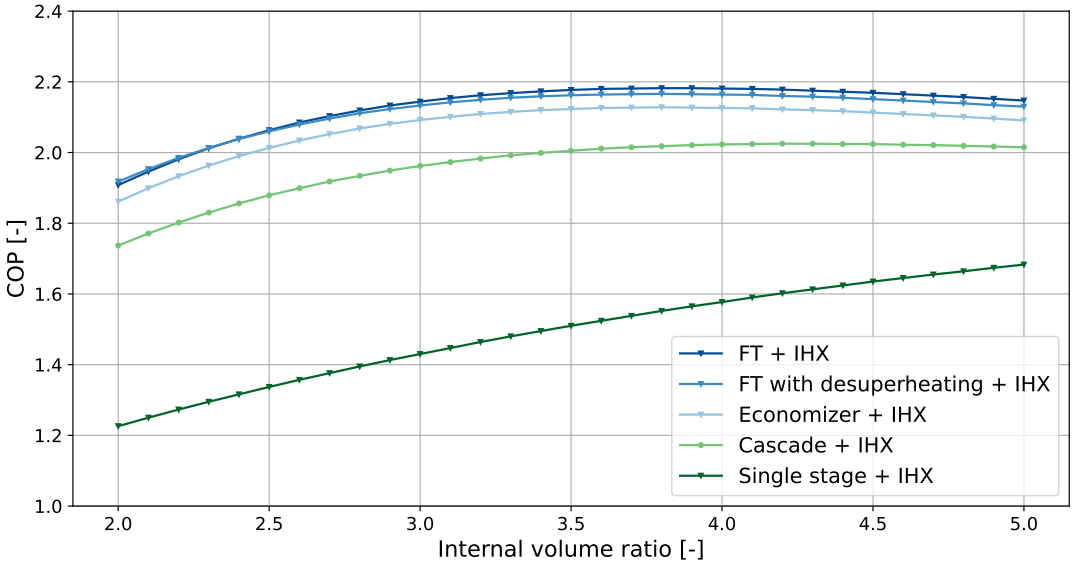

Figure 5.12: New performances of the different configurations while varying the internal volume ratio.

5.2.4 Compressor sizing

With the optimal configuration for Case 1 using a single evaporator identified, the sizing of each compressor can now be performed :

Low pressure compressor :

- Nominal power at 3000rpm : $W_{LP} = 6,926$ kW
- Displacement volume : $V_{LP} = 3,915 \cdot 10^{-4}$ m^3
- Internal volume ratio : $r_{v,in} = 3,7$
- Supply/exhaust pressure : 1,711 bar / 7,057 bar

High pressure compressor :

- Nominal power at 3000rpm : $W_{HP} = 9,910$ kW
- Displacement volume : $V_{HP} = 1,756 \cdot 10^{-4}$ m^3
- Internal volume ratio : $r_{v,in} = 3,7$
- Supply/exhaust pressure : 7,057 bar / 22,920 bar

5.3 Case 2 : Two evaporators

As for the first case, here is a reminder of the operating conditions for the heat pump :

- Refrigerant : R-1233zd(E).
- Nominal heating power : $\dot{Q}_{cd}$ = 36,728kW.
- Condensation temperature/pressure : T_{cd} = 140°C / P_{cd} = 22,920 bar.
- Middle pressure evaporator temperature/pressure : T_{ev} = 71°C / P_{ev} = 5,246 bar
- Heating power avalaible at medium pressure : $\dot{Q}_{ev,1}$ = 10,930 kW
- Low pressure evaporator temperature/pressure : T_{ev} = 35°C / P_{ev} = 1,83 bar.
- Middle to high pressure ratio : r_p = 4,369.
- Low to middle pressure ratio : r_p = 2,867.
- Total pressure ratio : r_p = 12,52.

As prevously introduced in Chapter 3, all the configurations studied in this case use an internal heat exchanger for the low pressure part of the cycle and the internal volume ratio of the compressor is fixed to his optimal value of $r_{v,in}$ = 2,8. The comparison in this case is therefore focused on the different configurations use for the high pressure part of the cycle. The chosen method to calculate the intermediate pressure is the one already developed for the first case, this pressure is set to have the external volume ratio of each compressors equal and allows the variation of the internal volume ratio to affect the compressors in the same way.

5.3.1 Performances

The values of the COP while varying the internal volume ratio of the high pressure compressors are illustrated in Figure 5.13. The first observation is that using two compressors for the high-pressure part of the heat pump achieves its best performance at smaller internal volume ratios. This type of configuration is designed for high pressure ratios, therefore, smaller pressure ratio leads to overcompression, which decreases the isentropic efficiency of the compressors and, consequently, the performance of the heat pump. On the other hand, the configurations using a single compressor shows the opposite behavior. Indeed, smaller pressure ratio reduces undercompression in the compressor, thereby increasing its isentropic efficiency and the performance of the heat pump. Moreover, it can be noted the remarkable 21% increases of the performances of the single stage configuration when using vapor injection compressor.

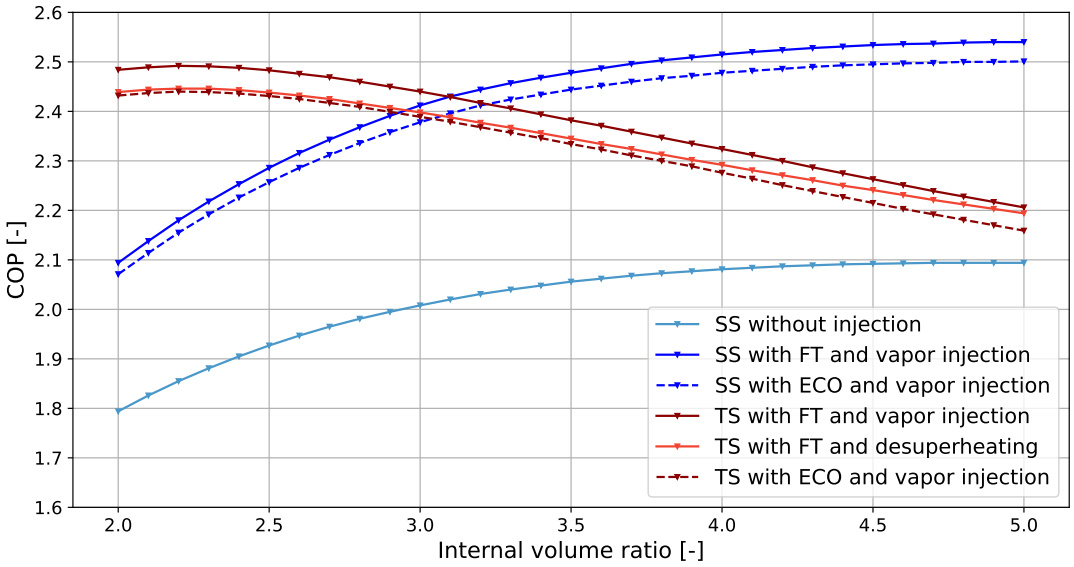

Figure 5.13: Influence of $r_{v,in}$ and configurations on the COP.

5.3.2 Evaporator available heating power

In this case, the evaporator is directly connected to the washer, it is important to verify that it could provide the heating power required for an evaporation temperature of 35°C. Using the best results, this required heating power is $\dot{Q}_{ev}$ = 13,110 kW and the total power available at the washer is $\dot{Q}_{\text{washer}}$ 17,433 kW. However this is the power if the water is cooled down from 47,5°C to 37,5°. As already explained, each heat exchanger has a temperature approach of 5K, so the real power available at the washer if the evaporator temperature is 35°C is the power available if the water is cool down from 47,5°C to 40°C :

$$\dot{Q}_{\text{washer}} = 7,5 \cdot 1,754\text{kW} = 13,074\text{kW} < 13,110\text{kW} = \dot{Q}_{ev} \tag{5.1}$$

As the heating requirement can not be satisfied, the same analysis of the evaporator heating requirements as a function of the evaporation temperature did for the first case must be realised. The results are illustrated in Figure 5.14 and shows that the intersection of the two lines is just below 35°C. The new evaporation temperature is therefore fixed to 34°C

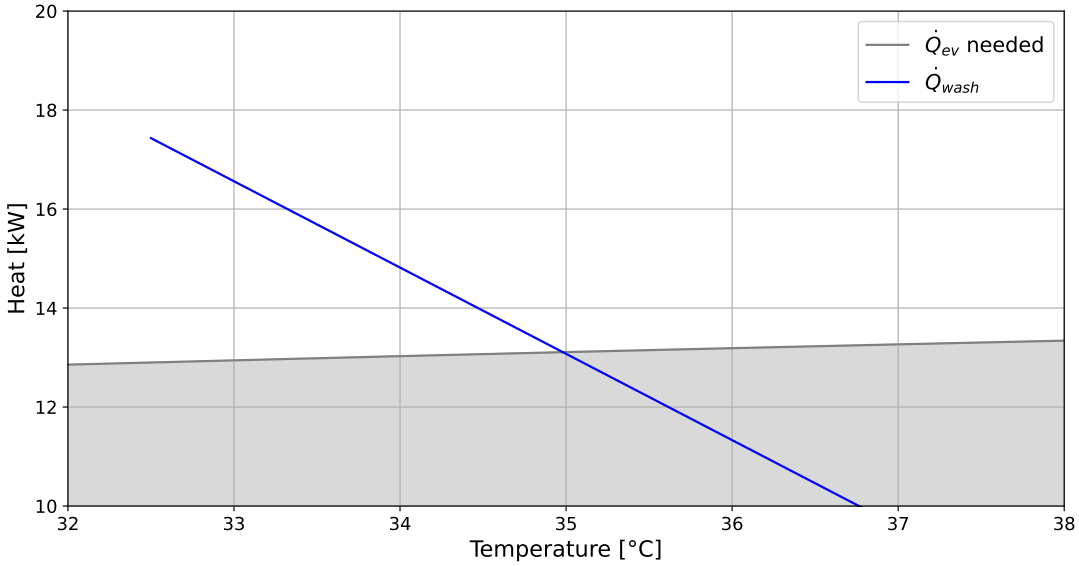

Figure 5.14: Evaporator heat duty in function of the evaporation temperature.

The new results, calculated with this evaporation temperature of 34°C are illustrated in Figure 5.15. As the temperature lift and pressure ratio slightly increases with the new evaporation temperature, the COP of the best configurations is therefore slightly reduce to 2,47 for the configurations using a flash tank with two compressors and to 2,52 for the configuration using a flash tank with one vapor injection compressor.

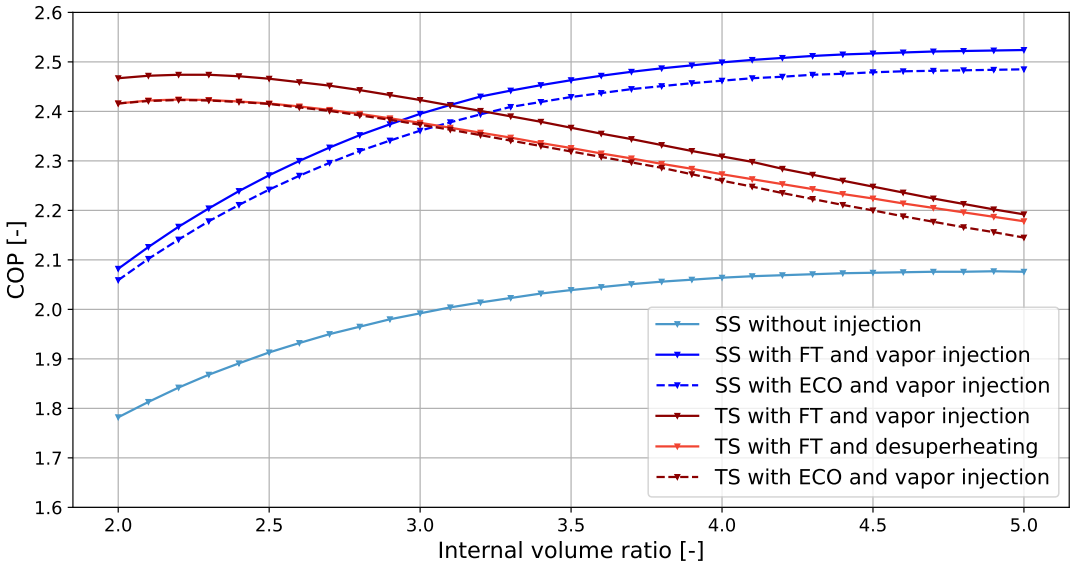

Figure 5.15: Influence of $r_{v,in}$ and configurations on the COP.

5.3.3 Compressor sizing

With the optimal configuration for Case 2 using two evaporators being identified, the sizing of each compressor can now be performed :

1) Two-stage with flash tank and vapor injection compressor

Low pressure compressor :

- Nominal power at 3000rpm : $W_{LP} = 3,692$ kW
- Displacement volume : $V_{LP} = 2,569 \cdot 10^{-4}$ m^3
- Internal volume ratio : $r_{v,in} = 2,8$
- Supply/exhaust pressure : 1,770 bar / 5,246 bar

Vapor injection compressor :

- Nominal power at 3000rpm : $W_{inj} = 10,860$ kW
- Displacement volume for the first isentropic compression : $V_{inj,1} = 1,69 \cdot 10^{-4}$ m^3
- Displacement volume for the second isentropic compression : $V_{inj,2} = 1,136 \cdot 10^{-4}$ m^3
- Internal volume ratio : $r_{v,in} = 5$
- Supply/exhaust pressure : 5,246 bar / 22,920 bar

2) Three stages with flash tank

Low pressure compressor :

- Nominal power at 3000rpm : $W_{LP} = 3,933$ kW
- Displacement volume : $V_{LP} = 2,737 \cdot 10^{-4}$ m^3
- Internal volume ratio : $r_{v,in} = 2,8$.
- Supply/exhaust pressure : 1,770 bar / 5,246 bar

Medium pressure compressor :

- Nominal power at 3000rpm : $W_{MP} = 4,959$ kW
- Displacement volume : $V_{MP} = 1,717 \cdot 10^{-4}$ m^3
- Internal volume ratio : $r_{v,in} = 2,2$
- Supply/exhaust pressure : 5,246 bar / 11,469 bar

High pressure compressor :

- Nominal power at 3000rpm : $W_{HP} = 5,952$ kW
- Displacement volume : $V_{HP} = 1,104 \cdot 10^{-4}$ m^3
- Internal volume ratio : $r_{v,in} = 2,2$
- Supply/exhaust pressure : 11,469 bar / 22,920 bar

5.4 Energy consumptions

5.4.1 Energy saving

The goal of this thesis being to find the optimal configurations to minimize the energy consumption of the carbon capture pilot plant, Table 5.1 summarizes the COP and energy consumption for each case and optimal configurations. The results show a significant reduction in energy consumption at the reboiler, reaching up to 60.6% for the second case with a two-stage flash tank with vapor injection compressor and internal heat exchanger configurations. As discussed in Chapitre 1, this energy consumption is one of the main obstacles to the industrial development of post-combustion capture processes using amines such as the one studied in this work. These results are therefore encouraging and may increase interest in this technology of CO_2 capture process.

	Case 1	**Case 2**	
Optimal configuration	Two-stage FT with IHX	Two stage FT with VI compressor and IHX	Three stage FT with IHX
COP	2,18	2,52	2,47
Total power [kW]	16,836	14,552	14,843
Energy consumption [GJ/ton CO_2]	1,662	1,427	1,456
Energy saving [%]	54,1	60,3	59,5

Table 5.1: Summary of performances and energy consumptions for each case and configurations.

5.4.2 Load variation

One of the objectives of the CO2 capture pilot project will be to analyze the process performance, particularly when its capacity decreases or increases. This means that the power required at the reboiler will not be fixed to the nominal value but will vary depending on the experiments conducted on the pilot. Therefore, an analysis of performance at partial load or increased load is necessary for each case. Although the utilization plan for the capture pilot plant is not yet well defined, an estimate of the variations in the amount of CO_2 captured suggests that the power required at the reboiler would range from a minimum of 10 kW to a maximum of 70 kW.

The most commonly used methods to vary the power of a heat pump are varying the rotational speed, changing the displacement volume, using a bypass, or simply turning the heat pump on and off [22]. For scroll compressors and for a load reduction ratio below 5, the use of a variable-speed compressor is preferred over other techniques [72] [73][74]. Under these conditions, it is the variation in the compressor's rotational speed that will vary the heat pump's power.

To perform a valuable load variation performance analysis, each compressor is sized for the nominal power, therefore the displacement volume, the leakage Area and the internal volume ratio of each compressor are fixed. The analysis is done for the best configurations of each cases and the results are represented in Figure 5.16.

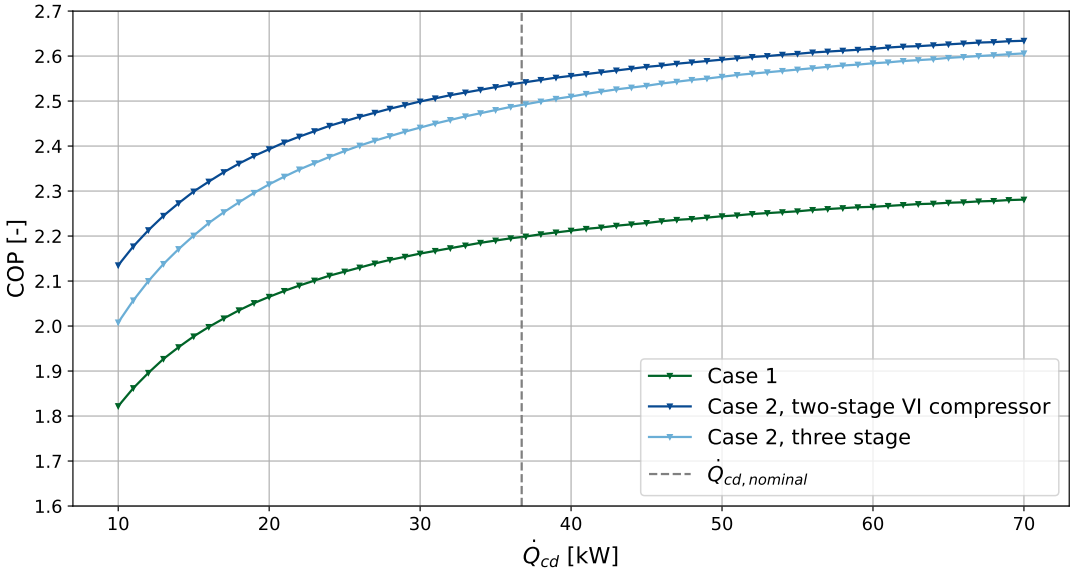

Figure 5.16: COP variation with the load for the different configurations.

The three curves show good performance when the power required at the reboiler increases because the volumetric efficiency of each compressor increases. Indeed, the increase of the rotational speed of each compressor reduces leakage losses. However, it is important to note that friction losses increase as the compressor's rotational speed increases. Since these losses are not accounted for in the models, the increase in COP may be slightly overestimated. Nevertheless, the decreases of the rotational speed has the exact opposite effect on the performances. Indeed, the rotational speed of each compressor for a heat duty of $\dot{Q}_{cd}$ = 10 kW become too small and the increases of leakages losses has a bigger effect on the COP, as illustrated on the left in Figure 5.16. Additionally scroll compressor rotational speeds typically range between 1000 and 10000 rpm. In this analysis, the rotational speed for the minimal and maximal reboiler heat duty corresponds respectively to 950 and 5500 rpm, regardless of the configurations.

This analysis indicates that the compressors are at the lower limit of the operational range for scroll compressors with a reboiler power of 10 kW and also exhibits poor performance at this power level. If this power level is frequently required in the capture pilot's utilization plan, it would be relevant to size the compressor for a lower power than the nominal power. This would, on one hand, increase the rotational speed corresponding to 10 kW and move it away from the lower limit of scroll compressors, and on the other hand, improve the performance of the heat pump when operating at this low power level.

Chapter 6

Case 3 : Modification of the process

The primary objective of this thesis was to optimize the integration of a heat pump into the CO_2 capture process without modifying the operating conditions (with 2 bar at the stripper). Now that this objective has been achieved, this chapter will present an analysis of modifications to the process itself. Indeed, decreasing the pressure in the stripper leads to a reduction in the temperature required for CO_2 desorption. This temperature reduction would decrease the temperature lift of the heat pump as well as the pressure ratio, thereby improving the heat pump's performance and especially its COP. However, this required temperature decrease is accompanied by an increase in the reboiler's power demand.

To illustrate this phenomenon, the temperature at the base of the stripper and the reboiler heat duty were calculated for stripper pressures of 1.75, 1.5, 1.25, 1, 0.75, and 0.5 bar. The results, represented in Figure 6.1, do not allow for determining the optimal pressure directly. To do this, this chapter will consider each stripper pressure, analyze which heat pump configurations would yield the best results and COP, and finally compare the results and the total energy consumption of the compressor for each considered pressure.

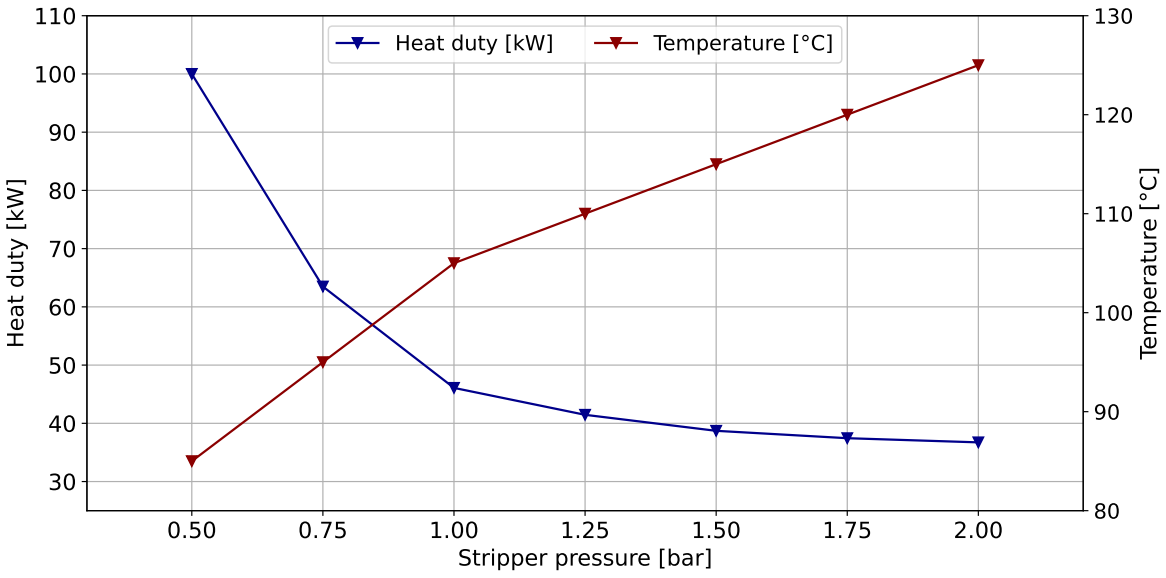

Figure 6.1: Stripper pressure influence on the stripper temperature and reboiler heat duty.

6.1 Operating conditions

Although most of the flow rates, temperatures, and pressures remain identical in the part of the process including the absorber, the direct contact cooler and the washer, the reduction in stripper temperature and the increase in reboiler heat duty nevertheless impact the flow rate and temperature of the mixture exiting the stripper, which consists of CO2 and water vapor. This, in turn, alters the amount of recoverable heat at the condenser at the stripper outlet. As shown in Figure 6.2, these temperatures and heating/cooling power must be determined to establish the operating conditions of the heat pump for each pressure.

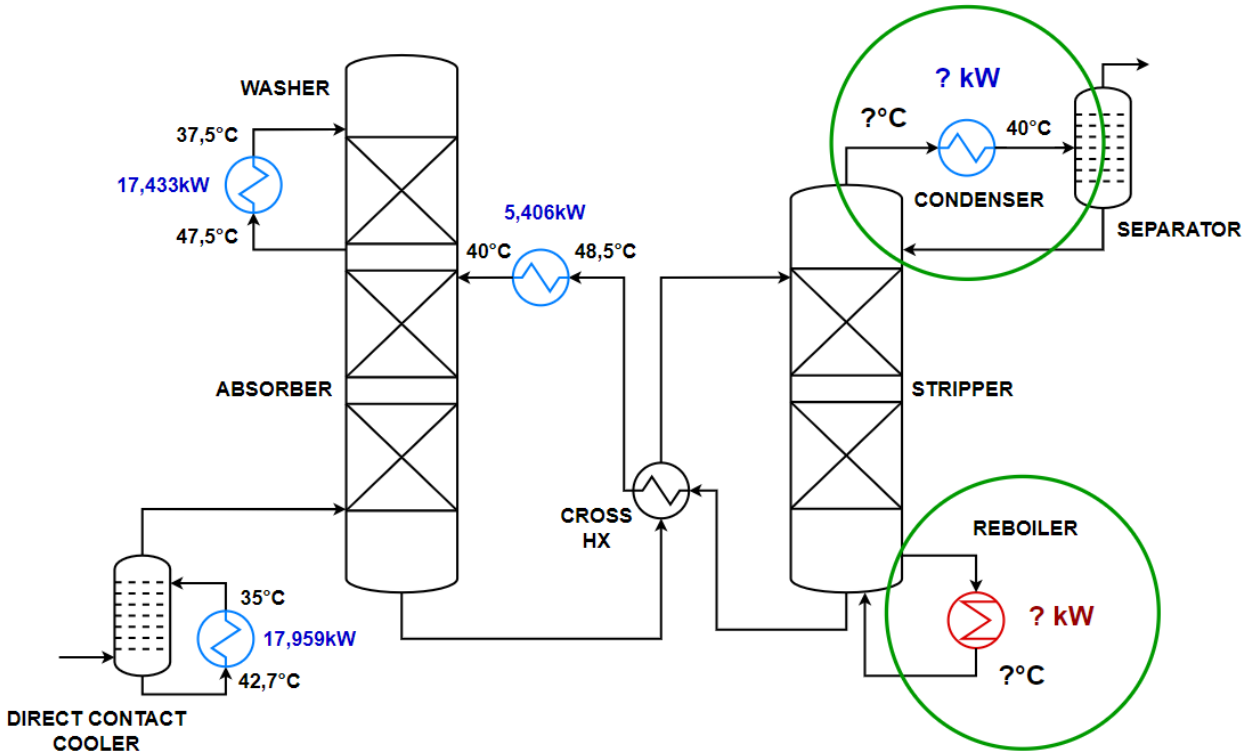

Figure 6.2: Unknowns new operating conditions.

The first part of this study showed that using the high temperature avalaible at the outlet of the stripper by dividing the condensation process into two stages with a heat pump featuring two evaporators at different pressures (case 2) resulted in better performance compared to a heat pump simply connected to the cooling circuit using a single evaporator (case 1). Therefore, only the configuration with two evaporators will be used to determine the optimal stripper pressure.

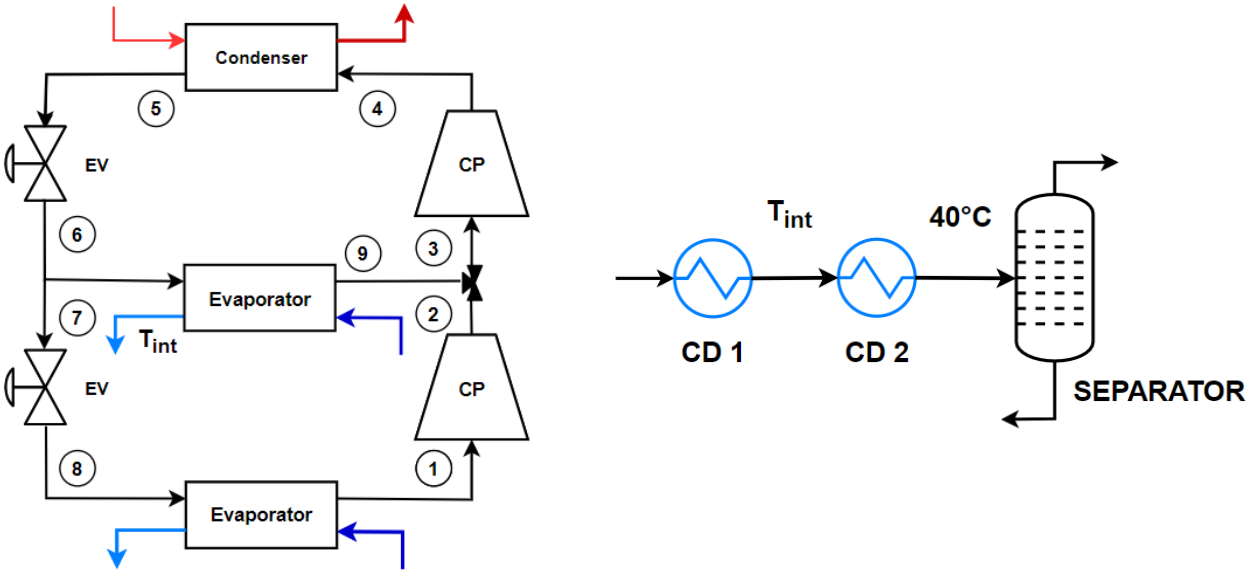

(a) Two evaporators configuration.

(b) Condenser separation.

Figure 6.3: Two evaporators heat pump specifications.

Figure 6.3 serves as a reminder. To use this configuration, the condenser at the stripper outlet must be separated into two stages, and the intermediate temperature that offers the highest COP must be determined for each set of operating conditions corresponding to each pressure. However since the procedure has already been detailed in Chapter 3, it will not be reiterated for each pressure in this chapter and the operating conditions are therefore summarized in Table 6.1.

Stripper pressure [bar]	**1,75**	**1,5**	**1,25**	**1**	**0,75**	**0,5**
Heat duty / $\dot{Q}_{cd}$ [kW]	37,445	38,712	41,462	46,084	63,487	100
Condensation temperature [°C]	135	130	125	120	110	100
Condensation pressure [bar]	20,92	19.06	17,34	15.73	12.86	10.39
Intermediate power available [kW]	11,28	12,37	14,273	19,074	30,9	59,23
Intermediate evaporator temperature [°C]	69,4	67.8	66,7	66,5	65,7	64,9
Intermediate evaporator pressure [bar]	5,032	4,82	4,68	4,66	4,54	4,467
Low evaporator temperature [°C]	35	35	35	35	35	35
Low evaporator pressure [bar]	1,83	1,83	1,83	1,83	1,83	1,83
Low to medium pressure ratio	2,75	2,637	2,561	2.548	2,481	2,441
Medium to high pressure ratio	4,158	3,952	3,701	3,377	2,836	2,33
Total pressure ratio	11,43	10,42	9,47	8,6	7,03	5,68

Table 6.1: Heat pump operating conditions for each stripper's pressure.

6.2 Simulation and results

6.2.1 Heat pump configurations

In order to analyze the performance corresponding to each set of operating conditions as effectively as possible, the results from the previous chapter are used. Specifically, to avoid redundancy and facilitate the interpretation of the results, only the configurations that demonstrated the highest COP will be employed and analyzed in this chapter. Therefore, the configuration employing two compressors and a flash tank (FT) for the high pressure part of the cycle, as well as the configuration using one compressor featuring vapor injection and a flash tank for the high pressure cycle, are illustrated as a reminder in Figure 6.4. As for the first and second case, the intermediate pressure for the two-stage configurations is fixed to obtain the same external ratio for each compressors in order to make the variation of the internal volume ratio relevant.

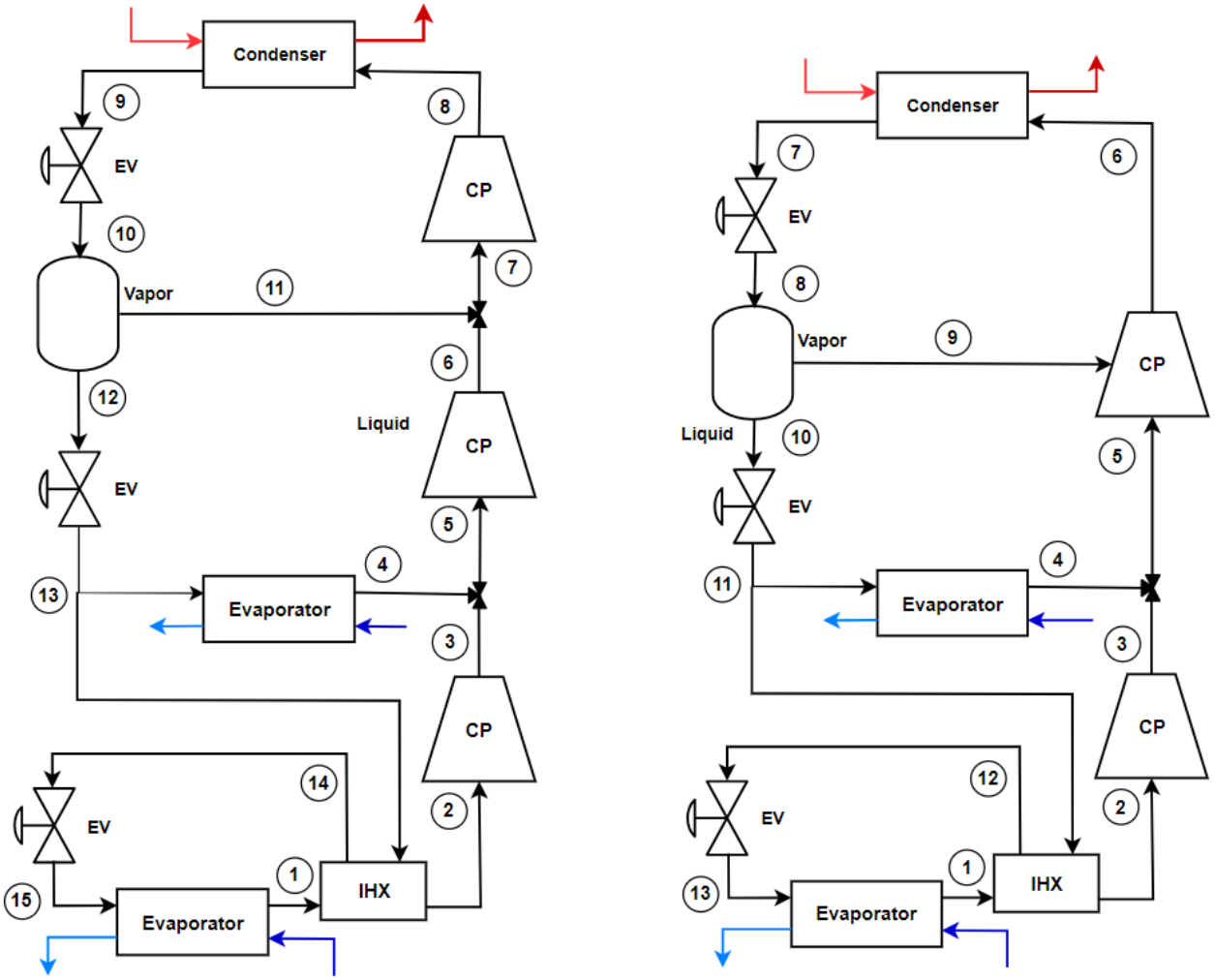

(a) TS with FT.

(b) SS with FT.

Figure 6.4: Best configurations used in this chapter.

6.2.2 Two-stage FT

Figure 6.5 shows the evolution of the COP for the configuration using two compressors and a flash tank in the high-pressure part of the cycle as a function of the internal volume ratio of each compressor and for each pressure level in the stripper studied except 0.5 bar. Indeed, the required heat duty at the reboiler for this pressure became too significant, making the calculated values for the heat pump irrelevant. In order to not make the analysis and visualization of the important results harder, the results obtained for this pressure are not represented in this chapter.

As expected, it shows that the COP increases as the pressure in the stripper decreases. Moreover, it can be observed that the internal volume ratio of the two compressors has an increasing influence due to the decrease in the pressure ratio from medium to high pressure which significantly deteriorates the performance of the two-compressor cycle. This cycle is recommended for high pressure ratios and exhibits therefore substantial overcompression in each compressor.

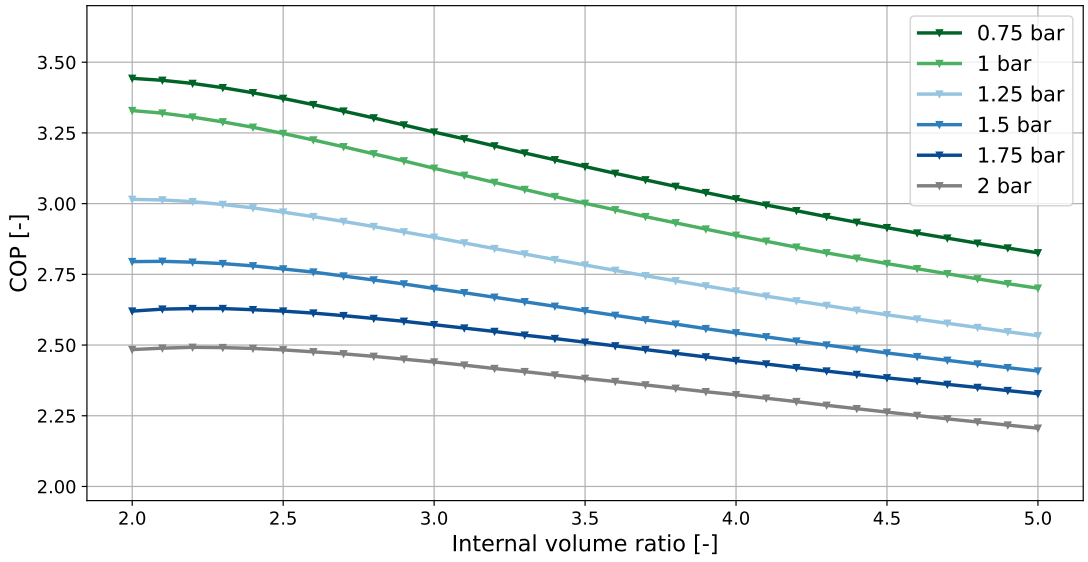

Figure 6.5: Effect of the stripper pressure and $r_{v,in}$ on the COP for the three stages configurations.

6.2.3 Single stage FT with vapor injection compressor

As with the previous configuration, the performance and consequently the COP of the heat pump also increase. However, this increase is more pronounced; since this configuration uses only one compressor, it is better suited to the lower pressure ratios compared to the previous configuration. Nevertheless, the influence of the internal volume ratio can still be observed. Indeed, as the pressure decreases, the pressure ratio decreases, and the optimal internal volume ratio also decreases, shifting this optimum to the left in Figure 6.6.

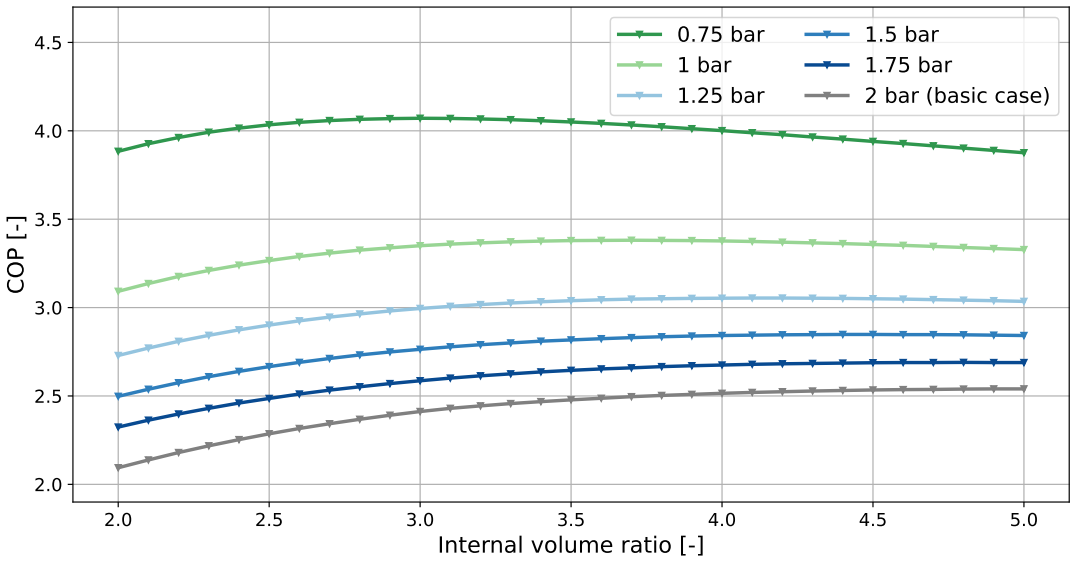

Figure 6.6: Effect of the stripper pressure and $r_{v,in}$ on the COP for the VI configuration.

6.2.4 Compressor total power

Although the performance of each configuration improves with decreasing pressure, this does not mean that their total electrical consumption decreases because of the increase of the heat duty required at the stripper. To assess whether lowering the pressure in the stripper reduces the energy required for the CO_2 capture process, the total electrical consumption of the compressors for each configuration is calculated using the internal volume ratio that maximizes the COP for each pressure studied.

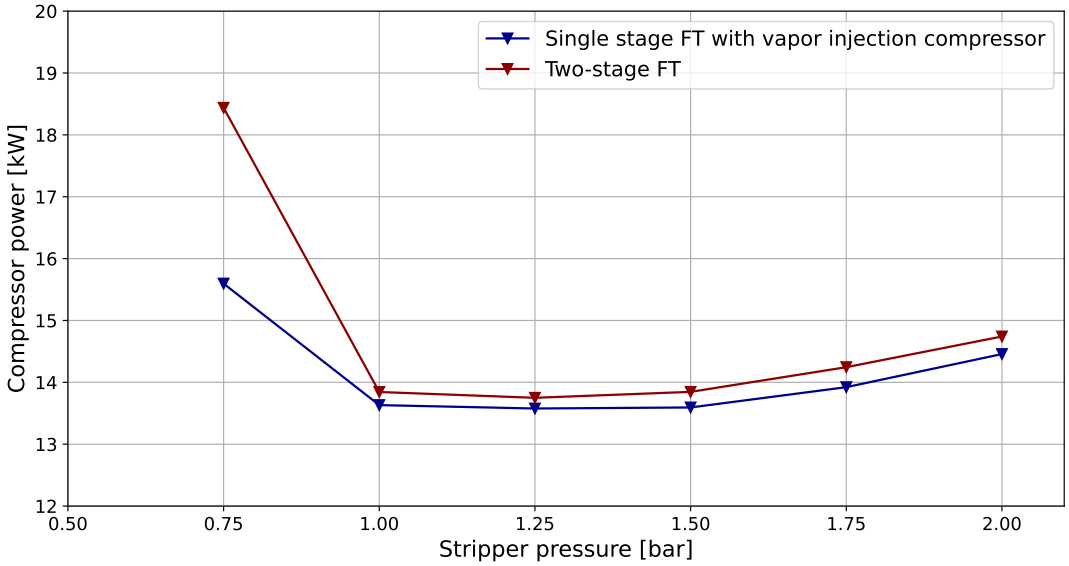

Figure 6.7: Stripper pressure effect on the compressor required power.

The lowest electrical consumption in Figure 6.7 corresponds to the single-stage configuration at a pressure of 1.25 bar in the stripper, which correspond to a condensation temperature of 125°C and an electrical power of 13,577 kW.

6.2.5 Evaporator available heating power

As for the second case, the evaporator is directly connected to the washer, it is important to verify that it could provide the heating power required. For the highest COP of 2,54 obtained the vapor injcetion and flash tank configuration, this required heating power is $\dot{Q}_{ev}$ = 15,206 kW and the total power avalaible at the washer is $\dot{Q}_{\text{washer}}$ 17,433 kW. However, this is the power if the water is cooled down from 47,5°C to 37,5° which represent a cooling power of 1,754 kW/K. So the real power available at the washer if the evaporator temperature is 35°C is the power available if the water is cool down to 47,5°C to 40°C :

$$\dot{Q}_{\text{washer}} = 7,5°\text{C} \cdot 1,754\text{kW} = 13,074\text{kW} < 15,206\text{kW} = \dot{Q}_{ev} \tag{6.1}$$

As the heating requirement can not be satisfied, the same analysis of the evaporator heating requirements as a function of the evaporation temperature did for the two first cases must be realised. The results are illustrated in Figure 6.8 and shows that the intersection of the two lines is just below 34°C. The new evaporation temperature is therefore fixed to 33°C

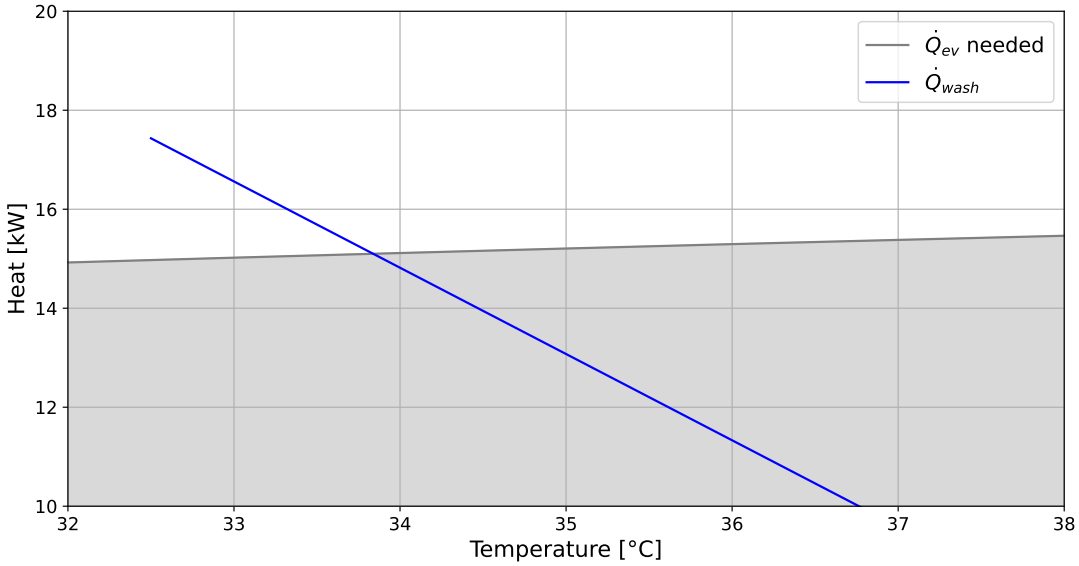

Figure 6.8: Evaporator heat duty in function of the evaporation temperature.

This new evaporation slightly decreases the performances of the cycles but not in a significant way. Indeed, the maximum COP recalculated is now 3,007 which represent a decrease of 1,54% compared to the previous value.

6.2.6 Compressor sizing

Finally, with the optimal pressure in the stripper, the corresponding condensation temperature and the corresponding optimal configurations being identified, the sizing of each compressor can now be performed :

Low pressure compressor :

- Power : $W_{LP} = 3,633$ kW.
- Displacement volume : $V_{LP} = 2,904 \cdot 10^{-4}$ m^3.
- Internal volume ratio : $r_{v,in} = 2,5$.
- Supply/exhaust pressure : 1,711 bar / 4,688 bar.

Vapor injection compressor :

- Power : $W_{inj} = 10,175$kW.
- Displacement volume for the first isentropic compression : $V_{inj,1} = 2,080 \cdot 10^{-4}$ m^3.
- Displacement volume for the second isentropic compression : $V_{inj,2} = 1,381 \cdot 10^{-4}$ m^3.
- Internal volume ratio : $r_{v,in} = 4,1$.
- Supply/exhaust pressure : 4,688 bar / 17,350 bar.

6.2.7 Conclusion

The aim of this chapter was to analyze the performance and energy consumption of the heat pump when the pressure maintained in the CO_2 capture process stripper was reduced. This reduction in pressure is interesting because it lowers the temperature required for CO_2 desorption, but it also increases the heat duty required for this desorption, which is less favorable. The results of this analysis show that it is indeed beneficial to lower the stripper pressure to 1.25 bar. Finally, a comparison of the required power and thus the energy consumption for each case studied in this thesis is illustrated in Table 6.2. It can be observed that the last case studied presents the lowest energy consumption, with a reduction of 62.4% compared to the process without heat pumps.

	Case 1	**Case 2**		**Case 3**
Optimal configuration	Two-stage FT with IHX	Two stage FT with VI compressor and IHX	Three stage FT with IHX	Two stage FT with VI compressor and IHX
Total power [kW]	16,836	14,552	14,843	13,788
Energy consumption [GJ/-ton CO_2]	1,662	1,427	1,456	1,352
Energy saving [%]	54,1	60,3	59,5	62,4

Table 6.2: Summary of performances and energy consumptions for each case and configurations.

Chapter 7

Conclusions and perspectives

This study aimed to explore the technical possibilities of reducing the energy consumption of the CO_2 capture pilot plant by integrating a high-temperature heat pump in the process. This integration has been thoroughly investigated through numerical modeling and simulations on EES and AspenPlus software. After introducing the main challenge of the post combustion amine based carbon capture process in Chapter 1 and a comprehensive review on heat pump technologies and its previous integration to the CO_2 capture process in Chapter 2. The study first explored the heat sources available from the cooling requirements of the CO_2 capture process in Chapter 3. Two cases were considered: a single evaporator heat pump connected to the cooling circuit of the process and a two-evaporator heat pump utilizing the high-temperature of the mixture exiting the stripper. For each cases, the heat pump cycles were optimized to provide the best performances.

The results of the simulations using the refrigerant R-1233zd(E) in Chapter 5 demonstrated significant potential for energy savings. Indeed, for the first case, the two-stage configurations using a flash tank and an internal heat exchanger reachs a maximal COP of 2,18 and reduced the initial energy consumption of the process by 54,1%. For the second case study, two configurations achieved similar results: The three-stage configuration with an internal heat exchanger for the low-pressure side and a flash tank for the high-pressure side achieved a COP of 2,47, reducing the initial energy consumption by 59,5%. The two-stage configuration using an internal heat exchanger for the low-pressure side but with a single vapor injection compressor for the high-pressure side achieved a of 2,52, reducing the initial energy consumption by 60,3%. For the best configurations of the two first cases, simulation results of the system's behavior under variable load demonstrate that, depending on the pilot's needs, it would be appropriate to size the compressors for lower power than the nominal power.

Subsequently, the study delves into modifications of the carbon capture process itself to enhance the energy performance of the second case in Chapter 6. Specifically, an analysis of the impact of reducing the pressure in the stripper was conducted. The results of this analysis demonstrate that the energy consumption of the heat pump can be further decreased by lowering the pressure in the stripper. The best results were obtained at a pressure of 1,25 bar, using a two-stage heat pump configuration with an internal heat exchanger for the low-pressure side and a vapor injection compressor for the high-pressure side, achieving a 62,4% reduction in initial energy consumption.

It is important to remain critical of these results. Indeed, the simulations are based on purely theoretical models, and the assumptions used in Chapter 4 may have influenced the outcomes. Moreover, the behavior of scroll compressors at high temperatures is not yet well understood experimentally, adding another layer of uncertainty. Additionally, ambient losses, pressure drops and friction losses were neglected, which which can affect the accuracy of the results. These limitations highlight the need for caution when interpreting the findings.

Nevertheless, the main drawback of CO_2 capture processes being their high energy consumption, the results of this work demonstrate that integrating a high-temperature heat pump can significantly reduce this energy demand, which is highly encouraging. To further validate these findings, experimental testing on the pilot plant project is necessary. Such testing would provide a clearer understanding of the real-world energy savings and offer insights into the behavior of scroll compressors at high temperatures. Additionally, these experiments could reveal how the integration of the heat pump impacts the overall capture process. This, in turn, could enhance the feasibility and attractiveness of CO_2 capture technologies, potentially driving further advancements and optimizations in the field.

Bibliography

[1] In: *Climate Action tracker* (2023). URL: https://climateactiontracker.org/global/temperatures/.

[2] David Chandler. "Explained : Greenhouse Gases". In: *MIT News* (2023). URL: https://climate.mit.edu/explainers/greenhouse-gases.

[3] "Shaping the hydrogen and carbon infrastructure for Belgium". In: 2021. URL: https://www.fluxys.com/en/about-us/energy-transition/hydrogen-carbon-infrastructure/infosession-20210126.

[4] Madejski et al. "Methods and Techniques for CO2 Capture: Review of Potential Solutions and Applications in Modern Energy Technologies". In: (2022). URL: https://www.mdpi.com/1996-1073/15/3/887.

[5] Aseem Dubey and Akhilesh Arora. "Advancements in carbon capture technologies: A review". In: *Journal of Cleaner Production* 373 (2022), p. 133932. ISSN: 0959-6526. URL: https://www.sciencedirect.com/science/article/pii/S0959652622035041.

[6] K. Vatopoulos et al. "Study on the state of play of energy efficiency of heat and electricity production technologies". In: *Publ Office Eur Union* (Jan. 2012), pp. 1–102.

[7] Robert Czarnota et al. "CARBON DIOXIDE SEPARATION TECHNOLOGIES". In: *Archives of Mining Sciences* vol. 64.No 3 (2019), pp. 487–498. URL: http://journals.pan.pl/Content/112904/PDF/Archiwum-64-3-02-Czarnota.pdf.

[8] Fanzhi Meng et al. "Research progress of aqueous amine solution for CO2 capture: A review". In: *Renewable and Sustainable Energy Reviews* 168 (2022), p. 112902. ISSN: 1364-0321. URL: https://www.sciencedirect.com/science/article/pii/S1364032122007845.

[9] Beguin Brieuc. "Simulation and Adaptation of a Biomass Combined Heat and Power Plant with CO2 Capture". MA thesis. University of Liège, 2022. URL: http://hdl.handle.net/2268.2/14396.

[10] Dipa Das, Tushar Agarwal, and Arun Kumar Biswal. "A review on different methods of CO2 capture, separation and utilization." In: *Brazilian Journal of Chemical Engineering* (2023). URL: https://link.springer.com/article/10.1007/s43153-023-00378-z.

[11] Ikhlas Ghiat and Tareq Al-Ansari. "A review of carbon capture and utilisation as a CO2 abatement opportunity within the EWF nexus". In: *Journal of CO2 Utilization* 45 (2021), p. 101432. ISSN: 2212-9820. URL: https://www.sciencedirect.com/science/article/pii/S2212982020310623.

[12] Alicja Krzemień et al. “Risk Assessment of a Post-Combustion and Amine-Based CO2 Capture Ready Process”. In: *Journal of Sustainable Mining* 12.4 (2013), pp. 18–23. ISSN: 2300-3960. URL: https://www.sciencedirect.com/science/article/pii/S2300396015300653.

[13] Ludovic Raynal et al. “From MEA to demixing solvents and future steps, a roadmap for lowering the cost of post-combustion carbon capture”. In: *Chemical Engineering Journal* 171.3 (2011). Special Section: Symposium on Post-Combustion Carbon Dioxide Capture, pp. 742–752. ISSN: 1385-8947. URL: https://www.sciencedirect.com/science/article/pii/S1385894711000350.

[14] Zhiwu (Henry) Liang et al. “Recent progress and new developments in post-combustion carbon-capture technology with amine based solvents”. In: *International Journal of Greenhouse Gas Control* 40 (2015). Special Issue commemorating the 10th year anniversary of the publication of the Intergovernmental Panel on Climate Change Special Report on CO2 Capture and Storage, pp. 26–54. ISSN: 1750-5836. URL: https://www.sciencedirect.com/science/article/pii/S1750583615002704.

[15] Cordin Arpagaus et al. “High temperature heat pumps: Market overview, state of the art, research status, refrigerants, and application potentials”. In: *Energy* 152 (2018), pp. 985–1010. ISSN: 0360-5442. URL: https://www.sciencedirect.com/science/article/pii/S0360544218305759.

[16] Anton Kiss and Carlos Ferreira. *Heat Pumps in Chemical Process Industry*. Sept. 2016. ISBN: 978-1-4987-1895-0. DOI: 10.1201/9781315371030.

[17] Hatem Houhou, W Yuan, and G Wang. “Simulation of Solar Heat Pump Dryer Directly Driven by Photovoltaic Panels”. In: *IOP Conference Series: Earth and Environmental Science* 63 (May 2017), p. 012007. DOI: 10.1088/1755-1315/63/1/012007.

[18] Vincent Lemort. *Applied thermodynamics and introduction to heating and cooling systems*. Université de Liège, Liège, Belgium. 2022.

[19] Cordin Arpagaus et al. “Multi-temperature heat pumps: A literature review”. In: *International Journal of Refrigeration* 69 (2016), pp. 437–465. ISSN: 0140-7007. URL: https://www.sciencedirect.com/science/article/pii/S0140700716301190.

[20] Fadi Alsouda et al. “Vapor Compression Cycle: A State-of-the-Art Review on Cycle Improvements, Water and Other Natural Refrigerants”. In: *Clean Technologies* 5.2 (2023), pp. 584–608. URL: https://www.mdpi.com/2571-8797/5/2/30.

[21] Benjamin Zühlsdorf et al. “High-Temperature Heat Pumps. Task 1 – Technologies.: Task Report”. In: *Annexe 58* 1 (2023). URL: https://heatpumpingtechnologies.org/annex58/task1/.

[22] Vincent Lemort. *Cooling and low temperature heating systems*. University of Liège, Liège, Belgium. 2023.

[23] Zhenying Zhang and Lili Tian. “Effect of Suction Nozzle Pressure Drop on the Performance of an Ejector-Expansion Transcritical CO2 Refrigeration Cycle”. In: *Entropy* 16.8 (2014), pp. 4309–4321. URL: https://www.mdpi.com/1099-4300/16/8/4309.

[24] S. Taslimi Taleghani et al. “Performance investigation of a two-phase transcritical CO2 ejector heat pump system”. In: *Energy Conversion and Management* 185 (2019), pp. 442–454. ISSN: 0196-8904. URL: https://www.sciencedirect.com/science/article/pii/S0196890419301578.

[25] ASHRAE. “Update on New Refrigerants Designations and Safety Classifications”. In: (2022). URL: https://www.ashrae.org/file%20library/technical%20resources/bookstore/factsheet_ashrae_english_november2022.pdf.

[26] S.B. Riffat et al. “Natural refrigerants for refrigeration and air-conditioning systems”. In: *Applied Thermal Engineering* 17.1 (1997), pp. 33–42. ISSN: 1359-4311. URL: https://www.sciencedirect.com/science/article/pii/1359431196000300.

[27] Ioan Sarbu. “A review on substitution strategy of non-ecological refrigerants from vapour compression-based refrigeration, air-conditioning and heat pump systems”. In: *International Journal of Refrigeration* 46 (2014), pp. 123–141. ISSN: 0140-7007. URL: https://www.sciencedirect.com/science/article/pii/S0140700714000991.

[28] P. Makhnatch. “New refrigerants for vapour compression refrigeration and heat pump systems: evaluation in a context of the requirements set by the F-gas Regulation and the Paris Agreement goals.” In: *(PhD dissertation, Universitetsservice US-AB)* (2019). URL: https://www.diva-portal.org/smash/get/diva2:1347734/FULLTEXT01.pdf.

[29] Sachin Dubey et al. “Energy, environmental and economic analysis of low GWP refrigerant heat pumps for simultaneous heating and cooling applications”. In: *Thermal Science and Engineering Progress* 51 (2024), p. 102605. ISSN: 2451-9049. URL: https://www.sciencedirect.com/science/article/pii/S2451904924002233.

[30] European environment agency. “Risks of PFAS for human health in Europe”. In: *European zero solution dashboard* (2024). DOI: 10.5194/acp-21-14833-2021. URL: https://www.eea.europa.eu/en/european-zero-pollution-dashboards/indicators/risk-of-pfas-in-humans.

[31] Marina G. Evich et al. “Per- and polyfluoroalkyl substances in the environment”. In: *Science* 375.6580 (2022), eabg9065. URL: https://www.science.org/doi/abs/10.1126/science.abg9065.

[32] ECHA. “ECHA publishes PFAS restriction proposal”. In: (2023). URL: https://echa.europa.eu/-/echa-publishes-pfas-restriction-proposal#:~:text=ECHA%20publishes%20PFAS%20restriction%20proposal%20ECHA%2FNR%2F23%2F04%20The%20details,and%20the%20environment%2C%20and%20the%20impacts%20on%20society.

[33] Xudong Ma et al. “A comprehensive review of compression high-temperature heat pump steam system: status and trend”. In: *International Journal of Refrigeration* (2024). ISSN: 0140-7007. URL: https://www.sciencedirect.com/science/article/pii/S014070072400152X

[34] Carlos Mateu-Royo et al. “Theoretical evaluation of different high-temperature heat pump configurations for low-grade waste heat recovery”. In: *International Journal of Refrigeration* 90 (2018), pp. 229–237. ISSN: 0140-7007. URL: https://www.sciencedirect.com/science/article/pii/S0140700718301233.

[35] Cordin Arpagaus et al. “High temperature heat pumps - Theoretical study on low GWP HFO and HCFO refrigerants”. In: (Aug. 2019). URL: https://www.researchgate.net/publication/335882942_High_temperature_heat_pumps_-_Theoretical_study_on_low_GWP_HFO_and_HCFO_refrigerants.

[36] Fernando M. Tello-Oquendo, Emilio Navarro-Peris, and José Gonzálvez-Maciá. “Comparison of the performance of a vapor-injection scroll compressor and a two-stage scroll compressor working with high pressure ratios”. In: *Applied Thermal Engineering* 160 (2019), p. 114023. ISSN: 1359-4311. URL: https://www.sciencedirect.com/science/article/pii/S1359431119308622.

[37] Carlos Mateu-Royo et al. “Advanced high temperature heat pump configurations using low GWP refrigerants for industrial waste heat recovery: A comprehensive study”. In: *Energy Conversion and Management* 229 (2021), p. 113752. ISSN: 0196-8904. URL: https://www.sciencedirect.com/science/article/pii/S0196890420312759.

[38] Xing-Qi Cao et al. “Performance analysis of different high-temperature heat pump systems for low-grade waste heat recovery”. In: *Applied Thermal Engineering* 71.1 (2014), pp. 291–300. ISSN: 1359-4311. URL: https://www.sciencedirect.com/science/article/pii/S1359431114005298.

[39] Bin Hu et al. “Exergy analysis of R1234ze(Z) as high temperature heat pump working fluid with multi-stage compression”. In: *Frontiers in Energy* 11 (Nov. 2017). URL: https://www.researchgate.net/publication/321060373_Exergy_analysis_of_R1234zeZ_as_high_temperature_heat_pump_working_fluid_with_multi-stage_compression.

[40] Sho Fukuda et al. “Low GWP refrigerants R1234ze(E) and R1234ze(Z) for high temperature heat pumps”. In: *International Journal of Refrigeration* 40 (2014), pp. 161–173. ISSN: 0140-7007. URL: https://www.sciencedirect.com/science/article/pii/S0140700713002922.

[41] Adrián Mota-Babiloni et al. “Optimisation of high-temperature heat pump cascades with internal heat exchangers using refrigerants with low global warming potential”. In: *Energy* 165 (2018), pp. 1248–1258. ISSN: 0360-5442. URL: https://www.sciencedirect.com/science/article/pii/S0360544218319601.

[42] Cordin Arpagaus et al. “High Temperature Heat Pump using HFO and HCFO refrigerants - System design, simulation, and first experimental results”. In: (Aug. 2018). URL: https://www.researchgate.net/publication/326847793_High_Temperature_Heat_Pump_using_HFO_and_HCFO_refrigerants_-_System_design_simulation_and_first_experimental_results.

[43] Guido Francesco Frate, Lorenzo Ferrari, and Umberto Desideri. “Analysis of suitability ranges of high temperature heat pump working fluids”. In: *Applied Thermal Engineering* 150 (2019), pp. 628–640. ISSN: 1359-4311. URL: https://www.sciencedirect.com/science/article/pii/S1359431118353602.

[44] Cordin Arpagaus et al. “High temperature heat pump using HFO and HCFO refrigerants - System design and experimental results”. In: (Aug. 2019). URL: https://www.researchgate.net/publication/335882749_High_temperature_heat_pump_using_HFO_and_HCFO_refrigerants_-_System_design_and_experimental_results#fullTextFileContent.

[45] Opeyemi Bamigbetan et al. “Theoretical analysis of suitable fluids for high temperature heat pumps up to 125°C heat delivery”. In: *International Journal of Refrigeration* 92 (2018), pp. 185–195. ISSN: 0140-7007. URL: https://www.sciencedirect.com/science/article/pii/S0140700718301750.

[46] arlos Mateu-Royo et al. “Thermodynamic analysis of low GWP alternatives to HFC-245fa in high-temperature heat pumps: HCFO-1224yd(Z), HCFO-1233zd(E) and HFO-1336mzz(Z)”. In: *Applied Thermal Engineering* 152 (2019), pp. 762–777. ISSN: 1359-4311. URL: https://www.sciencedirect.com/science/article/pii/S1359431118357582.

[47] Di Wu et al. “The performance comparison of high temperature heat pump among R718 and other refrigerants”. In: *Renewable Energy* 154 (2020), pp. 715–722. ISSN: 0960-1481. URL: https://www.sciencedirect.com/science/article/pii/S0960148120303566.

[48] P. Giménez-Prades et al. “Novel molecules as working fluids for refrigeration, heat pump and organic Rankine cycle systems”. In: *Renewable and Sustainable Energy Reviews* 167 (2022), p. 112549. ISSN: 1364-0321. URL: https://www.sciencedirect.com/science/article/pii/S1364032122004488.

[49] Daniella Johansson, Jonas Sjöblom, and Thore Berntsson. "Heat supply alternatives for CO2 capture in the process industry". In: *International Journal of Greenhouse Gas Control* 8 (2012), pp. 217–232. ISSN: 1750-5836. URL: https://www.sciencedirect.com/science/article/pii/S1750583612000382.

[50] Kefang Zhang et al. "Process integration analysis and improved options for an MEA CO2 capture system based on the pinch analysis". In: *Applied Thermal Engineering* 85 (2015), pp. 214–224. ISSN: 1359-4311. URL: https://www.sciencedirect.com/science/article/pii/S1359431115003348.

[51] Abdullah Alabdulkarem, Yunho Hwang, and Reinhard Radermacher. "Multi-functional heat pumps integration in power plants for CO2 capture and sequestration". In: *Applied Energy* 147 (2015), pp. 258–268. ISSN: 0306-2619. URL: https://www.sciencedirect.com/science/article/pii/S0306261915002871.

[52] Bingyao Ge et al. "Innovative process integrating high temperature heat pump and direct air capture". In: *Applied Energy* 355 (2024), p. 122229. ISSN: 0306-2619. URL: https://www.sciencedirect.com/science/article/pii/S0306261923015933.

[53] Veronika Wilk et al. "Improving Energy Efficiency of Carbon Capture Processes with Heat Pumps". In: *International Sustainable Energy Conference - Proceedings* 1 (Apr. 2024). URL: https://www.researchgate.net/publication/380084638_Improving_Energy_Efficiency_of_Carbon_Capture_Processes_with_Heat_Pumps.

[54] Ebbe Hauge Jensen et al. "Electrification of amine-based CO2 capture utilizing heat pumps". In: *Carbon Capture Science Technology* 10 (2024), p. 100154. ISSN: 2772-6568. URL: https://www.sciencedirect.com/science/article/pii/S2772656823000581.

[55] Aspen Technology, Inc. *Aspen Plus*. Version 14. Burlington, MA, 2024. URL: https://www.aspentech.com/en/products/engineering/aspen-plus.

[56] F-Chart Software. *Engineering Equation Solver (EES) Version 10.507*. Madison, WI, 2024. URL: http://www.fchart.com/ees/.

[57] Eric Winandy, Claudio Saavedra, and Jean Lebrun. "Experimental analysis and simplified modelling of a hermetic scroll refrigeration compressor". In: *Applied Thermal Engineering* 22.2 (2002), pp. 107–120. ISSN: 1359-4311. URL: https://www.sciencedirect.com/science/article/pii/S1359431101000837.

[58] Jean Lebrun and Vincent Lemort. *Machines et systèmes thermiques*. University of Liège, Liège, Belgium. 2007.

[59] Cristian Cuevas and Jean Lebrun. "Testing and modelling of a variable speed scroll compressor". In: *Applied Thermal Engineering* 29.2 (2009), pp. 469–478. ISSN: 1359-4311. URL: https://www.sciencedirect.com/science/article/pii/S1359431108001397.

[60] Cristian Cuevas et al. "Characterization of a scroll compressor under extended operating conditions". In: *Applied Thermal Engineering* 30.6 (2010), pp. 605–615. ISSN: 1359-4311. URL: https://www.sciencedirect.com/science/article/pii/S1359431109003330.

[61] Eric Winandy and Jean Lebrun. "Scroll compressors using gas and liquid injection: experimental analysis and modelling". In: *International Journal of Refrigeration* 25.8 (2002), pp. 1143–1156. ISSN: 0140-7007. URL: https://www.sciencedirect.com/science/article/pii/S0140700702000038.

[62] Vincent Lemort. "Contribution to the characterization of scroll machines in compressor and expander modes". PhD thesis. University of Liège, 2008.

[63] G Meramveliotakis, G Kosmadakis, and S Karellas. “Identifying the performance and losses of a scroll compressor with vapour injection and R1234ze(E) [version 2; peer review: 2 approved”. In: *Open Research Europe* 2.49 (2022). URL: https://open-research-europe.ec.europa.eu/articles/2-49.

[64] Christ Jan et al. “Semi-empirical Scroll Compressor Model with Optional Vaporinjection”. In: *INTERNATIONAL COMPRESSOR ENGINEERING CONFERENCE* (2022). URL: https://docs.lib.purdue.edu/cgi/viewcontent.cgi?article=3790&context=icec.

[65] Paul Byrne, Redouane Ghoubali, and Jacques Miriel. “Scroll compressor modelling for heat pumps using hydrocarbons as refrigerants”. In: *International Journal of Refrigeration* 41 (2014), pp. 1–13. ISSN: 0140-7007. URL: https://www.sciencedirect.com/science/article/pii/S0140700713001503.

[66] Wenhua Li. “Simplified steady-state modeling for variable speed compressor”. In: *Applied Thermal Engineering* 50.1 (2013), pp. 318–326. ISSN: 1359-4311. URL: https://www.sciencedirect.com/science/article/pii/S1359431112005649.

[67] Eric Winandy, Claudio Saavedra O, and Jean Lebrun. “Simplified modelling of an open-type reciprocating compressor”. In: *International Journal of Thermal Sciences* 41.2 (2002), pp. 183–192. ISSN: 1290-0729. URL: https://www.sciencedirect.com/science/article/pii/S1290072901012960.

[68] Rubén Ossorio, Javier Marchante-Avellaneda, and Emilio Navarro-Peris. “Development of compact empirical models for variable-speed compressors for the prediction of energy consumption, mass flow and discharge temperature”. In: *Applied Thermal Engineering* 244 (2024), p. 122666. ISSN: 1359-4311. URL: https://www.sciencedirect.com/science/article/pii/S135943112400334X.

[69] Umer Khalid Awan. “Experimental analysis of variable capacity heat pump system equipped with vapour injection and permanent magnet motor”. MA thesis. KTH, Applied Thermodynamics and Refrigeration, 2012, p. 79. URL: https://www.diva-portal.org/smash/record.jsf?pid=diva2%3A565195&dswid=3514.

[70] “Semi-empirical model of scroll compressors and its extension to describe vapor-injection compressors. Model description and experimental validation”. In: *International Journal of Refrigeration* 106 (2019), pp. 308–326. ISSN: 0140-7007. URL: https://www.sciencedirect.com/science/article/pii/S0140700719302944.

[71] Laurent Dardenne et al. “Semi-empirical modelling of a variable speed scroll compressor with vapour injection”. In: *International Journal of Refrigeration* 54 (2015), pp. 76–87. ISSN: 0140-7007. URL: https://www.sciencedirect.com/science/article/pii/S0140700715000511.

[72] John P. Elson et al. “Scroll Technology: An Overview of Past, Present and Future Developments”. In: 2008. URL: https://api.semanticscholar.org/CorpusID:19431062.

[73] Sugun Tej Inampudi and Stefan Elbel. “Experimental comparison and seasonal performance evaluation of different scroll compressor capacity modulation methods in an R410A water to water system”. In: *Applied Thermal Engineering* 247 (2024), p. 123033. ISSN: 1359-4311. URL: https://www.sciencedirect.com/science/article/pii/S1359431124007014

[74] E.Pereira Perreira and J.A.R. Parise. “Performance analysis of capacity control devices for heat pump reciprocating compressors”. In: *Heat Recovery Systems and CHP* 13.5 (1993), pp. 451–461. ISSN: 0890-4332. URL: https://www.sciencedirect.com/science/article/pii/089043329390046X.